INAUGURAL DISSERTATION

submitted to the Combined Faculty of Natural Sciences and Mathematics of the Ruperto Carola University Heidelberg, Germany for the degree of Doctor of Natural Sciences

Presented by

M. Sc. Tolga Lokumcu

Born in Borçka, Turkey

Date of Oral Examination: 20.01.2022

Metabolic, proteomic, transcriptomic, and fatty acid profiling of glioblastoma stem cells and their small extracellular vesicles

Referees: Prof. Dr. Ursula Klingmüller

Prof. Dr. Stefan Pfister

Declaration

I hereby declare that I have written the submitted dissertation “Metabolic, proteomic, transcriptomic, and fatty acid profiling of glioblastoma stem cells and their small extracellular vesicles” myself and in this process have not used any other sources than those expressly indicated.

I hereby declare that I have not applied to be examined at any other institution, nor have I used the dissertation in this or any other form at any other institution as an examination paper, nor submitted it to any other faculty as a dissertation.

Tolga Lokumcu

Contents

Table of Figures

Summary

Glioblastoma is the most frequent and lethal brain tumor, showing a high degree of intra- and intertumoral heterogeneity. Despite the multimodal treatments (surgical resection, irradiation, and chemotherapy), overall survival of patients is still less than 15 months. The inevitable relapse of glioblastoma is mainly attributed to the subpopulation of tumor initiating cells, namely glioblastoma stem cells, which are shown to be refractory to standard treatments. The exceedingly heterogeneous nature of glioblastoma creates hurdles in developing effective therapies and makes it extremely difficult to eradicate. This project investigated the role of GSCs-derived sEVs in glioblastoma aggressiveness with the particular focus on the complexity of tumor-derived sEVs in terms of proteins, metabolites, fatty acids, and small RNAs. In this direction, protein, metabolite, fatty acid, and small-RNA contents of sEVs and their parent cells (NCH421k, NCH644, NCH705, and NCH711d) were profiled by utilizing mass spectrometry and high-throughput sequencing. Protein profiling of sEVs and their respective cell lines revealed the enrichment of proteins playing a role in amino acids, carboxylic acids, and organic acids transmembrane transport, together with the ones functioning in growth factor binding (including insulin-like growth factor I and transforming growth factor beta). In line with the proteomic analysis, metabolite screening of GSC-derived sEVs also displayed the existence of metabolites associated with alanine, aspartate, glutamate metabolism, arginine biosynthesis, and butanoate metabolism, suggesting the dual role of GSCs-derived sEVs, which is transferring proteins responsible for the transport of amino acids/carboxylic acids and providing metabolites that will be used in amino acid and carboxylic acid metabolism. In conjunction with proteomic and metabolic analysis, profiling of fatty acids (carboxylic acids with long aliphatic chains) has revealed the presence of different fatty acid species, especially saturated fatty acids, in GSCs-derived sEVs, further implying that loading of biological cargos into sEVs is a highly regulated process, and that GSCs-derived sEVs are important sources for tumor cells to maintain their cellular metabolism. Finally, small RNA sequencing of GSCs-derived sEVs and their parent cells was carried out to shed some light on the contribution of sEVs-derived small RNAs to heterogeneity of glioblastoma; however, due to technical problems in sequencing (very low reads counts, poor complexity of sequencing library) the data is unfortunately not reliable for comparative analysis.

In summary, this project revealed the complexity of GSCs-derived sEVs in terms of proteins, metabolites, fatty acids, and smRNAs (with limited degree), and unveiled their potential contribution to tumor heterogeneity and critical cellular processes commonly deregulated in glioblastoma.

Zusammenfassung

Das Glioblastom ist der häufigste und tödlichste Hirntumor und weist ein hohes Maß an intra- und intertumoraler Heterogenität auf. Trotz multimodaler Behandlung bestehend aus chirurgischer Resektion, Bestrahlung und Chemotherapie beträgt das Gesamtüberleben der Patienten immer noch weniger als 15 Monate. Der unvermeidliche Rückfall des Glioblastoms wird hauptsächlich auf eine Subpopulation der tumorauslösenden Zellen, den Glioblastom-Stammzellen (GSZ), zurückgeführt, die sich als therapieresistent gegenüber Standardbehandlungen erweisen. Die Heterogenität des Glioblastoms erschwert die Entwicklung wirksamer Therapien und macht eine Behandlung sehr schwierig. In diesem Projekt wurde die Rolle von GSZ-abgesonderten kleinen extrazellulären Vesikel (EVs) in Bezug auf die Aggressivität des Glioblastoms untersucht und hierbei den Fokus auf die Komplexität der vom Tumor stammenden EVs hinsichtlich der Proteine, Metabolite, Fettsäuren und kleiner RNA Moleküle gelegt. Aus diesem Grund wurde die Zusammensetzung der Proteine, Metabolite, Fettsäuren und kleiner RNA Moleküle in EVs und den dazu gehörigen Zelllinien (NCH421k, NCH644, NCH705 und NCH711d) mittels Massenspektrometrie und Hochdurchsatzsequenzierung analysiert. Die Proteomanalyse der EVs und den jeweiligen Zelllinien ergab eine Anreicherung von Proteinen, die beim Transmembrantransport von Aminosäuren, Carbonsäuren und organischen Säuren sowie bei der Bindung von Wachstumsfaktoren (einschließlich des insulinähnlichen Wachstumsfaktors I und des transformierenden Wachstumsfaktors beta) eine Rolle spielen. In Übereinstimmung mit der Proteomanalyse zeigte die Metabolomanalyse von EVs auch das Vorkommen von Metaboliten, die mit dem Alanin-, Aspartat- und Glutamat-Stoffwechsel, der Arginin-Biosynthese sowie dem Butanoat-Stoffwechsel in Verbindung gebracht werden. Dies deutet auf eine duale Rolle von EVs hin, die die Übertragung von Proteinen, die für den Transport von Aminosäuren/Carbonsäuren verantwortlich sind, und die Bereitstellung von Metaboliten, die im Aminosäure- und Carbonsäure-Stoffwechsel verwendet werden, umfasst. Zusammen mit der Proteom- und Metabolomanalyse hat die Untersuchung von Fettsäuren (Carbonsäuren mit langen aliphatischen Ketten) ergeben, dass verschiedene Fettsäurearten, insbesondere gesättigte Fettsäuren, in EVs vorliegen. Dies deutet darauf hin, dass die Beladung der EVs mit biologischen Molekülen ein stark regulierter Prozess ist und dass die EVs eine wichtige Quelle für Tumorzellen zur Aufrechterhaltung ihres Zellstoffwechsels sind. Schließlich wurde die Sequenzierung kleiner RNA Moleküle aus EVs und den dazu gehörigen Zelllinien durchgeführt, um den Beitrag der aus EVs stammenden kleinen RNAs zur Heterogenität des Glioblastoms besser zu verstehen. Aufgrund technischer Probleme bei der Sequenzierung (sehr niedrige Lesezahlen, geringe Komplexität der Sequenzierbibliothek) waren die Daten für eine vergleichende Analyse jedoch leider nicht auswertbar.

Zusammenfassend hat dieses Projekt die Komplexität der aus GSZs-stammenden EVs in Bezug auf Proteine, Metabolite, Fettsäuren und kleiner RNA Moleküle (in begrenztem Umfang) aufgezeigt und ihren potenziellen Beitrag zur Tumorheterogenität und zellulären Prozessen, die beim Glioblastom häufig dereguliert sind, offengelegt.

Abbreviations

ATCC	American Tissue Culture Collection
BCA	Bicinchoninic acid
BLAST	Basic Local Alignment Search Tool
BSA	Bovine serum albumin
CCM	complete conditioned medium
CL	Classical
CNS	Central Nervous System
DMEM	DMEM (Dulbecco's modified eagle medium)
DMSO	Dimethyl sulfoxide
DNA	Deoxyribonucleic acid
dNTP	Deoxynucleoside triphosphate
DTT	Dithiotreitol
ECL	Enhanced chemiluminescence
EDTA	Ethylenediaminetetraacetate
EGF	Epidermal Growth Factor
EGFR	Epidermal growth factor receptor
EM	Electron microscopy
ESCRT	Endosomal sorting complex required for transport
EVs	Extracellular vesicles
FACS	Fluorescence-activated cell sorting
FAME	Fatty Acid Methyl Ester
FBS	Fetal bovine serum
FCS	Fetal calf serum
FGF	Fibroblast Growth Factor
G-CIMP	CpG island methylator phenotype
GBM	Glioblastoma
GC-MS	Gas Chromatography-Mass Spectrometry
gDNA	Genomic deoxyribonucleic acid

GFP	Green fluorescent protein
GSC	Glioblastoma stem cells
GTPases	Guanosine triphosphatases
HEK	Human Embryonic Kidney
HM	Homogenization media
HSC70	Heat shock cognate 71 kDa protein
HSP70	Heat shock 70 kDa protein
IDH1	Isocitrate dehydrogenase 1
ILVs	Intraluminal vesicles
LB	Luria-Bertani
MES	Mesenchymal
MGMT	O6-methylguanine–DNA methyltransferase
MOI	Multiplicity of Infection
MVB	Multivesicular body
NE	Neural
NGS	Next-generation sequencing
NTA	Nanoparticle tracking analysis
PBS	Phosphate buffered saline
PCR	Polymerase chain reaction
PDGFRA	Platelet-derived growth factor receptor alpha
PI	Propidium iodide
PI3K	Phosphoinositide 3-kinase
PN	Proneural
PVDF	Polyvinylidene difluoride
RB	Retinoblastoma
RFP	Red fluorescent protein
RNA	Ribonucleic acid
RNAi	RNA interference
RTK	Receptor tyrosine kinase
scRNA-seq	Single-cell RNA-sequencing

SDS	Sodium dodecyl sulfate
sEVs	Small extracellular vesicles
shRNA	Short-hairpin ribonucleic acid
SNAP-23	Synaptosomal-associated protein 23
TBE	TRIS-Borat-EDTA
TBS	TRIS buffered saline
TCGA	The Cancer Genome Atlas Research Network
TMZ	Temozolomide
TP53	Tumor protein 53
VPS32	Vacuolar protein sorting-associated protein 32
WS	Working Solution

1. Introduction

1.1 Tumors of the Central Nervous System

Central nervous system (CNS) tumors refer to diverse group of neoplasms arising from cells within the brain, brainstem or spinal cord[1]. World Health Organization (WHO) has recently classified over 130 types of CNS tumor into categories of gliomas, glioneuronal and neuronal tumors, ependymal tumors, choroid plexus tumors, embryonal tumors, pineal tumors, cranial and paraspinal nerve tumors, meningiomas, mesenchymal non-meningothelial tumors, melanocytic tumors, hematolymphoid tumors, germ cell tumors, tumors of the sellar region and metastases to the CNS[2].

According to Central Brain Tumor Registry of the United States (CBTRUS) statistical report, published in 2020, about 30% of all primary CNS tumors were malignant, and from those, glioblastoma was the most common primary malignant brain tumor by comprising 48.6% of malignant tumors. On the other hand, meningioma was the most prevalent (54.5% of non-malignant tumors) primary non-malignant tumor (**Figure 1**). Malignant tumors of the pituitary had the highest median survival with 11.5 years, whereas glioblastoma had the lowest median survival with 8 months[3].

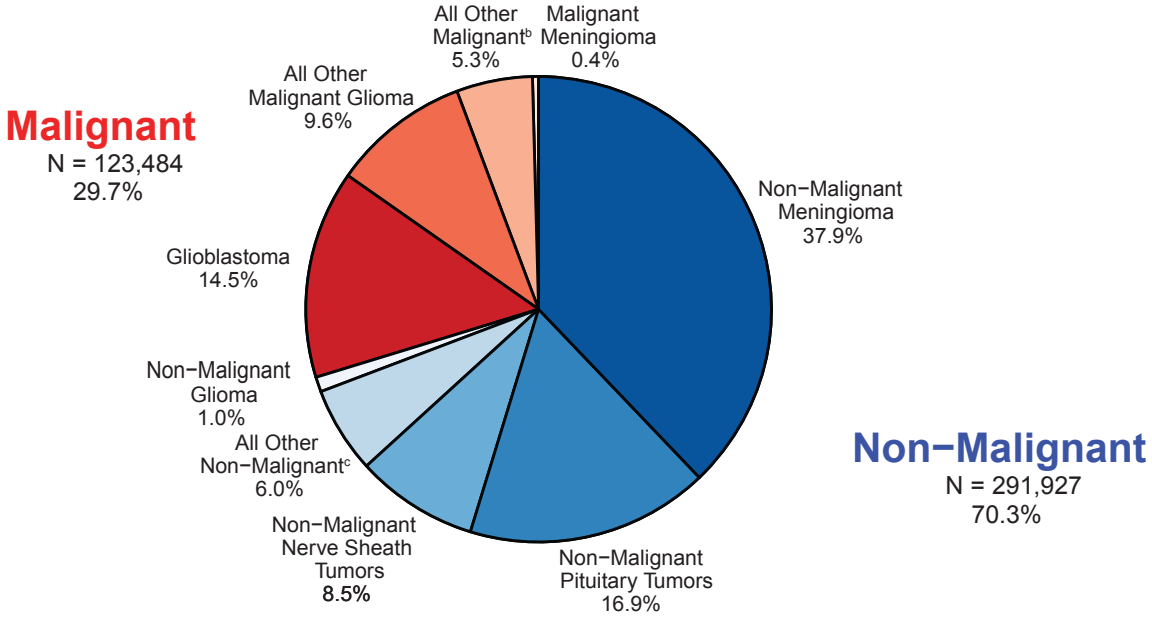

a. Percentages may not add up to 100% due to rounding.
b. Includes histologies with ICD−O−3 behavior code of /3 from choroid plexus tumors, neuronal and mixed neuronal−glial tumors, tumors of the pineal region, embryonal tumors, nerve sheath tumors, mesenchymal tumors, primary melanocytic lesions, other neoplasms related to the meninges, lymphoma, other hematopoietic neoplasms, germ cell tumors, cysts and heterotopias, tumors of the pituitary, craniopharyngioma, hemangioma, neoplasm unspecified, and all other.
c. Includes histologies with ICD−O−3 behavior code of /0 or /1 from neuronal and mixed neuronal−glial tumors, tumors of the pineal region, embryonal tumors, other tumors of cranial and spinal nerves, mesenchymal tumors, primary melanocytic lesions, other neoplasms related to the meninges, other hematopoietic neoplasms, germ cell tumors, cysts and heterotopias, craniopharyngioma, hemangioma, neoplasm unspecified, and all other.

Figure 1. Percent distribution of primary brain and other central nervous system tumors

Distributions and incidence of malignant/non-malignant brain and other CNS tumors reported during 2013-2017. Figure taken from Ostrom et al., 2020[3].

1.2 Gliomas

Gliomas are primary brain tumors arising from neuroglial stem or progenitor cells and account for approximately 25% of all primary brain and CNS tumors. Histologically, gliomas are classified as astrocytomas, oligodendrogliomas and ependymomas. The majority of gliomas (about 62%) occur in the supratentorial region of the brain, while only a small fraction of gliomas arises from the CNS areas other than the brain[3,4].

1.2.1 Classification of Gliomas

Historically, the classification of CNS tumors was based on histological features of the tumors. In recent years, studies focusing on molecular markers of tumors have provided valuable information on tumor characteristics and paved the way for more accurate classification of the central nervous system tumors.

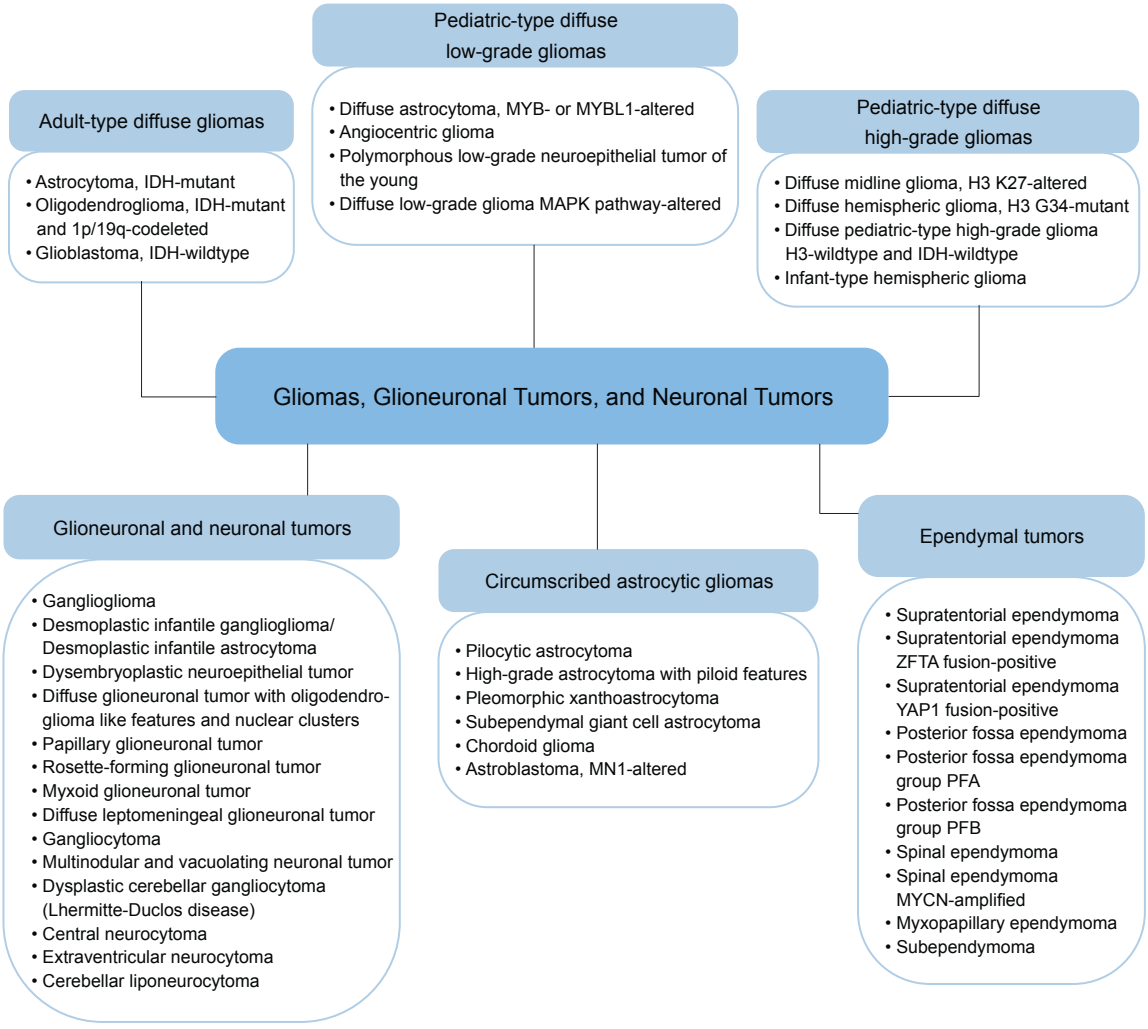

Figure 2. WHO Classification (2021) of Gliomas, Glioneuronal Tumors, and Neuronal Tumors

World Health Organization (WHO) has recently classified central nervous system tumors by integrating molecular diagnostics with histology and immunohistochemistry. According to the WHO Classification of CNS Tumors (2021), Gliomas, Glioneuronal Tumors, and Neuronal Tumors have been divided into six different families, namely Adult-type diffuse gliomas (1), Pediatric-type diffuse low-grade gliomas (2), Pediatric-type diffuse high-grade gliomas (3), Circumscribed astrocytic gliomas (4), Glioneuronal and neuronal tumors (5), and Ependymal tumors (6)[2] (**Figure 2**).

1.2.2 Prognostic markers for gliomas

Recent advances in molecular diagnostic techniques have greatly facilitated the identification of genomic drivers implicated in gliomagenesis. From those, isocitrate dehydrogenase 1 and 2 (IDH1 and IDH2) mutations, chromosome 1p/19q codeletion, O6-methylguanine-DNA methyltransferase (MGMT) promoter methylation, glioma CpG island methylator phenotype (G-CIMP) methylation, telomerase reverse transcriptase (TERT) promoter mutations, epidermal growth factor receptor (EGFR) alterations, BRAF V600E and histone H3 mutations are the ones deeply studied in gliomagenesis and glioma prognostication (**Table 1**)[5].

Table 1. Summary of prognostic molecular markers found in glioma*

Molecular Marker	Functional Significance	Prognostic value
IDH mutations	Accumulation of oncometabolite 2-HG Inhibition of 2-OG dependent enzymes Alteration in epigenetic state	Favorable prognosis
1p/19q codeletion	Deletion of tumor suppressor genes	Favorable prognosis
MGMT promoter methylation	Inhibition of MGMT expression Resistance to alkylating agents	Favorable prognosis
G-CIMP methylation	Silencing of tumor suppressor and mismatch repair genes	Favorable prognosis
TERT promoter mutations	Telomerase reactivation and telomere maintenance	Poor prognosis
EGFR alterations	Constitutively active EGFR pathway	Poor prognosis
BRAF V600E mutations	Constitutively active MAPK pathway	Favorable prognosis (in young patients)
Histone Mutations (H3K27, H3G34)	Deregulation of transcription	Poor prognosis

* based on Aquilanti et al., 2015[5]

IDH1 and IDH2 are metabolic enzymes that catalyze the oxidative carboxylation of isocitrate to alpha-ketoglutarate. Recurrent *IDH* mutations substituting arginine to histidine mostly at residue 132 (R132H for IDH1) or 172 (R172H for IDH2) give rise to accumulation of oncometabolite R-2-hydroxyglutarate (2-HG) that inhibit several 2-oxoglutarate (2-OG)-dependent enzymes, resulting in alterations of epigenetic state[6,7]. IDH mutant gliomas show CpG island methylator phenotype (CIMP), which facilitates to keep glioma cells in stem cell-like state and promote tumorigenesis[8–10]. *IDH* mutations (R132H) can be detected up to 80-90% of grade 2 and 3 gliomas and 12% of glioblastomas[11,12]. Besides, *IDH1* and *IDH2* mutations occur relatively early in gliomagenesis and have been associated with improved prognosis in glioma[13].

Heterozygous loss of the short arm of chromosome 1 (1p) and the long arm of chromosome 19 (19q) is associated with the tumors of the oligodendroglial lineage by promoting tumor growth via the inactivation of Capicua Transcriptional Repressor (*CIC*) and Far Upstream Element Binding Protein 1 (*FUBP1*) tumor suppressor genes[14]. The co-deletion of 1p/19q confers longer progression-free survival and is predictive of an improved response to therapy[15,16].

O^6-methylguanine-DNA methyltransferase (MGMT) is a DNA repair protein that removes alkyl groups from the DNA and reverses DNA damage induced by alkylating agents such as temozolomide. *MGMT* promoter methylation results in silencing of *MGMT* gene and decreased ability of tumors cells to repair such DNA damage. *MGMT* promoter methylation is more common in glioblastoma than in lower grade gliomas and considered as a favorable prognostic factor[17–19].

CpG islands are genomic regions that are enriched in CpG dinucleotides and are mainly located in or near promoter region of genes[20]. Glioma CpG island methylator phenotype (G-CIMP) was first described in colorectal cancer by Toyota et al. in 1999[21]. In 2010, Noushmehr et al. has also identified a group of glioblastoma tumors having similar methylation alterations and showed their association with *IDH* mutations. Although it is unclear whether this is related to the *IDH* mutations, G-CIMP phenotype is often correlated with improved overall survival[22].

Telomeres are repetitive nucleotide sequences (TTAGGG) located at the termini of chromosomes, which shorten following cell division. Telomerase reverse transcriptase (TERT) is a catalytic subunit of telomerase and is responsible for the maintenance of telomeric DNA. Cancer cells show increased telomerase activity, giving them unlimited proliferative capacity, whereas this is not the case in normal cells[23]. Mutations in *TERT* promoter region result in the reactivation of telomerase and can be detected about 80% of IDH-wildtype glioblastomas, as well as in the majority of oligodendrogliomas[24–26]. *TERT* promoter mutations are associated with the decrease survival in IDH-wildtype gliomas[27].

Finally, EGFR alterations, BRAF V600E and histone H3 mutations are also considered as prognostic markers for glioma. From those, amplification of EGFR is detected in ~ 40-50% of primary glioblastoma,

and its high expression has been shown to associated with poor prognosis[28–30]. Similarly, mutation in *BRAF* gene at the V600E position, which results in constitutive activation of B-Raf, has been identified in several cancer types, including diffuse gliomas, glioneuronal tumors, and glioblastoma. Although the outcome of *BRAF* mutations on glioma prognosis is still not entirely clear, a meta-analysis shows that the presence of this mutation is associated with improved survival in pediatric patients and younger adults (<35 y)[31,32]. Furthermore, histone mutations at K27 (K27M, lysine-to-methionine substitution) and G34 (G34R or G34V, glycine-to-arginine or glycine-to-valine substitution, respectively) have also been identified in high grade gliomas and are associated with decreased overall survival[33–35].

1.3 Glioblastoma

Glioblastoma (GBM) is the most frequent brain and central nervous system (CNS) tumor, accounting for 48.6% of primary malignant brain tumors and 14.5% of all primary brain and CNS tumors. Despite aggressive treatments (surgical resection, irradiation and chemotherapy), glioblastoma still has a dismal prognosis with the median survival less than 15 months[36,37]. Glioblastoma is classified into primary and secondary subtypes that originate from different precursor cells, harbor different genetic alterations, and have differences in prognosis. Whereas primary glioblastomas (*de novo*) develop mostly in older patients, without clinical and histological evidence of pre-existing lower grade lesions, secondary glioblastomas progress from lower-grade astrocytoma or oligodendrogliomas[36–39].

1.3.1 Classification of glioblastoma

Glioblastoma (GBM) is a highly aggressive type of brain tumor that harbors several genomic alterations such as chromosomal rearrangements, copy number changes, activating/deactivating mutations, and DNA methylation, resulting in malignant transformation. In 2008, The Cancer Genome Atlas Research Network (TCGA) initiated a project to provide comprehensive data to better understand the development and progression of human glioblastomas. The integrated multi-dimensional analyses of the genomic changes, gene expression and aberrant DNA methylation revealed that three core pathways, namely receptor tyrosine kinase (RTK)/phosphoinositide 3-kinase (PI3K) signaling, tumor protein 53 (TP53) and retinoblastoma (RB) tumor suppressor pathways, play pivotal roles in glioblastoma tumorigenesis[40,41]. Afterwards, gene expression profiling studies paved the way to define prognostic and subtype specific gene signatures, allowing the classification of high-grade gliomas (HGGs). Phillips et al., using gene expression profiling, defined a gene signature to stratify HGGs (Grade III and Grade IV astrocytoma) into subclasses named proneural, mesenchymal, and proliferative, relating PN and MES to favorable and poor outcome, respectively[42]. In addition, subsequent analysis of TCGA expression profile revealed four glioblastoma subtypes termed as proneural (PN), neural (NE), classical (CL), and mesenchymal (MES)[43]. After distinguishing glioblastoma specific mRNAs from those associated with nontumor cells, glioblastoma subtypes were revisited as proneural, classical, and mesenchymal[44]. Furthermore, epigenetic analysis of TCGA samples identified that a subset of tumor samples harbor promoter DNA

hypermethylation at several loci, revealing a CpG island methylator phenotype (G-CIMP). G-CIMP+ samples display similar gene expression profile with proneural tumors and are highly associated with secondary and recurrent tumors. Besides, a vast majority of G-CIMP tumors contain IDH1 mutations and have better prognosis, making G-CIMP as a discrete subset of human gliomas[22].

1.3.2 Heterogeneity

Tumor heterogeneity describes the genetic, epigenetic, transcriptomic, and phenotypic differences between cancer cells within a single tumor and between tumors from different patients. Tumor heterogeneity can be divided into two categories, namely intratumoral heterogeneity and intertumoral heterogeneity.

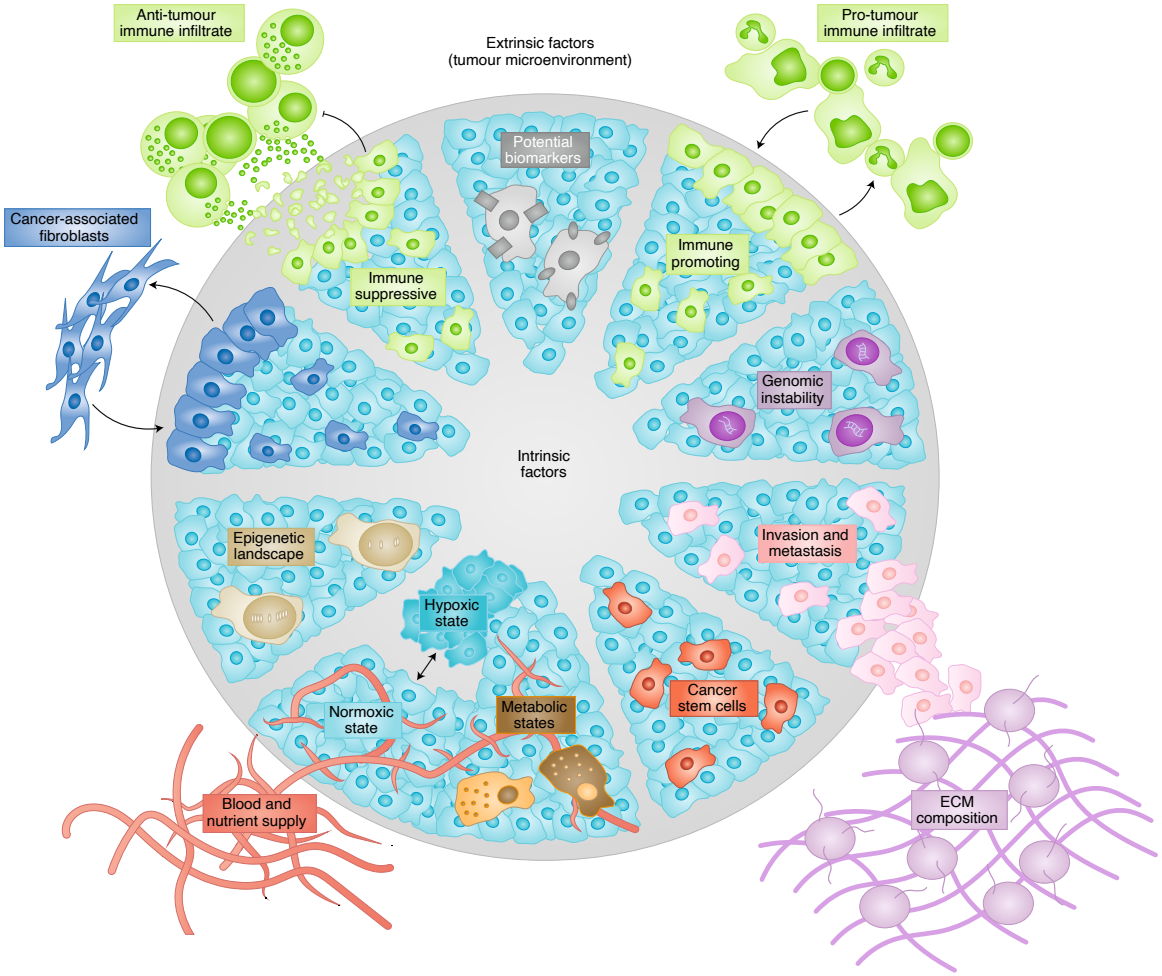

Figure 3. Intrinsic and extrinsic factors that regulate tumor heterogeneity

Tumors contain heterogenous cell populations that are regulated by both intrinsic and extrinsic factors. Intrinsic factors (epigenetic landscape, hypoxic/metabolic states, genomic instability, invasion potential and biomarker expression) and extrinsic factors (immune filtration, vascular density, ECM composition and types of surrounding cells) may contribute to the tumor heterogeneity. Figure taken from Lawson et al., 2018[45]

While intratumoral heterogeneity refers to heterogeneity between the tumor cells of an individual patient, intertumoral heterogeneity describes the differences between tumors of the same histological type in different patients. Overall, tumor heterogeneity is considered as one of the major causes of treatment failure and therapy resistance, revealing the importance of developing more efficient individualized therapies[46,47].

Tumor heterogeneity is generated through cell-intrinsic and cell-extrinsic driving forces such as genomic instability, alterations in gene expression, clonal evolution/selection of tumor cells, epigenetic changes, and tumor microenvironment (**Figure 3**)[45]. Genomic instability might result from aberrations in DNA replication, DNA repair, telomere maintenance, chromosome segregation, and oxidative stress and is one of the most extensively investigated intrinsic driving force of intratumoral heterogeneity[48]. However, genomic instability alone is not sufficient to develop tumor heterogeneity and promote tumorigenesis. Clonal diversity is generated by acquisition of mutations, which confer a proliferative and/or survival advantage to new clones, allowing them to outcompete ancestral clones[47].

Glioblastoma is an extremely aggressive tumor showing high degree of intra- and inter-tumoral heterogeneity. The exceedingly heterogeneous nature of glioblastoma creates a major challenge to implement better treatment strategies. A study by Patel et al. showed that, using single-cell transcriptome analysis by RNA-sequencing (scRNA-seq), individual glioblastoma cells have heterogenous gene expression profiles and correspond to different glioblastoma subtypes[49]. In addition, given that most glioblastomas harbor receptor tyrosine kinase (RTK) amplification, two commonly amplified RTK genes EGFR and PDGFRA were detected in variable proportions among cells from the same tumor specimen, showing a mutually exclusive pattern of amplification in the majority of the cells[50]. With the help of single cell whole-genome sequencing, the existence of EGFR mutation variants has also been revealed in mutually exclusive clones in a single glioblastoma tumor[51].

The genomic and transcriptomic results have been extended by functional studies revealing that single cell clones established from a fresh tumor specimen have distinct characteristics of differentiation, proliferation and tumorigenicity and exhibit differential response to chemotherapeutics. Importantly, drug screening in treatment-naïve single cell-clones showed the pre-existence of TMZ-resistant cells in primary glioblastomas, paving the way for the development of clone-specific treatment strategies[52].

In addition to extensive intratumoral heterogeneity of primary glioblastomas, recurrent glioblastomas also exhibit a high degree of intratumoral heterogeneity, making the successful treatment of the disease unlikely. Whole-genome and exome sequencing studies of primary tumors and matched recurrences shows that while some recurrences harbor the mutations detected in primary glioblastoma, many other recurrences possess a different set of mutations not present in the matching primary tumors, which suggests both clonal and ancestral origins of glioblastoma recurrence[53]. Furthermore, spatiotemporal evolution of glioblastoma was unveiled by revealing that distally recurred tumors retained a minority of

initial mutations, whereas locally recurred tumors maintained a majority of initial mutations, further indicating divergent and linear evolution of recurrence, respectively[54].

1.3.3 Treatment

The current treatment of newly diagnosed glioblastoma consists of maximal surgical resection followed by radiotherapy with concomitant and adjuvant temozolomide (a DNA alkylating agent) chemotherapy. Radiotherapy is the integral part of glioblastoma treatment for years, with an unquestionable survival benefit[55]. Additionally, Stupp et al. showed that concomitant treatment of newly diagnosed glioblastoma with temozolomide and radiotherapy improved the median survival from 12.1 months to 14.6 months as compared to radiotherapy alone[56,57]. Besides, an increased efficacy of temozolomide was revealed in patients with glioblastoma with MGMT (O6-methylguanine–DNA methyltransferase) promotor methylation[18,58]. On the other hand, the treatment regimen for recurrent glioblastoma is not well established and clinical decisions are made by considering previous treatments, tumor size, age, and patterns of relapse. Treatment of recurrent glioblastoma may include second surgery, reirradiation, and monotherapy/combination therapy of temozolomide, bevacizumab and nitrosoureas[59,60].

1.4 Extracellular Vesicles

Extracellular vesicles (EVs) are lipid bilayer structures released by various cell types and include many different membranous structures. Extracellular vesicles can now be broadly classified into two categories, namely exosomes and microvesicles (ectosomes/microparticles)[61]. The invagination of the endosomal membrane leads to the formation of intraluminal vesicles (ILVs), resulting in a cell compartment called a multivesicular body (MVB)[62]. Extracellular vesicles released upon fusion of MVBs with the plasma membrane are referred as exosomes and range in size from 50-150 nm[63].

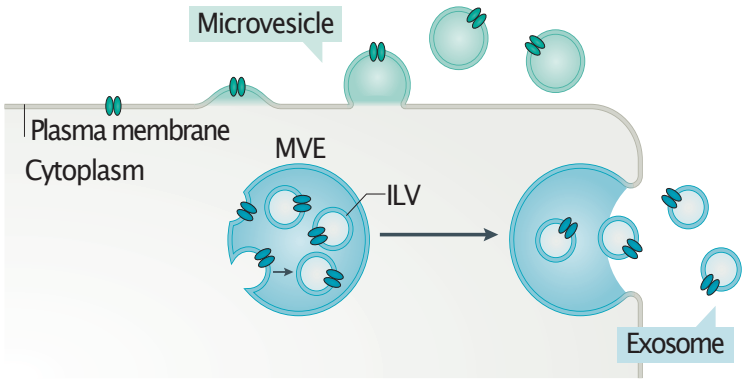

Figure 4. Extracellular vesicles are broadly classified into exosomes (small EVs) and microvesicles (ectosomes)

Microvesicles are extracellular vesicles generated by outward budding of plasma membrane, while exosomes are the ones generated through the endocytic pathway. Figure taken from Niel et al., 2018[63]

Exosomes are highly heterogenous due to their varying sizes, composition, cellular origin and functional impact on recipient cells, which makes them an interesting biological structure for the cell-to-cell communication[64], cellular homeostasis[65] and disease progression[66]. Other types of extracellular vesicles are generated by the outward budding of plasma membrane and classified as ectosomes, microvesicles,

oncosomes, microparticles and apoptotic bodies. These types of vesicles range in the size from 50 nm to 5000 nm[67] (**Figure 4**).

Extracellular vesicles can carry various biomolecules such as proteins, lipids, nucleic acids and metabolites to regulate several biological processes including gene transcription, survival and proliferation, angiogenesis, cellular waste disposal, immune response, cell differentiation, migration and metabolic reprogramming[68].

1.4.1 The Biogenesis of Extracellular vesicles

The biogenesis of extracellular vesicles covers several machineries including endosomal sorting complex required for transport (ESCRT), sphingomyelinase-generated ceramides, lipid flipping, tetraspanins and depolymerization of the actin cytoskeleton. Although some extracellular budding mechanisms have been revealed specifically in exosome or ectosome generation, they may take part in the biogenesis of both types of extracellular vesicles[67,69].

The biogenesis of exosomes is initiated by the inward budding of endosomal membrane, which results in the formation of intraluminal vesicles (ILVs) and ultimately multivesicular bodies (MVBs). Several proteins and protein complexes are involved in the biogenesis of exosomes. From those, ESCRT-0 complex, together with ESCRT-I complex, recognizes the ubiquitylated transmembrane cargoes in the endosomal membrane and recruits ESCRT-III complex, which is necessary for the scission of ILVs (future exosomes) into MVB lumen[70]. Moreover, syntenin and ESCRT accessory protein ALIX (ALG-2 interacting protein-X) have been identified as important regulators of exosome biogenesis due to their bridging role between cargoes and the ESCRT-III subunit VPS32 (Vacuolar protein sorting-associated protein 32)[71]. On the other hand, the existence of ESCRT-independent mechanisms of exosome formation was revealed by the inactivation of key subunits of four ESCRT complexes (ESCRT-0, I, II, and III)[72]. Neutral type sphingomyelinase (nSMase) hydrolyses sphingomyelin to ceramide, resulting in the formation of membrane microdomains, which triggers domain-induced budding[73,74]. In addition to sphingomyelinase-mediated exosome generation, tetraspanin family proteins (i.e., CD63, CD9, CD81, CD82) have also been shown to modulate ESCRT-independent exosome production by sorting cargo molecules to exosomes and forming membrane microdomains that will eventually bud. Additional molecular players such as chaperons heat shock 70 kDa protein (HSP70) and heat shock cognate 71 kDa protein (HSC70) have also been identified in the transfer of cytosolic proteins to ILVs (**Figure 5**).

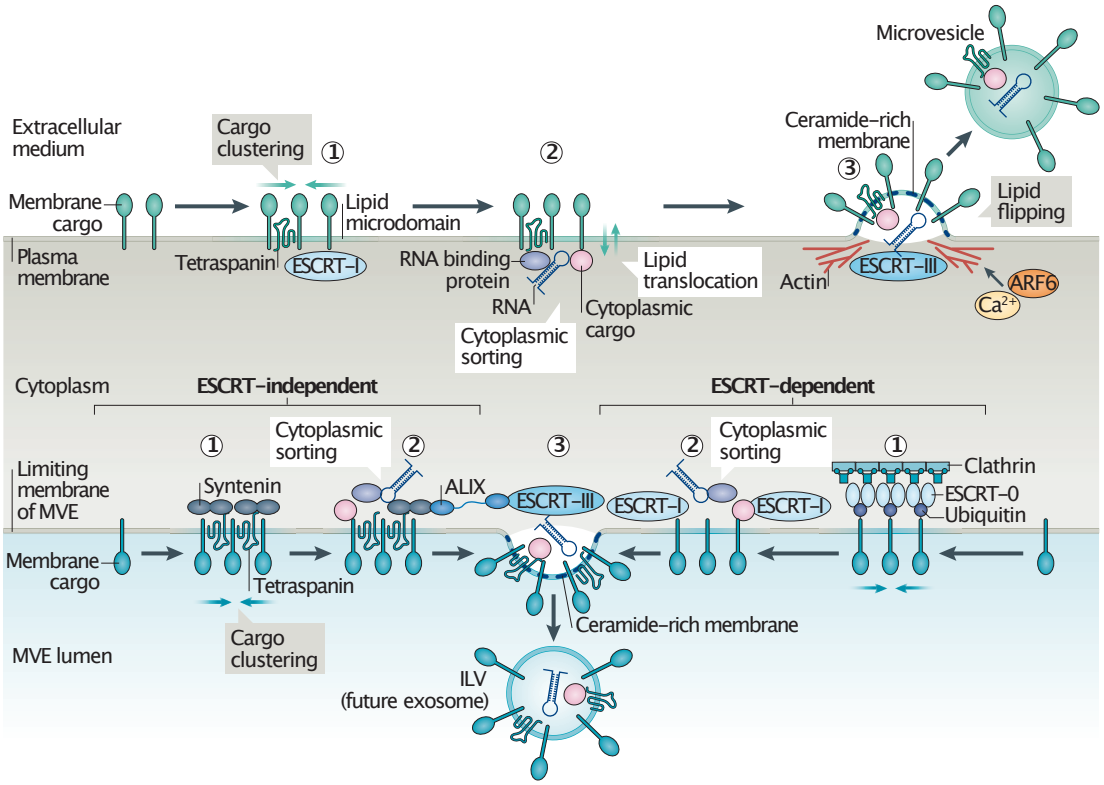

Figure 5. Biogenesis of extracellular vesicles

Several sorting machineries take part in the different steps of the biogenesis of microvesicles (top) and exosomes (bottom). Clustering of lipids and membrane-associated proteins (1), sorting and recruitment of soluble cargos (2) and membrane budding towards the extracellular space/the lumen of the multivesicular endosome (MVE) (3) are the main steps required for the biogenesis of microvesicles and exosomes. Figure taken from Niel et al., 2018[63]

1.4.2 The Secretion of Extracellular vesicles

The Rab family of small guanosine triphosphatases (GTPases) regulates many intracellular transport pathways by transferring vesicles from one intracellular compartment to another. In humans, a wide range of Rab proteins have been identified, and their roles in orchestrating the biogenesis, transport, docking and fusion of vesicles have been elucidated[75,76]. RNA interference (RNAi)-based screening revealed that the perturbation of Rab proteins, namely Rab2b, Rab5a, Rab9a, Rab27a and Rab27b, blocked exosome secretion without disrupting the secretion of soluble proteins[77]. In addition, it has been discovered that, by comparing wild-type and active mutant, another Rab family member Rab11a facilitates the homotypic fusion of multivesicular bodies (MVBs) in the presence of Ca^{+}, which is critical for the exosome biogenesis and secretion[78,79]. Besides, the inhibition of Rab35 function in oligodendroglial cells by siRNA knockdown or transfection with dominant-negative mutant ($Rab35^{N120I}$) resulted in reduced exosome release, suggesting its crucial role in exosome secretion in the central nervous system[80].

In addition to active role of Rab family proteins in vesicular trafficking and release, SNAREs (soluble N-ethylmaleimide-sensitive fusion attachment protein receptors) mediate the fusion of MVBs with the plasma membrane by generating SNARE complexes, thus releasing the vesicular cargo into surrounding environment. SNARE proteins such as YKT6[81,82], Syntaxin-1a[83] and Syntaxin-5[84] have been involved in exosome secretion in different organisms, including *Drosophila, Caenorhabditis elegans* and humans. Besides, the inhibition of another SNARE proteins SNAP-23 (synaptosomal-associated protein 23) and Syntaxin-4 decrease the MVB-PM fusion rate in HeLa cells, supporting the role of SNAREs in exosome release and tumorigenesis[85,86].

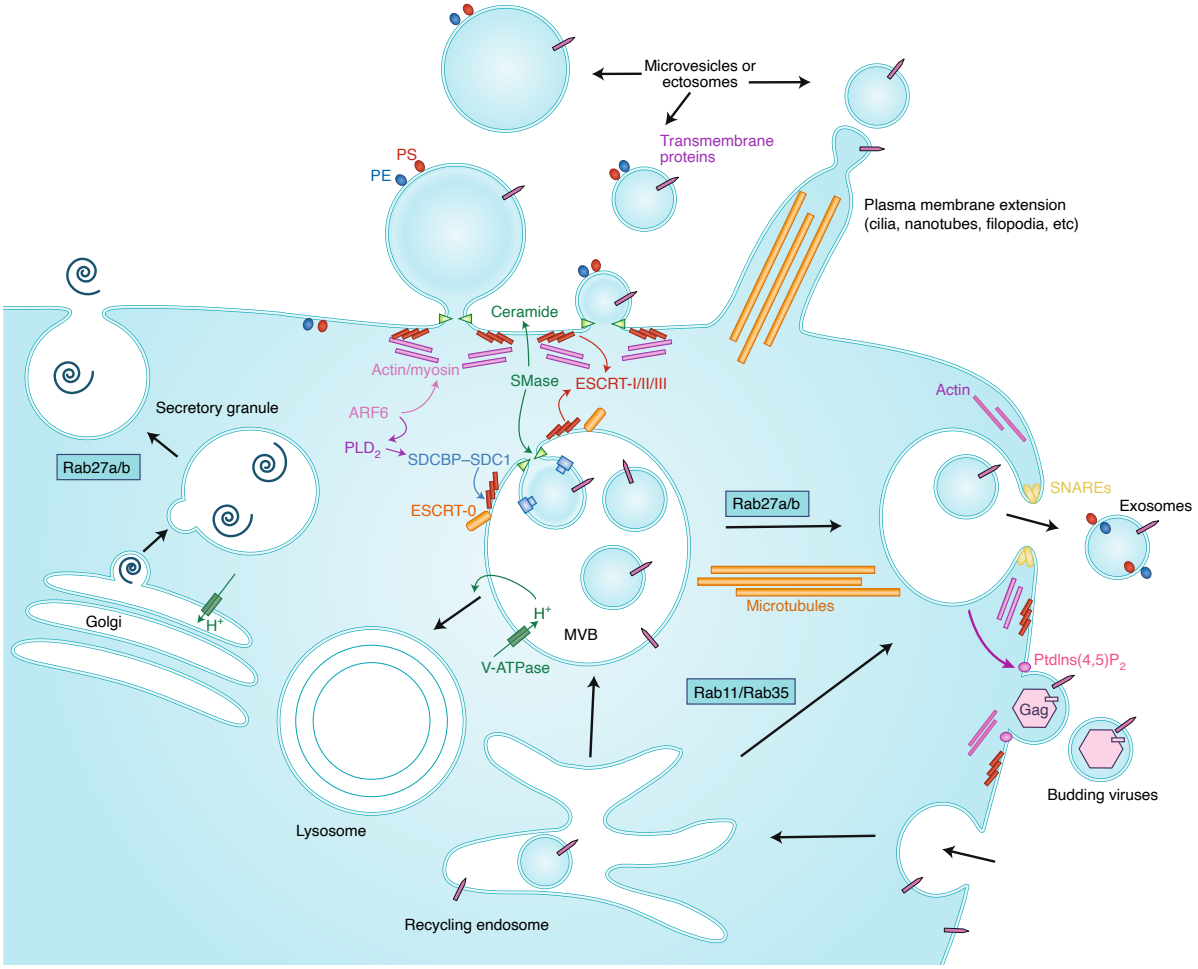

Figure 6. The secretion of extracellular vesicles

Intracellular molecular machineries are involved in the secretion of microvesicles and exosomes. Rab proteins facilitate the MVB-dependent secretion of exosomes. Ceramide (formed by SMAses) and ESCRT proteins are required for the formation of vesicles at the plasma membrane or inside MVBs. Actin depolymerization and ARF6 promote the secretion of microvesicles and exosomes. SNAREs are required for the fusion of MVBs with plasma membrane. Figure taken from Mathieu et al., 2019[64].

Cytoskeleton proteins, together with Rab GTPases and SNAREs, are also essential for the budding and release of extracellular vesicles from the plasma membrane. Once loaded with cargo, microvesicles are pinched of the plasma membrane via actin polymerization followed by acto-myosin contraction[87]. Moreover, microtubules and motor proteins (mainly kinesins and dyneins) are crucial for the spatial distribution of endocytic compartments, and the transport of MVBs to the plasma membrane is facilitated by this complex cytoskeleton network formed by microtubules, actin filaments and motor proteins[88]. **Figure 6** summarizes the molecular machineries playing a role in the secretion extracellular vesicles.

1.4.3 The uptake of Extracellular Vesicles

Extracellular vesicles are delivered to recipient cells with the help of specific molecular interactions incorporating membrane-bound sugars, lipids, and proteins, or through unspecific mechanisms such as micropinocytosis and macropinocytosis[63,89]. In direct route of cargo delivery, EVs fuse with the plasma membrane of the recipient cells and release their content directly into the cytosol. The binding of extracellular vesicles to acceptor cells is coordinated by several mediators including integrins, lectins, proteoglycans, tetraspanins and extracellular matrix (ECM) components.

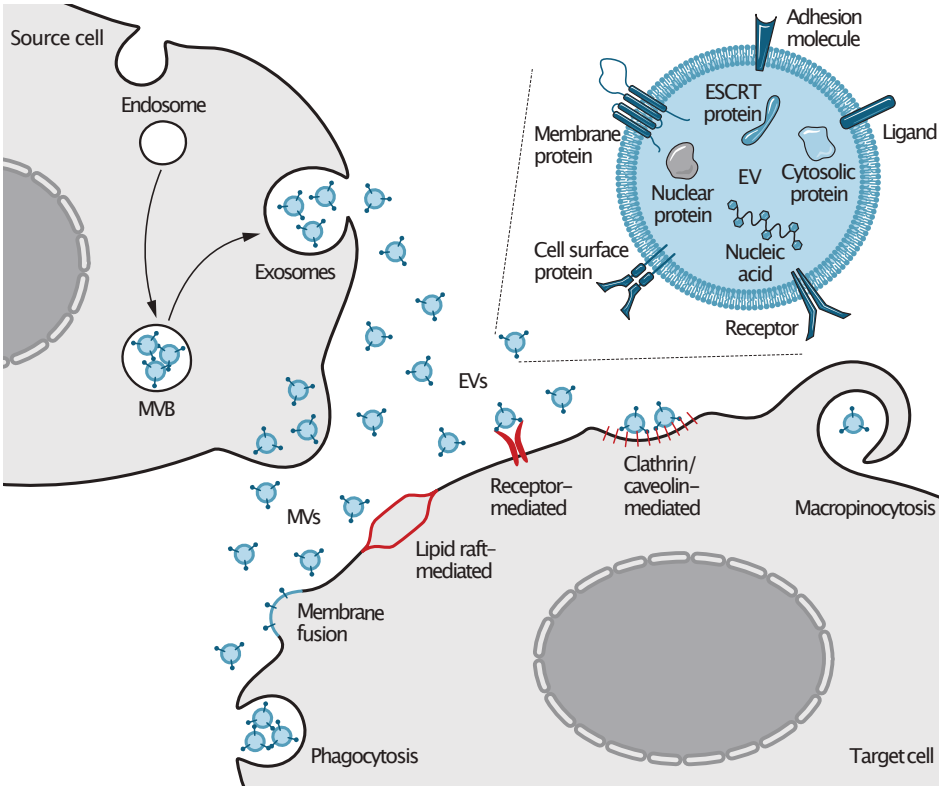

Figure 7. Mechanisms of extracellular vesicle uptake

Extracellular vesicles are internalized by different mechanisms including phagocytosis, membrane fusion, lipid raft-mediated endocytosis, clathrin/caveolin-mediated endocytosis, macropinocytosis, and receptor-mediated endocytosis. Figure taken from Wiklander et al., 2019[90]

Integrins located on the surface of extracellular vesicles can interact with adhesion molecules (i.e., intercellular adhesion molecules, ICAMs) and extracellular matrix proteins (fibronectin and laminin) to initiate the binding of extracellular vesicles to recipient cells[91–94]. Moreover, heparan sulfate proteoglycans (Glypican 1) and cell surface glycoproteins (CD44) have also been shown to be involved in docking and uptake of exosomes[95] and microvesicles[96], respectively. In addition, lipid rafts, which are membrane microdomains that are highly enriched in cholesterol and glycosphingolipids, are also involve in both clathrin- and caveolin-mediated endocytosis of extracellular vesicles[97,98]. On the other hand, the indirect route of EV uptake involves the docking, internalization and targeting of vesicles to endosomes. Internalized extracellular vesicles are either targeted for lysosomal degradation or recycled in the extracellular space. Alternatively, internalized EVs might escape from endosome and deliver their intraluminal cargo into the cytosol of the recipient cells[99].

1.5 Sources of Tumor Heterogeneity and Therapy Resistance

1.5.1 Glioblastoma Stem Cells (GSCs)

Cancer stem cells (CSCs) are a subpopulation of cells within tumors, which have self-renewal and differentiation capabilities similar to those of normal stem cells[100]. Singh et al. for the first time showed the existence of $CD133^+$ glioblastoma stem cells (GSCs) with the ability of initiating tumor growth *in vivo*. A small number of $CD133^+$ cells (100 cells) were sufficient to initiate tumor formation in immunodeficient mice, whereas injection of 10^5 $CD133^-$ did not form any tumor, supporting the hypothesis that only a certain fraction of tumor cells can recapitulate the original tumor[101].

It has been revealed that the ablation of GSCs rendered glioblastomas susceptible to temozolomide, impeded tumor growth and prolonged survival in glioblastoma mouse model[102]. Likewise, Liau et al. uncovered that GSCs can evade anti-proliferative therapies by reorganizing their chromatin through H3K27 demethylases KDM6A/B and by upregulating Notch pathway genes, supporting the pivotal role of GSCs in promoting tumor malignancy, therapy resistance and disease recurrence[103]. In addition to their role in drug resistance, GSCs can also promote radioresistance by increasing DNA repair capacity via activation of the DNA damage response. Ionizing radiation (IR) treatment of glioblastoma cultures and xenografts increased the fraction of $CD133^+$ cells (glioblastoma stem cells), which evaded radiation-induced apoptosis by increasing activating phosphorylation of Chk1 and Chk2 checkpoint proteins, allowing for more efficient repair of DNA damage[104]. Radioresistance of glioblastoma stem cells is also mediated by Notch signaling, which is preferentially activated to maintain the stemness properties of these cells and is promoted by activation of the PI3K/Akt pathway and increased expression of prosurvival protein Mcl-1[105].

In addition to their stunning ability to develop protective adaptation mechanisms in response to treatments, already existing aberrant chromatin state of GSCs might also confer them the ability to

escape from chemo and/or radiotherapy rapidly. The chromatin profiling and transcriptional network analysis indicated that compared to normal astrocytes, GSCs show widespread loss of repressive histone marks and promiscuous activation of transcription factor networks, making them highly flexible to develop alternative pathways in response to therapy[106]. Besides their transcriptional flexibility, GSCs are also more flexible in using different metabolic pathways than differentiated glioblastoma cells. Although Warburg et al. first described that majority of cancer cells preferentially use less efficient aerobic glycolysis rather than oxidative phosphorylation, GSCs can switch between aerobic glycolysis and oxidative phosphorylation as they express both pyruvate kinase isozyme 2 (PKM2) and both pyruvate kinase isozyme 1 (PKM1), which are associated with aerobic glycolysis and oxidative phosphorylation, respectively[107].

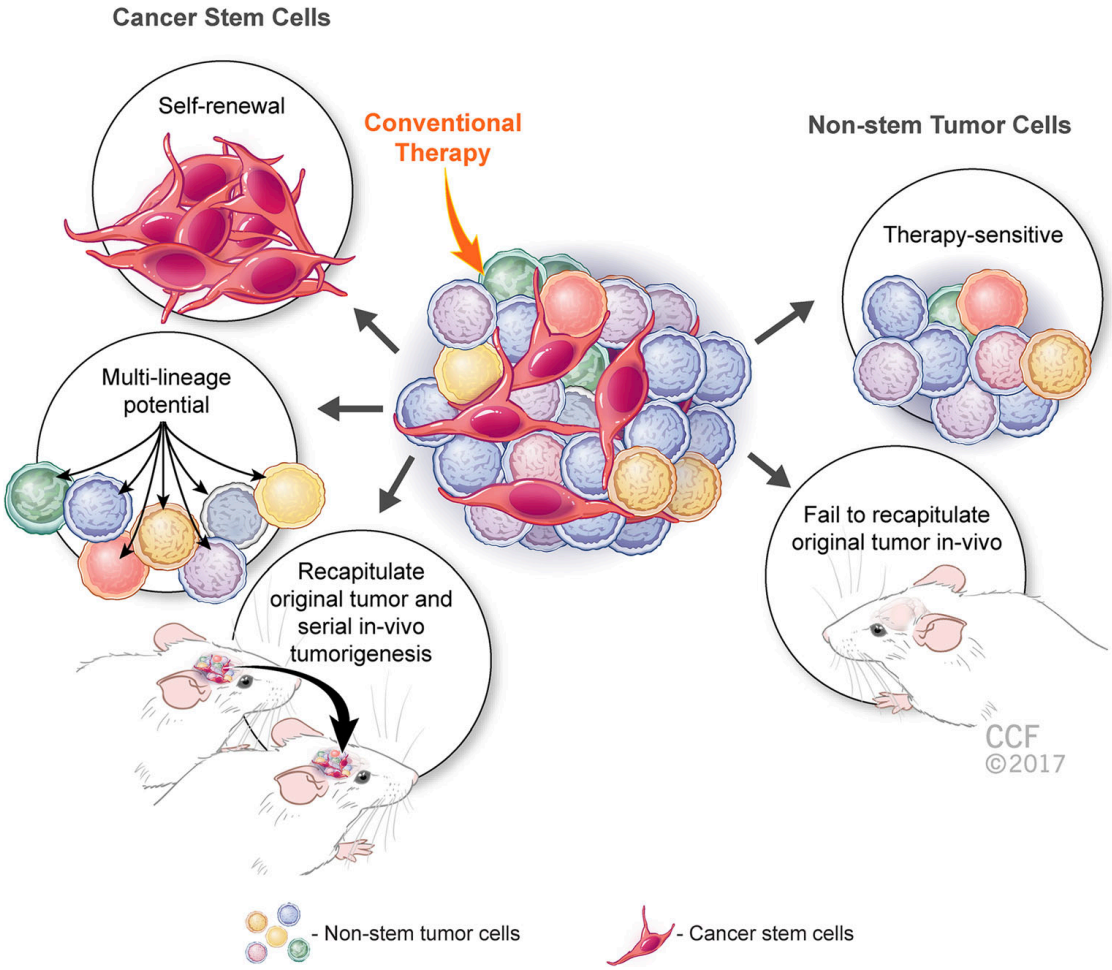

Figure 8. Scheme describing the functional characteristics of cancer stem cells (CSCs)

Cancer stem cells (CSCs) have an ability to self-renew, differentiate into different lineages, and recapitulate original tumor. Non-stem tumor cells are unable to recapitulate the original tumor and are generally more sensitive to therapy. Figure taken from Abou-Antoun et al., 2017[108]

1.5.2 Cancer Cell Plasticity

Cellular plasticity describes the ability of cells to switch between different phenotypic states and is required for proper cell function, normal development, and regeneration. However, cancer cells have ability to hijack these biological processes to evolve towards phenotypically plastic state, which allows them to develop therapeutic resistance (**Figure 9**)[109,110].

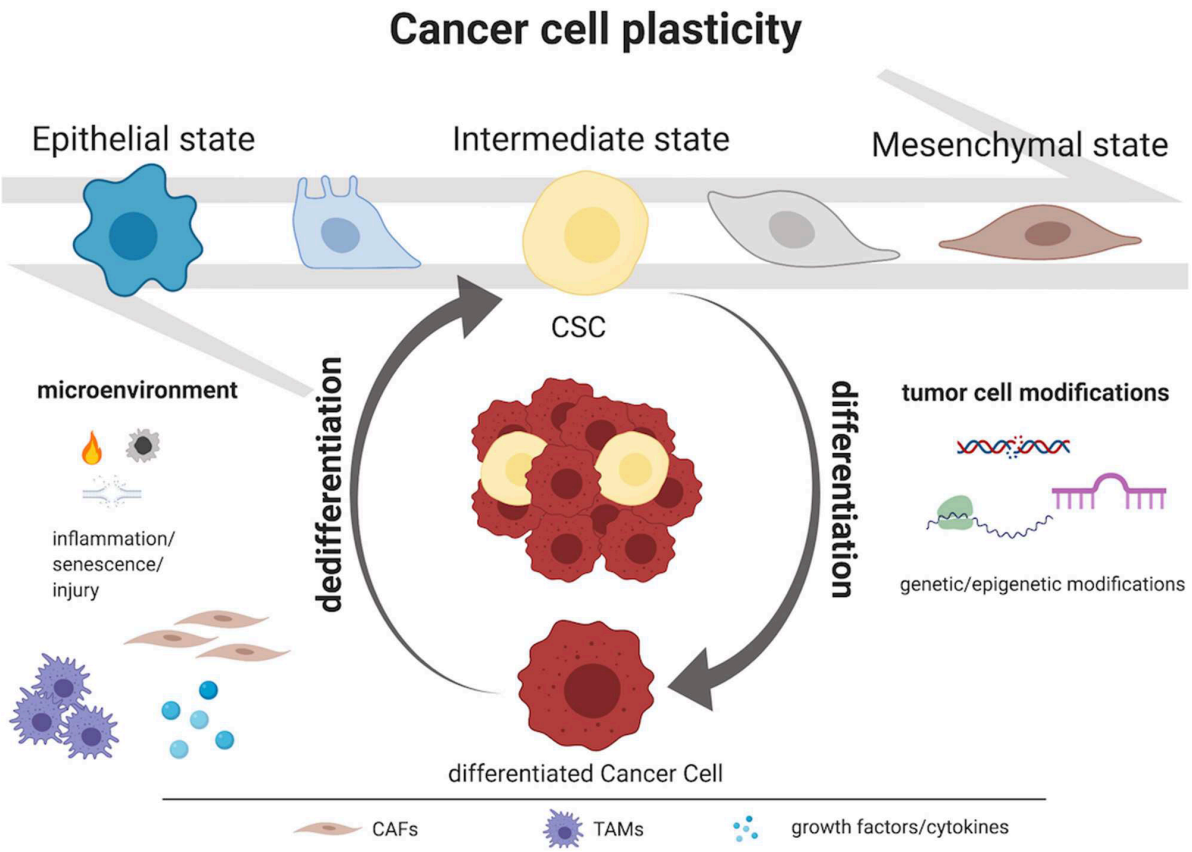

Figure 9. Mechanisms driving cancer stem cell plasticity

Genetic/epigenetic modifications, microenvironmental stresses (such as inflammation, senescence, and injury), and epithelial-to-mesenchymal transition (EMT) program are the main driving forces of cancer cell plasticity. In addition to genetic/epigenetic modifications, signals transmitted by the tumor microenvironment (CAFs, TAMs, cytokines, and growth factors) also support the plasticity of cancer cells. Figure taken from Fanelli et al., 2020[109].

The epithelial-to-mesenchymal transition (EMT) is one of the best characterized mechanisms of phenotypic switching that cancer cells exploit to acquire resistance to therapy and develop disease recurrence[110]. The inhibition/downregulation of apoptotic pathways, decrease in cancer stem cell proliferation rate, enhanced drug efflux capacity, promoted immune evasion, and increased protection against molecular targeted agents are the most prevalent therapy resistance mechanisms conferred by EMT[111]. Accordingly, several studies have postulated that increased expression of EMT markers is associated with promoted migration and increased proliferation of glioblastoma cells[112–114].

Cancer cell can also switch between a drug-sensitive proliferative state and a drug-tolerant state when they are exposed to drugs. These drug-tolerant persisters (DTP) have been identified in different cancer entities including non- small-cell lung cancer (NSCLC)[115], melanoma[116], colon cancer[117] and glioblastoma[103]. DTPs could generate drug-sensitive cells once the drug was discontinued, suggesting that drug-resistant state is transient rather than genetic inheritance, and that DTPs are not a pre-existing cell population but rather originate from a dynamically fluctuating cell population. For instance, Liau et al. nicely showed that GSCs can reversibly transition between naïve, receptor tyrosine kinase (RTK) sensitive state and persister-like state upon RTK inhibitor treatment by reorganizing their chromatin with H3K27 demethylases KDM6A/B[103].

Taken together, these data suggest that cancer cells are phenotypically plastic and capable of exploiting various biological processes to render themselves more aggressive and resistant to therapy.

1.5.3 Spatial Heterogeneity

Glioblastoma is a very aggressive and lethal type of brain tumor that shows high degree of intratumoral and intertumoral heterogeneity, making it extremely difficult to eradicate. In addition to above mentioned factors, emerging evidence revealed that spatial distribution of the tumor cells also contributes to the intratumoral heterogeneity of glioblastoma. Jin et al. showed by image-guided multiregional glioblastoma sampling followed by expression profiling that glioblastoma cells display distinct transcriptional profiles depending on anatomical regions of the tumors. Interestingly, whereas tumor cells from the peripheral portion of tumor (tumor edge) preferentially express proneural genes (DLL3, OLIG2, ASCL1, CD133), tumor core cells show high expression of mesenchymal genes (CD44, CHI3L1, TIMP1, TGFB1). On the other hand, intermediate tumor regions exhibit a mixed transcriptional profile associated with proneural and classical gene expression[118]. Similarly, Bastola et al. also showed a distinct molecular signature of tumor core and edge cells, and that tumor core cells promoted the malignancy and irradiation resistance of the edge cells in a HDAC-CD109 dependent manner[119].

In addition to its role in creating distinct transcriptional profiles within the tumor, anatomical distribution of glioblastoma cells, together with their phenotypic plasticity, also contribute to the aggressiveness and therapy resistance of glioblastoma. Minata et al. demonstrated that invading edge and tumor core harbor

distinct type of GSCs resembling proneural and mesenchymal subtypes, respectively, and that CD133 expressing invasive edge cells start expressing CD109 mesenchymal surface marker in a C/EBP-β-dependent manner in response to ionizing radiation. Subsequently, increased expression of CD109 enhances the oncogenic signaling, which confers promoted clonogenicity and radioresistance to the cells[120].

Finally, Puchalski et al. also revealed the spatial heterogeneity of glioblastoma by creating an anatomic transcriptional atlas of human glioblastoma using in situ hybridization (ISH), laser microdissection (LMD) and RNA sequencing (RNA-seq). They first established the tumor's anatomic features as leading edge (LE), infiltrating tumor (IT), cellular tumor (CT), pseudopalisading cells around necrosis (PAN), and microvascular proliferation (MVP), and nicely presented their gene expression profiles together with the genomic alterations[121]. Taken together, all these studies suggest that anatomically distinct glioblastoma cell populations show distinct transcriptional patterns, inevitably interact with each other, contribute to the intratumoral heterogeneity and therapy resistance.

1.6 Cell-to-Cell Communications

1.6.1 Secreted Factors

Various biological molecules, including cytokines, chemokines, and growth factors, take part in the communication of tumor cells with each other and with the cells from tumor microenvironment. Cytokines and chemokines are intercellular signaling proteins released in response to cellular stresses, infection, and inflammation. These secreted signaling proteins suppress tumor formation by stimulating a host response to minimize the cellular stress and damage. However, tumor cells exploit host-derived cytokines and chemokines to favor their growth, viability, and metastasis. Many cytokines such as IL-1, IL-6, IL-12, IL-15, IFN-γ, M-CSF, GM-CSF, TNF-α, MIF and TGF-β have been shown to associated with the pathogenesis of different cancer types including melanoma, lymphoma, sarcoma, leukemia, breast, skin, and colon[122,123].

1.6.2 Extracellular Vesicles

Tumor cells have a striking ability to mold their environment through extracellular vesicles to facilitate their growth, resistance, immune evasion, and metastasis. For instance, glioblastoma cells can stimulate tubule formation by delivering mRNA, miRNA and angiogenic proteins to surrounding endothelial cells by means of microvesicles, resulting in increased angiogenesis and malignancy[124]. In addition, glioblastoma cells can exchange oncogenic proteins such as epidermal growth factor receptor variant III (EGFRvIII), conferring growth advantage and increased invasiveness[125]. In addition to their role in tumor cell proliferation and invasiveness, glioblastoma-derived EVs could also mediate the immune evasion of tumor cells by inhibiting the T cell activation through PD-L1 dependent mechanism[126].

Extracellular vesicles have also been involved in critical processes associated with cell migration and invasion[127]. EVs secreted from highly metastatic human mammary tumor cells enhanced the migration of less malignant tumor cells that internalized these vesicles, supporting that EV-mediated transfer of biomolecules could convey tumor supporting phenotype to recipient cells[128]. Moreover, in orthotopic mouse models of breast cancer, it has been shown that mouse fibroblast L cells-derived exosomes harbor Wnt11 and that the internalization of Wnt11 loaded exosomes by breast cancer cells induced their motility and metastasis by modulating Wnt/Planar cell polarity (PCP) signaling[129]. Besides, exosomal integrins and fibronectins can stimulate migration, invasion and metastasis of cancer cells and determine organ-specific metastasis[94,130]. Finally, matrix metalloproteinases (MMPs) delivered by extracellular vesicles can remodel surrounding tissues by degrading the extracellular matrix (ECM), supporting the invasion and migration of cancer cells[131–134].

The tumor microenvironment consists of numerous cell types, including fibroblasts, endothelial cells, pericytes, and infiltrating immune cells, as well as microglia, astrocytes, lymphocytes, dendritic cells, neutrophils, and infiltrating macrophages in the brain. The pivotal role of growth factors, chemokines, cytokines, and small molecules in tumor cell-to-cell communication has been widely shown in various cancer entities. In recent years, a great number of studies have also revealed that EVs take essential part in cell-to-cell communication in the tumor microenvironment[135–137]. For instance, oncogenic EGFF can be transferred via microvesicles to endothelial cells and activates MAPK and Akt signaling pathways followed by increased expression of VEGF[138]. Moreover, it has been shown that exosomes secreted by hypoxic glioblastoma cells can induce angiogenesis and enhance tumor growth by modulating endothelial cells via transferring hypoxia-regulated mRNAs and proteins, which results in the activation of the ERK1/2 MAPK, PI3K/AKT, and FAK pathways[139]. Besides, prostate cancer EVs can transfer transforming growth factor beta 1 (TGF-b1) to fibroblasts and induce their differentiation to myofibroblasts, facilitating angiogenesis and tumor growth[140].

The tumor microenvironment harbors a variety of immune cells; however, their ability to kill tumor cells is often inhibited by PD-1 and CTLA-4 signaling. Tumor-associated macrophages (TAMs) are the major immune cells in glioblastoma tumor microenvironment and are often implicated in PD-L1 and CTLA-4-mediated suppression of T cells, NK T cells and NK[137,141]. TAMs can also express TRAIL and FAS ligands and induce caspase-dependent cell death in T cells, resulting in tumor-promoting immunosuppression[142]. Tumor-derived EVs can also promote an immunosuppressive macrophage phenotype as exemplified by glioblastoma secreted EVs, where tumor-supportive monocyte-to-macrophage differentiation takes place upon incubation with these EVs[143]. In addition, it has been revealed that glioblastoma-derived EVs transfer miR-451 and miR-21 to microglia, resulting in the downregulation of *c-Myc* mRNAs followed by changes in the gene expression and shift to tumor supportive phenotype[144].

Moreover, several studies have uncovered that EVs can also serve as pivotal priming factors that facilitate the dissemination of tumor cells to distant organs by creating premetastatic niches[145,146]. For example, melanoma-derived exosomes transfer MET oncoprotein to bone marrow progenitor cells and promote tumor growth and metastasis by educating them toward a pro-vasculogenic and pro-metastatic phenotype[147]. In addition, pancreatic ductal adenocarcinoma-derived exosomes deliver macrophage migration inhibitory factor (MIF) to Kupffer cells, triggering TGF-β production by these cells, which in turn, increase the expression of fibronectin. Afterwards, bone marrow-derived cells such as macrophages and granulocytes migrate to fibronectin-enriched hepatic sites, creating liver pre-metastatic niche for the arrival of metastatic cells[148].

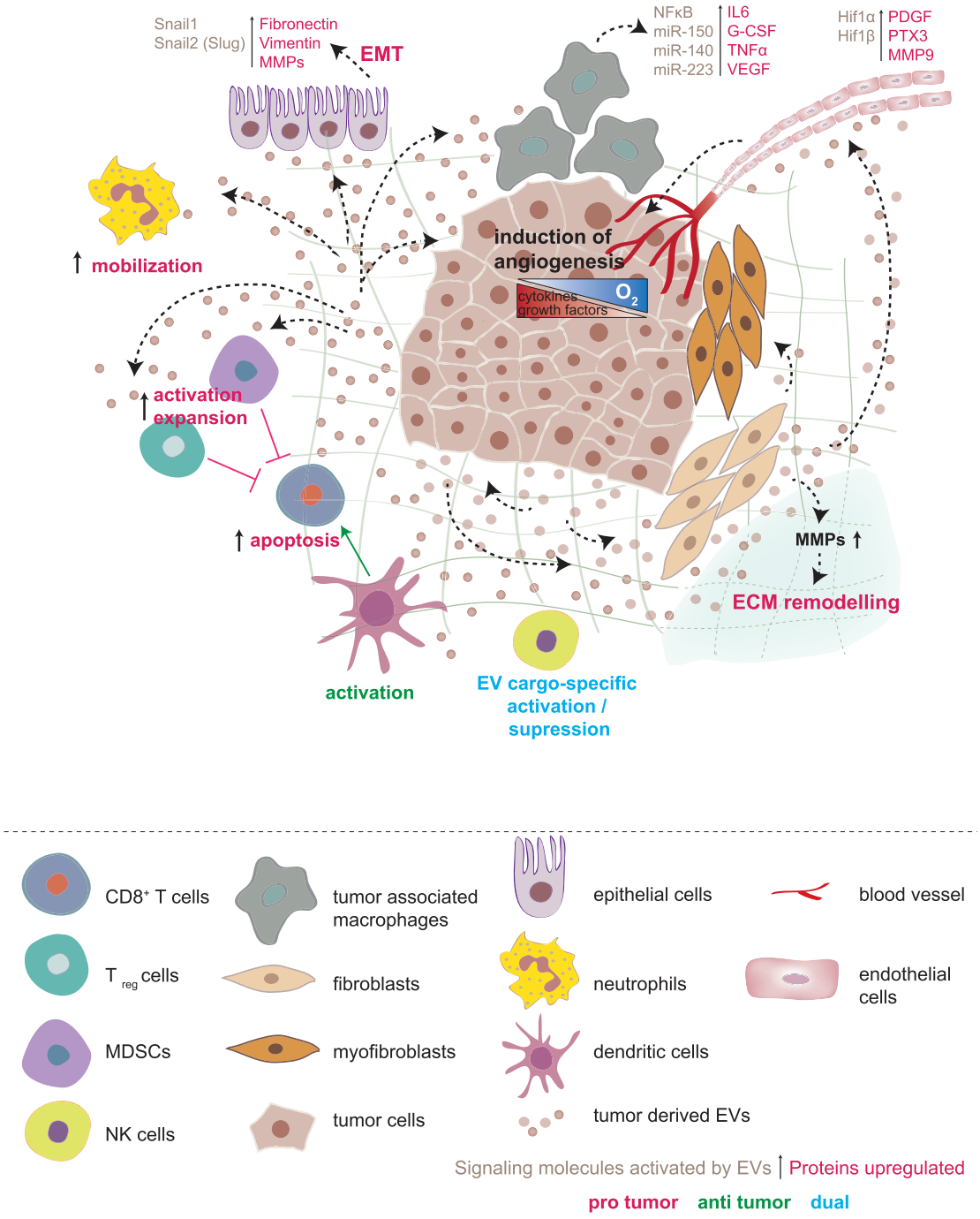

Figure 10. The role of tumor-derived extracellular vesicles in cell-cell communication in the tumor microenvironment

Extracellular vesicles play a crucial role in cell-cell communication between tumor cells and surrounding cells including T cells, tumor associated macrophages (TAMs), epithelial cells, fibroblasts, neutrophils, endothelial cells, myeloid-derived suppressor cells (MDSCs), myofibroblasts, dendritic cells and natural killer (NK) cells. Figure taken from Becker et al., 2016[149]

1.7 Aim of the study

Glioblastoma is the most frequent and aggressive brain tumor accounting for about half of all primary malignant brain tumors. Despite the multimodal aggressive treatments including surgical resection, irradiation, and chemotherapy, the prognosis of glioblastoma remains very poor. The high degree of intratumoral and intertumoral heterogeneity in glioblastoma creates a major hurdle for the complete eradication of the disease. Over the past decades several studies have revealed many cell-intrinsic and cell-extrinsic factors, which contribute to heterogenous, aggressive and lethal nature of glioblastoma, making it extremely difficult to eradicate. From those, the increased ability of glioblastoma cells to communicate with each other and with neighboring stromal cells in their microenvironment is considered as one of the main sources of elevated tumor cell plasticity and heterogeneity in glioblastoma. In this direction, this project mainly focuses on characterizing the content of small extracellular vesicles from different glioblastoma subtypes (namely mesenchymal and proneural) at the proteomic, metabolomic, fatty acid and small-RNA level to better understand their contribution to glioblastoma heterogeneity. To this end, protein, metabolite, fatty acid, and small-RNA contents of sEVs and their respective cell lines were assessed using mass spectrometry and high-throughput sequencing, and potential roles of these biomolecules in glioblastoma heterogeneity, plasticity, and aggressiveness were further investigated.

2. Materials and Methods

2.1 Materials

2.1.1 Antibodies

Antibody	Company	Product Number
Anti-β-Actin	Cell Signaling Technology, Danvers, USA	3700S
Anti-α-Tubulin	Sigma-Aldrich, Munich, Germany	T9026
Anti-human CD133	Biolegend, San Diego, USA	372805
Anti-human CD44	Biolegend, San Diego, USA	338815
APC Mouse IgG1, κ Isotype Ctrl (FC)	Biolegend, San Diego, USA	400121
Brilliant Violet 421™ Rat IgG2a, κ Isotype Ctrl	Biolegend, San Diego, USA	400535
Brilliant Violet 711™ Mouse IgG1, κ isotype Ctrl	Biolegend, San Diego, USA	400167
FITC Mouse IgG1, κ Isotype Ctrl (FC)	Biolegend, San Diego, USA	400109
PE/Cy7 Mouse IgG1, κ isotype Ctrl	Biolegend, San Diego, USA	400125
Anti-RPLP0	Atlas Antibodies, Bromma, Sweden	HPA003512
Anti-Cytochrome c	Biolegend, San Diego, USA	612503
Anti-GM130	Cell Signalling Technology, Danvers, USA	12480
Anti-Lamin B1	Abcam, Cambridge, UK	16048
Anti-Enolase	Abcepta, San Diego, USA	AP6526c
Anti-CD9	Cell Signalling Technology, Danvers, USA	13403
Anti-CD138	Biolegend, San Diego, USA	352301
Anti-mouse IgG, HRP-linked	Cell Signalling Technology, Danvers, USA	7076
Anti-rabbit IgG, HRP-linked	Cell Signalling Technology, Danvers, USA	7074

2.1.2 Buffers and Solutions

Solutions	Composition
1x Phosphate buffered saline (PBS)	137 mM NaCl, 2.7 mM KCl, 9.2 mM Na2HPO4, 1.8 mM KH2 PO4, pH 7.4
1x Transfer buffer	25 mM Tris, 200 mM glycine, 20 % methanol, pH 8.8
1x TRIS buffered saline (TBS)	150 mM NaCl, 10 mM Tris, pH 7.5
1x TRIS-Borat-EDTA (TBE)	0.445 M Tris-Borat, 10 mM EDTA, pH 8
Blocking buffer	5 % milk powder or 5 % BSA in TBS-T
FACS buffer	5 % FCS in PBS
Loading buffer (6x)	30 % Glycerine, 0.25 % Bromophenol blue
EDTA (0.5M)	46.5 g EDTA in 250 ml ddH20, pH 8.0
Tris-HCl (60 nM)	1.9 g Tris-HCl in 250 ml ddH20
Homogenization media (HM)	17.1 g Sucrose (HPLC) 4 ml EDTA (0.05M) 33.3 ml TRIS/HCL (60mM) 162.7 ml ddH20 Adjust pH to 7.4
OptiPrep™ Density Gradient Medium	Sigma-Aldrich, Munich, Germany
Working Solution (WS)	17.1 g Sucrose (HPLC) 24 ml EDTA (0.05M) 1.9 g TRIS/HCL 176 ml ddH20 Adjust pH to 7.4

2.1.3 Bacterial Culture Media

Medium	Composition
LB (Luria-Bertani)	0.5 % (w/v) NaCl, 1 % (w/v) Tryptone, 0.5 % (w/v) Yeast extract
LB Agar	0.5 % (w/v) NaCl, 1 % (w/v) Tryptone, 0.5 % (w/v) Yeast extract, 1.6 % (w/v) Agarose

2.1.4 Biochemicals and Reagents

Substance	Company
Agarose	Sigma-Aldrich, Munich, Germany
Ampicillin	Roche Diagnostics, Mannheim, Germany
Bicinchoninic acid (BCA)	Sigma-Aldrich, Munich, Germany
Bovine serum albumin	New England Biolabs (NEB), Ipswich, USA
Bromophenol blue	Waldeck GmbH, Münster, Germany
Complete mini protease inhibitors	Roche Diagnostics, Mannheim, Germany
cOmplete™, EDTA free protease inhibitor cocktail	Roche Diagnostics, Mannheim, Germany
Dithiotreitol (DTT) (0.1 M)	Thermo Fisher Scientific, Langenselbold, Germany
DNA loading dye (6x)	Thermo Fisher Scientific, Langenselbold, Germany
DNA marker (1kb)	Fermentas, St Leon-Rot, Germany
dNTP mix (100 µM each)	Thermo Fisher Scientific, Langenselbold, Germany
Ethanol	Merck Millipore, Darmstadt, Germany
Ethyl acetate, 99.7 %	Sigma-Aldrich, Buchs SG, Switzerland
Ethylenediaminetetraacetate (EDTA) (25 mM)	Thermo Fisher Scientific, Langenselbold, Germany
Glycerol	Carl Roth, Karlsruhe, Germany
HEPES (1M) pH 7.2-7.6	Corning Inc., Corning, USA
IP lysis buffer	Thermo Fisher Scientific, Langenselbold, Germany
Methanol	Sigma-Aldrich, Munich, Germany
$MgCl_2$ solution (1M)	Sigma-Aldrich, Munich, Germany
Nuclease-free water	Ambion, Austin, USA

NuPAGE® LDS sample buffer (4x)	Life Technologies, Darmstadt, Germany
NuPAGE® SDS running buffer (20x)	Life Technologies, Darmstadt, Germany
Oligo-d(T) nucleotides	Thermo Fisher Scientific, Langenselbold, Germany
PCR nucleotide mix	Roche Diagnostics, Mannheim, Germany
Pierce ECL Western blotting substrate	Thermo Fisher Scientific, Langenselbold, Germany
Random primer mix	New England Biolabs NEB), Ipswich, USA
RIPA-lysis buffer	Sigma-Aldrich, Munich, Germany
RIPA Buffer (10X)	Abcam, Berlin, Germany
Sodium dodecyl sulfate (SDS)	Sigma-Aldrich, Munich, Germany
Sodium fluoride (NaF)	Carl Roth, Karlsruhe, Germany
Sodium orthovanadate (Na3VO4)	Carl Roth, Karlsruhe, Germany
Spectra multicolor broad range protein ladder	Fermentas, St Leon-Rot, Germany
Tris-(hydroxymethyl)-aminomethan (TRIS)	Carl Roth, Karlsruhe, Germany
Triton X-100	Sigma-Aldrich, Munich, Germany
TE Buffer	Qiagen, Hilden, Germany
Tween-20	Sigma-Aldrich, Munich, Germany
Whole milk powder	Carl Roth, Karlsruhe, Germany
Methoxyamine hydrochloride	Sigma-Aldrich, Munich, Germany
Pyridine anhydrous, 99.8%	Sigma-Aldrich, Munich, Germany
N-Methyl-N-trimethylsilyltrifluoracetamid	Sigma-Aldrich, Munich, Germany
Fatty Acid Methyl Ester (FAME) Standards	Sigma-Aldrich, Munich, Germany

2.1.5 Cell Culture Reagents and Materials

Reagent	Company
2-Mercaptoethanol (98 %)	Sigma-Aldrich, Munich, Germany
96-well plates (white, non-binding with clear bottom)	Greiner/Sigma-Aldrich, Munich, Germany
Cell culture flasks (T25, T75, T175)	Sarstedt, Nümbrecht, Germany
Accutase solution	Sigma-Aldrich, Munich, Germany
B-27™ Supplement (50X), minus vitamin A	Thermo Fisher Scientific, Langenselbold, Germany
Cryo tubes	Nunc, Wiesbaden, Germany
Dimethyl sulfoxide (DMSO)	Sigma-Aldrich, Munich, Germany
DMEM (Dulbecco's modified eagle medium)	Sigma-Aldrich, Munich, Germany
DMEM/Ham's F12	Sigma-Aldrich, Munich, Germany
Human Epidermal Growth Factor (EGF) Protein	Thermo Fisher Scientific, Langenselbold, Germany
Heparin sodium salt from porcine intestinal mucosa	Sigma-Aldrich, Munich, Germany
Fibroblast Growth Factor basic	Biomol GmbH, Hamburg, Germany
Fetal calf serum (FCS)	Merck Millipore, Darmstadt, Germany
L-Glutamine	Thermo Fisher Scientific, Langenselbold, Germany
Opti-MEM I reduced serum medium	Thermo Fisher Scientific, Langenselbold, Germany
Phosphate-Buffered Saline (PBS)	Thermo Fisher Scientific, Langenselbold, Germany
Penicillin/Streptomycin (10000 U/ml, 100 µg/ml)	Thermo Fisher Scientific, Langenselbold, Germany
Puromycin	VWR International, Darmstadt, Germany
Reagent reservoirs (sterile)	Corning Inc., Corning, USA
Syringe filters (0.22 µm and 0.45 µm)	Merck Millipore, Darmstadt, Germany

Membrane filter (0.02 µm)	GE Healthcare, Chicago, USA
TransIT®-LT1 transfection reagent	Mirus Bio, Madison, USA
Lipofectamine™ Transfection Reagent	Thermo Fisher Scientific, Langenselbold, Germany
LentiFuge™ Viral Concentration Reagent	Cellecta, Inc., California, USA
Trypsin EDTA solution (0.5 %)	Sigma-Aldrich, Munich, Germany

2.1.6 Cell Lines

Glioblastoma Stem-Like Cell Lines

Cell Line	Sex	Age (Years)	PFS (months)
NCH421k	Male	66	34
NCH711d	Male	20.4	Not available
NCH644	Female	67	30
NCH705	Not available	78	24

Other Cell Lines

Cell Line	Supplier
Human Embryonic Kidney (293T)	ATCC, Wesel, Germany

2.1.7 Bacteria

Cells	Supplier
OneShot ® STABL3 chemically competent E.coli	Thermo Fisher Scientific, Langenselbold, Germany

2.1.8 Databases

Databases	Address
ExoCarta	http://www.exocarta.org/
Vesiclepedia	http://microvesicles.org/

2.1.9 Equipment

Equipment	Company
Biofuge Fresco tabletop centrifuge	Haraeus Instruments, Hanau, Germany
BD LSRFortessa™	BD Biosciences, Heidelberg, Germany
Cytospin3-centrifuge	Thermo Fisher Scientific, Langenselbold, Germany
Heating block QBT	Grant Instruments, Cambridge, UK
Incubator HERA cell 150	Thermo Fisher Scientific, Langenselbold, Germany
L8-M ultracentrifuge	Beckmann Coulter, Krefeld, Germany
Leica TCS SP5 Confocal Microscope	Leica Biosystems, Wetzlar, Germany
Mini Trans-Blot® cell	Bio-Rad, Munich, Germany
Mithras LB 940 plate reader	Berthold Technologies, Bad Wildbad, Germany
NanoDrop®ND-1000 spectrometer	NanoDrop, Wilmington, USA
NanoSight LM10 system	Malvern Instruments, Worcestershire, UK
NextSeq 500 System	Illumina, Inc., San Diego, USA
QuickPoint electrophoresis cell	Novex, San Diego, USA
Qubit 2.0 Fluorometer	Thermo Fisher Scientific, Langenselbold, Germany
Vortex Genie 2	Scientific Industries Inc., New York, USA

Water bath B-480	Buchi AG, Flawil, Switzerland
XCell SureLock™ Mini-Cell electrophoresis system	Thermo Fisher Scientific, Langenselbold, Germany
Eppendorf® Concentrator Plus	Eppendorf, Hamburg, Germany
MPS Autosampler	Gerstel, Mülheim an der Ruhr, Germany
Agilent 7890 GC System	Agilent Technologies, Santa Clara, USA
Pegasus® BT	LECO Corporation, Michigan, USA
Intas Chemostar ECL Imager	Intas, Göttingen, Germany

2.1.10 Kits

Kit	**Company**
ABsolute SYBR® Green ROX mix	Thermo Fisher Scientific, Langenselbold, Germany
Plasmid Maxi/Midi/Mini Kit	Qiagen, Hilden, Germany
Blood & Cell Culture DNA Maxi Kit	Qiagen, Hilden, Germany
Monarch® PCR & DNA Clean-up Kit	New England Biolabs (NEB), Ipswich, USA
Monarch® DNA Gel Extraction Kit	New England Biolabs (NEB), Ipswich, USA
Rapid DNA dephos and ligation kit	Roche Diagnostics, Mannheim, Germany
NucleoSpin miRNA kit	MACHEREY-NAGEL GmbH & Co. KG, Düren, Germany
PKH26 Red Fluorescent Cell Linker Kit	Sigma-Aldrich, Munich, Germany
QIAshredder	Qiagen, Hilden, Germany
Qubit™ Protein Assay Kit	Thermo Fisher Scientific, Langenselbold, Germany
Qubit™ dsDNA HS Assay Kit	Thermo Fisher Scientific, Langenselbold, Germany
Rxi-5Sil MS Columns	Restek, Bellefonte, USA

SMARTer® smRNA-Seq Kit for Illumina®	Takara Bio Europe

2.1.11 Other Material

Article	Supplier
Falcon® 5 mL Round Bottom Polystyrene Test Tube	Corning inc., New York, USA
Falcon® tubes (15 ml and 30 ml)	Corning inc., New York, USA
NuPAGE® antioxidant	Life Technologies, Darmstadt, Germany
NuPAGE™ 4 to 12%, Bis-Tris, 1.0 mm, Mini Protein Gel	Life Technologies, Darmstadt, Germany
PCR tubes (0.2 ml)	Molecular BioProducts, San Diego, USA
Pipette tips (10 µl, 20 µl, 100 µl, 200 µl, 1000 µl)	Starlab, Ahrensburg, Germany
Polyvinylidene fluoride (PVDF) membrane	Sigma Aldrich, Munich, Germany
Reaction tubes (1.5 ml and 2 ml)	Eppendorf, Hamburg, Germany
Qubit™ Assay Tubes	Thermo Fisher Scientific, Langenselbold, Germany
Open-Top Thinwall Polypropylene Tube (38.5 ml)	Beckmann Coulter, Krefeld, Germany
Polyallomer tubes (14 ml)	Laborgeräte Beranek GmbH, Nußloch, Germany

2.1.12 Plasmids

Plasmid	Company
psPAX2	Addgene, Cambridge, USA
pMD2.G	Addgene, Cambridge, USA
pCSCW2-palmGFP	Kindly provided by Prof. Dr. Xandra O. Breakefield (MGH)and Dr. Charles Lai (IAMS)
pCSCW2-palmtdTomato	Kindly provided by Prof. Dr. Xandra O. Breakefield (MGH)and Dr. Charles Lai (IAMS)

2.1.13 Primers

Primers	Sequence
pDONR_FP	TAACGCTAGCATGGATCTC
pDONR_RP	GCAATGTAACATCAGAGAT

2.1.14 Software

Software	Source
Affinity Designer	Serif (Europe) Ltd
Basic Local Alignment Search Tool (BLAST)	blast.ncbi.nlm.nih.gov
GraphPad Prism 7	GraphPad, San Diego, USA
ImageJ	rsbweb.nih.gov/ij
Microsoft Excel/Word for Mac	Microsoft, Redmond, USA
NTA 3.0 software	Malvern Instruments, Worcestershire, UK
RStudio	RStudio, PBC, Boston, USA available at http://www.rstudio.com/
SnapGene software	GSL Biotech, available at http://www.snapgene.com
ChromaTOF Software	LECO Corporation, Michigan, USA available at https://www.leco.com/product/chromatof-software
MetaboAnalyst	https://www.metaboanalyst.ca/

2.2 Methods

The text of Methods section was taken from Lokumcu et al. (manuscript in preparation).

2.2.1 Cell Culture

GSC lines NCH421k, NCH644, NCH705, and NCH711d were established from primary glioblastoma patients undergoing surgery according to the research proposals approved by the Institutional Review Board at the Medical Faculty of Heidelberg.

Glioblastoma stem cells (GSC) were grown on hydrophobic growth surface cell culture flasks (Sarstedt) in Dulbecco's Modified Eagle's Medium/Nutrient Mixture F-12 Ham (Sigma-Aldrich) supplemented with 2% (v/v) B-27 minus Vitamin A (Life Technologies), 20 ng/mL epidermal growth factor (Life Technologies), 20 ng/mL basic fibroblast growth factor (Biomol) and 1 µg/mL heparin (Sigma-Aldrich). GSC neurospheres were dissociated using Accutase (Sigma Aldrich). HEK293 cell line was obtained from American Tissue Culture Collection (ATCC) and grown in DMEM (Life Technologies) supplemented with 10% FBS (Sigma-Aldrich) and 1% (v/v) penicillin/streptomycin (Life Technologies). All cells were cultured in a cell culture incubator at 37°C with 5 % CO2 and 95 % humidity and routinely tested for mycoplasma contamination (GATC Biotech).

2.2.2 Lentivirus production

4 x 10^6 HEK293T cells were plated in 10-cm plates (2 plates per construct) 24 hour prior to transfection. 4 µg of lentiviral packaging plasmids (psPAX2 and pMD2.G) and 8 µg of plasmid of interest (pCSCW2-palmGFP or pCSCW2-palmtdTomato) were mixed in 1200 µl of Opti-MEM I medium. Afterwards, 60 µl of TransIT-LT1 Reagent was added into the diluted DNA mixture and incubated at room temperature for 30 minutes. Subsequently, the cells were co-transfected with TransIT-LT1 Reagent: DNA complex drop-wise and incubated for 48 hours. At 24 hours post-transfection, the medium was replaced with fresh medium containing 10% FBS and 1% (v/v) penicillin/streptomycin to prevent undesirable carryover of plasmids. The virus-containing medium was collected from each plate at 48 hours post-transfection and filtered through 0.45 µm filter to eliminate packaging cells and debris. Subsequently, the lentiviral particles were concentrated by centrifugation at 25000 rpm for 90 minutes at 4 °C. Finally, lentiviral particles were resuspended in PBS and stored at -80 °C.

2.2.3 Viral Titer Determination

The titer of lentiviral particles was calculated by transducing 200 000 target cells with different amount viruses (0 µl, 0.050 µl, 0.100 µl, 0.175 µl, 0.250 µl, 0.375 µl) in 6-well plates in 2 ml of complete media. 72 hours after transduction, cells were harvested and dissociated into single cells by using Accutase. Dissociated cells were resuspended in 200 µl of FACS Buffer and the transduction efficiency was determined by GFP or tdTomato expression assessed by flow cytometry. Finally, the titer of the lentiviral stock was calculated by applying the formula below:

TU/ml = (# of cells at Transduction) × [MOI / (ml of Viral Stock used at Transduction)]

- # of cells at Transduction: The number of cells used at transduction
- MOI: Multiplicity of Infection, derived from the chart provided by Cellecta, Inc.
- ml of Viral Stock used at Transduction: The volume of the virus (ml) used at transduction

2.2.4 Bacterial transformation and plasmid preparation

Competent cells were thawed and incubated with plasmid DNA on ice for 20-30 minutes. After the incubation, competent cells were heat-shocked at 42 °C for 45 seconds and placed back on ice for 2 minutes. Subsequently, 250 µl of LB media (without antibiotic) was added to the competent bacteria and incubated for 45 minutes at 37 °C in a shaking incubator. 50 µl of transformation was plated on antibiotic agar plates and incubated at 37 °C overnight. Afterwards, well-separated colonies were picked and grown in LB media containing the appropriate antibiotic in 37 °C shaking incubator. Finally, plasmids were isolated by using a QIAprep® Miniprep kit following manufacturer's protocol.

2.2.5 Separation of sEVs

sEVs were separated using differential ultracentrifugation protocol. In brief, glioblastoma stem cells were cultured in DMEM/F12 medium supplemented with 2% (v/v) B-27 minus Vitamin A, 20 ng/mL EGF, 20 ng/mL bFGF and 1 µg/mL heparin for 3 days ($5x10^6$ cells/25 ml of complete medium in T175 flasks). Conditioned medium was collected and centrifuged at 300 g for 20 min, 10,000 g for 20 min at 4 °C. Afterwards, sEVs were pelleted by ultracentrifugation at 100,000 g for 70 min at 4°C in a SW40-Ti Rotor (Beckman Coulter) and resuspended in 0.22 µm-membrane filtered PBS (Sigma-Aldrich). The resuspended sEVs was loaded onto iodixanol density cushion (OptiPrep™, Sigma-Aldrich) and centrifuged again at 100,000 g for 70 min at 4°C. After centrifugation, the interphase was collected in a total volume of 2 ml and washed with 8 ml of 0.22 µm-membrane filtered PBS. Finally, sEVs were pelleted by ultracentrifugation at 100,000 g for 70 min at 4°C and stored at -80 °C.

2.2.6 Electron microscopy (EM)

Separated small extracellular vesicles (sEVs) were adsorbed onto glow discharged carbon coated copper grids, washed with bidestilled water followed by negative staining with 2% aqueous uranyl acetate. Electron micrographs were taken with a Zeiss EM 912 at 120kV (Carl Zeiss, Oberkochen, Germany) using a slow scan CCD camera (TRS, Moorenweis, Germany).

2.2.7 Nanoparticle tracking analysis (NTA)

Isolated sEVs were analyzed by nanoparticle tracking using a NanoSight LM10 system (Malvern Instruments, Worcestershire, UK) equipped with a blue laser (405 nm laser) following to manufacturer's guidelines. Samples were diluted 1:500 in 0.22 µm-membrane filtered PBS and analyzed by setting camera level and detection thresholds at 13 and 5, respectively. Five 60-seconds videos were recorded for each sample and analyzed by using the NTA 3.0 software (Malvern Instruments, Worcestershire, UK).

2.2.8 Monitoring sEVs uptake using flow cytometry and confocal microscopy

To visualize the sEVs uptake by confocal microscopy, the pelleted sEVs were first stained with fluorescent lipophilic dye PKH26 (Sigma-Aldrich; MINI26, 1:50) at room temperature for 30 minutes in the dark. After incubation with the staining solution, sEVs were washed with 0.22 µm-membrane filtered PBS, loaded onto iodixanol density cushion (OptiPrep™, Sigma-Aldrich; D1556) and centrifuged at 100,000 g for 70 min at 4°C. Subsequently, stained sEVs were carefully collected, washed with PBS, and centrifuged again at 100,000 g for 70 min at 4°C. The pelleted sEVs were resuspended in filtered PBS and used for confocal microscopy to visualize their internalization by recipient cells.

To measure the sEVs uptake using flow cytometry, NCH705 cells were stably transduced with a lentivirus vector expressing PalmtdTomato, tandem dimer Tomato fused at NH_2-termini with a palmitoylation signal, and sEVs (PalmtdTomato labelled) were separated by following the protocol described in Methods section. PalmGFP expressing NCH421k cells (recipient) were seeded in chambered coverslips (Ibidi, µ-Slide 8 Well) at a density of 10,000 cells per well, treated with PalmtdTomato-tagged NCH705 sEVs or PBB (control) and then the uptake of labelled sEVs uptake was measured every 2 hours for 8 hours using BD LSRFortessa™ (BD Biosciences). The data were analyzed by FlowJo software (FlowJo-LLC, USA).

2.2.9 Fractionation of conditioned medium

The conditioned medium was fractionated by differential centrifugation and filtration. In brief, the conditioned medium was centrifuged at 300 g for 20 min at 4°C to get rid of dead cells and cell debris (complete conditioned medium, CCM). Subsequently, the complete conditioned medium (CCM) was centrifuged at 2 000 g for 20 min at 4°C and the supernatant was collected (2 000 g supernatant, 2S). The 2 000 g supernatant was depleted at 10 000 g for 20 min at 4°C and the pellet containing cell debris and microvesicles was discarded. Afterwards, the 10 000 g supernatant (10S) was centrifuged at 100 000 g for 2 hours at 4°C to pellet the small extracellular vesicles (100P). The 100 000 g supernatant (100S) containing secreted proteins was also stored until use. Lastly, in addition to differential centrifugation, the complete conditioned medium was depleted with 0.02 µm-membrane filter (GE Healthcare) to eliminate the extracellular vesicles, sparing the soluble factors in flow-through.

2.2.10 Treating proneural cells with the different fractions of mesenchymal conditioned medium

Proneural (PN) cells were treated with the different fractions of conditioned medium of mesenchymal (MES) cells and the changes in abundance of well-known mesenchymal and proneural cell surface markers (CD44 and CD133, respectively) were measured using flow cytometry (BD LSRFortessa™, BD Biosciences). Briefly, mesenchymal cells (NCH705 or NCH711d) were seeded in cell culture flasks (2.5

x 10^6 cells in 12 ml of medium), cultured for 4 days and their conditioned medium was fractionated as described in section 2.2.12. NCH421k (PN) cells were seeded in cell culture flasks at a density of 1.5 x 10^6 cells in 6 ml of heparin-free medium, treated with 6 ml of different fractions (Own_CCM, MES_CCM, 2S, 10S, 100S and Filtered) of mesenchymal conditioned medium, and then cultured for 4 days prior to staining for cell surface markers. For 100P fraction, sEVs containing pellet was dissolved in 1 ml of heparin-free medium and transferred into a cell culture flask containing 1.5 x 10^6 NCH421k cells in 11 ml of heparin-free medium. After the incubation, the cells were harvested by centrifugation, dissociated with Accutase® (Sigma-Aldrich; A6964) and washed twice with DPBS (Sigma-Aldrich; D8537). The dissociated cells were stained with PE/Cy7 anti-human CD44 (Biolegend, # 338816) and APC anti-human CD133 (Biolegend, # 372805) antibodies in DPBS containing 5% FBS on ice for 30 minutes in the dark. Afterwards, antibody-stained cells were treated with propidium iodide (Sigma-Aldrich, # P4864) at a final concentration of 0.5 µg/ml for 5 minutes to discriminate dead cells from viable cells. Control stainings were performed by replacing each primary antibody with their nonimmune isotypes PE/Cy7 Mouse IgG1, κ or APC Mouse IgG1, κ (Biolegend, #400125 and #400121, respectively), at the same concentration and used for setting the gates for flow cytometry analysis. Finally, the data were acquired by flow cytometry (BD LSRFortessa™, BD Biosciences) and analyzed by FlowJo software (FlowJo-LLC, USA).

2.2.11 Protein extraction

Cells were pelleted by centrifugation at 300 g for 3 min at 4 °C and the supernatant was discarded. The pelleted cells were washed twice with ice-cold PBS and the supernatant was carefully decanted. 100 µl of RIPA buffer supplemented with 10 mM NaF, 10 mM Na_3VO_4 and complete mini protease inhibitor cocktail was added to the pelleted cells to resuspend. The lysate then was loaded into QIAShredder™ Columns and centrifuged at 13 000 rpm for 2 minutes. The flow-through containing proteins was collected and stored at -80°C. To isolate the proteins from sEVs, 2% SDS were mixed with the samples (1:10), vortexed for 30 seconds and incubated at room temperature 10 minutes. Afterwards, samples were centrifuged at 11000 g for 10 minutes, and protein containing supernatant was carefully recovered.

2.2.12 Protein quantitation

Pierce™ BCA Protein Assay Kit was used to quantify total protein by following manufacturer's protocol. Briefly, bovine serum albumin (BSA) protein standards (ranging from 25 µg/mL to 2000 µg/mL) were prepared by diluting albumin standard (2 mg/mL) using the same diluent as the samples. Afterwards, BCA working reagent was prepared by mixing BCA Reagent A and BCA Reagent B (50:1, Reagent A:B). The protein samples were diluted 1:5, 1:10, 1:20 and 1:40 in supplemented RIPA-lysis buffer and 10 µl of diluted protein samples/albumin standards was pipetted into a 96-well plate in duplicate. Subsequently, 200 µl of working reagent was added to each well and mixed thoroughly. The plate was covered with aluminum foil and incubated at 37°C for 30 minutes. Finally, the absorbance was measured

at 562 nm on a plate reader (Mithras LB 940). Protein concentration of sEVs samples was measured with Qubit 2.0 Fluorometer using Qubit™ Protein Assay Kit (Thermo Fisher Scientific) by following manufacturer's guidelines.

2.2.13 Western blot

Equal amounts of protein (10 µg) were prepared in LDS Sample Buffer (4X) supplemented with reducing agent DTT (10X) and denatured at 95°C for 5 minutes. Boiled protein samples were loaded into the wells of 4-12 % Bis-Tris Gels and electrophoresed at 250 V, 170 mA for 45 minutes in MES running buffer containing antioxidant. Afterwards, the gel was carefully placed in 1x transfer buffer, and the separated proteins were transferred onto a methanol-activated polyvinylidene difluoride (PVDF) membrane by performing a wet transfer in a Mini Trans-Blot wet gel transfer system, increasing the current 100 mA every 10 minutes for 50 minutes. Subsequently, the blot was blocked in blocking buffer at room temperature for 1 hour and incubated in the primary antibody solution at 4°C on a roller overnight. The membrane was rinsed three times in TBST and incubated in the horseradish peroxidase-conjugated secondary antibody solution for 2 hours at room temperature on a roller. Finally, the membrane was rinsed three times with TBST and incubated with the chemiluminescent substrate according to manufacturer's protocol. The chemiluminescent signal was captured on X-ray films.

2.2.14 Proteomics of glioblastoma stem cells and their sEVs

5 x 10^6 cells (NCH421k, NCH644, NCH705 and NCH711d) were seeded in each of twelve T175 cell culture flasks (Sarstedt, 83.3912.502) containing 25 ml of complete DMEM/Ham's F12 medium and allowed to grow for 3 days. Subsequently, conditioned medium was harvested from each cell culture flask and pooled for sEVs separation as described in section 2.2.8. Besides, sEVs-producing GSCs were recovered after the centrifugation at 300 g, washed with DPBS (Sigma-Aldrich, D8537), and dissociated into single cells with Accutase® (Sigma-Aldrich, A6964) for 3 minutes at 37°. The dissociated single cells were counted with Vi-CELL XR (Beckman Coulter), 1 x 10^7 cells were snap-frozen in liquid nitrogen and stored at -80°C until use. For proteomics, proteins were extracted from the cells following the protocol explained in Section 2.2.11. For mass spectrometry, 10 µg of full cell lysate and sEVs proteins were used. Data analysis was carried out by MaxQuant (version 1.6.14.0).

2.2.15 smRNA isolation and sequencing

Macherey-Nagel NucleoSpin® miRNA kit was used to isolate smRNA from the cells and exosomes by following manufacturer's guidelines. Small RNA libraries were prepared with 50 ng of RNA using SMARTer® smRNA-Seq Kit for Illumina® (Takara Bio Inc.), and sequenced using NextSeq 550 sequencer (Illumina, San Diego, CA).

2.2.16 Metabolite screening and fatty acid profiling by Gas Chromatography-Mass Spectrometry (GC-MS)

Sample extraction

Samples were treated with 380 µl of methanol supplemented with 0.2 mg/ml Ribitol at 70°C for 15 minutes. Afterwards, 200 µl of chloroform containing 20 mg/mL Heptadecanoic acid (C17:0) was added and samples were shaken at 37°C for 5 minutes. Subsequently, 400 µl of water was added and the samples were centrifuged at 11 000 x g for 10 minutes to separate polar and organic phases. For the derivatization, 700 µl of the polar phase (upper phase) was carefully transferred into a fresh GC vial and dried by using Eppendorf® Concentrator Plus without heating. To analyze total fatty acids, 150 µl of the lower organic phase (chloroform) was transferred to fresh vials and dried in a speed vacuum without heating. The protein phase has been used for the normalization.

Derivatization

Sequential on-line methoximation and silylation reactions were conducted with MPS autosampler (Gerstel GmbH & Co. KG) for the gas chromatographic (GC) screening of metabolites. Methoximation was carried out by treating each sample with 20 µl of 20 mg/ml methoxyamine hydrochloride (Sigma-Aldrich) in pyridine (Sigma-Aldrich) at 37°C for 90 minutes in a Gerstel MPS Agitator Unit (250 rpm). Afterwards, for the silylation reactions, the samples were treated with 45 µl of N-Methyl-N-trimethylsilyl-trifluoroacetamide (Sigma-Aldrich) supplemented with C4-C24 Fatty Acid Methyl Ester (FAME) Standards (1 µg/mL) and incubated at 37°C for 30 minutes with gentle shaking. Before the injection, samples were incubated at room temperature for 45 minutes.

For the total fatty acid analysis, sequential on-line transmethylation reactions were performed using a MPS autosampler (Gerstel GmbH & Co. KG). Briefly, the pellets were re-dissolved in 40 µL of TBME (tert-Butyl methyl ether, Sigma-Aldrich) for 5 minutes at 500 rpm at 50°C and incubated with 20 µl of TMSH (Trimethylsulfonium hydroxide, Sigma-Aldrich) for 45 minutes at 500 rpm at 50°C.

Gas Chromatography/Mass Spectrometry (GC/MS) analysis

In GC screening of metabolites, GC-TOF system (Agilent 7890 GC; Rxi®-5Sil MS Columns; Pegasus® BT) was used for the gas chromatography/mass spectrometry (GC/MS) analysis and data processing was performed with ChromaTOF® v5.50 software. The GC was operated at 250°C of injection temperature and 1 µl of sample was injected with splitless mode for the small extracellular vesicles and with split ratio of 1:10 for the cells by using the following conditions: 1 minute hold at 40°C; 6°C/min ramp to 210°C; 20°C/min ramp to 330°C; bake-out at 330°C for 5 minutes using Helium as carrier gas with constant linear velocity. Additionally, the ion source and interface temperatures were set at 250°C with

a solvent cut time of 8.5 minutes, a scan range (m/z) of 50 – 600 and an acquisition rate of 17 spectra/second.

For total fatty acids profiling, GC/MS-QP2010 Plus (Shimadzu®) fitted with a Zebron ZB 5MS column (Phenomenex®; 30 m x 0.25 mm x 0.25 µm) was used in GC/MS analysis. The GC was operated with an injection temperature of 230°C and 1 µL of sample was injected with splitless mode for the small extracellular vesicles and with a split ratio of 1:5 for cell samples using the following conditions: 1 minute hold at 40°C; 6°C/min ramp to 210°C; 20°C/min ramp to 330°C; bake-out at 330°C for 5 minutes using Helium as carrier gas with constant linear velocity. The mass spectrometer was operated with ion source and interface temperatures of 250°C, solvent cut time of 7 minutes and a scan range (m/z) of 40–700 with an event time of 0.2 seconds. The GCMS solution software (Shimadzu®) was used for data processing.

Data processing

The raw peak area values were normalized to the internal standards Ribitol and Heptadecanoic acid (C17:0) in GC screening and fatty acids profiling, respectively. The values obtained from extraction blank samples were subtracted from all sample values. Besides, normalized values measured in control sample (Mock sEVs isolation from cell-free conditioned medium) were subtracted from each sEVs sample to identify the metabolites and fatty acids truly associated with the sEVs. Finally, the metabolomics and fatty acid data were normalized to per µg of protein isolated from the cells and sEVs samples using protein phase formed in sample extraction step.

Data analysis

The partial least squares discriminant analysis (PLS-DA) score plots, hierarchical clustering heatmaps, Metabolite Set Enrichment Analysis (MSEA) plots, correlation heatmap, and Variable Importance in Projection (VIP) plots were generated using MetaboAnalyst[150] (https://www.metaboanalyst.ca/).

3. Results

The figures and part of the text in this section were taken from Lokumcu et al. (manuscript in preparation).

3.1 Classification of patient-derived glioblastoma stem cells (GSCs) into subtypes

To investigate the role of GSCs-secreted biomolecules in glioblastoma heterogeneity and cell plasticity, patient-derived glioblastoma stem cells (NCH421k, NCH644, NCH705, and NCH711d) were first classified into subtypes by single-sample gene set enrichment analysis (ssGSEA) using the gene signatures published by Wang et al. in 2017. According to ssGSEA, NCH421k and NCH644 cells were characterized as proneural (PN), while NCH705 and NCH711d cells were classified into mesenchymal (MES) subtype of glioblastoma (**Table 2**).

Table 2. Gene expression-based classification of glioblastoma stem cells (GSCs)

Single sample gene set enrichment analysis (ssGSEA) scores and respective p-values of GSC lines (NCH421k, NCH644, NCH705, NCH711d) were calculated by using Wang subtype signatures (PN: proneural, CL: classical, MES: mesenchymal). Subtype predictions were made based on the lowest p-values.

GSC Lines	ssGSEA Wang Signature Score			p-value			Prediction
	PN	CL	MES	PN	CL	MES	
NCH421k	6083	8448	1565	0.0348	0.4073	0.983	PN
NCH644	5720	5828	2707	0.0914	0.9998	0.7748	PN
NCH705	1963	7168	10952	1.0000	0.9758	0.0002	MES
NCH711d	3739	9372	5504	0.9072	0.0236	0.0046	MES

3.2 Investigating the role of GSCs-secreted biomolecules in cancer cell plasticity and tumor heterogeneity

To examine the role of GSCs-secreted biomolecules in cancer cell plasticity and tumor heterogeneity, proneural cells (NCH421k) were treated with the conditioned medium from mesenchymal cells (NCH705 and NCH711d), and the expression of CD44, a well-known mesenchymal GSCs marker, was measured by flow cytometry. NCH421k cells treated with NCH705 and NCH711d mesenchymal conditioned medium increased the abundance of CD44 significantly (**Figure 11**).

A

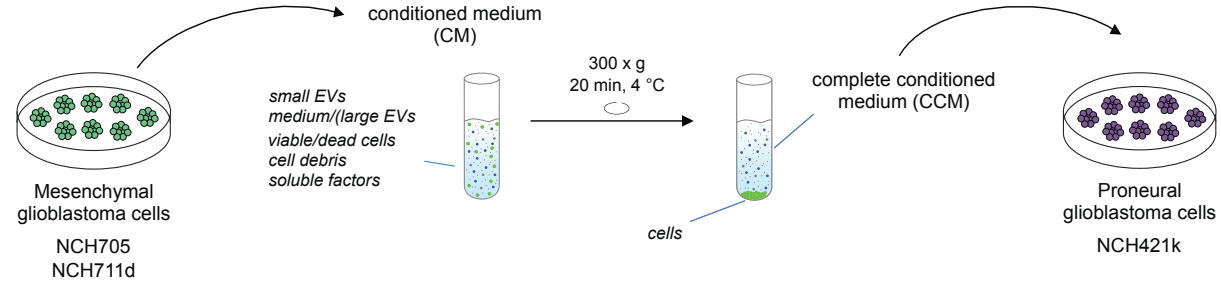

B

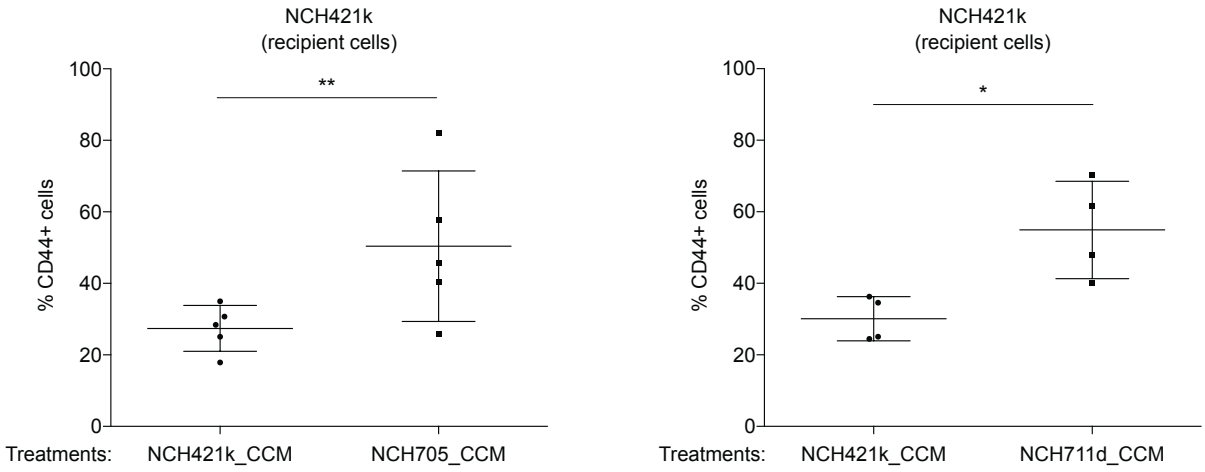

Figure 11. Treatment of proneural cells with the conditioned medium of mesenchymal cells

(A) Scheme showing the experimental setup.
(B) NCH421k cells (PN) were treated with the conditioned medium of mesenchymal NCH705 (left) and NCH711d (right) cells. Percent CD44-positivity was measured by flow cytometry. *p < 0.05, ** p < 0.01, as determined by ratio paired t-test. The graphs are showing the mean with SD, n=5 (left) and n=4 (right) biological replicates.

To understand which biomolecules are responsible for this change in CD44 positiveness, we fractionated mesenchymal conditioned medium by ultracentrifugation and filtering. Several centrifugation steps were introduced to separate proteins, small and large EVs as depicted in **Figure 12**.

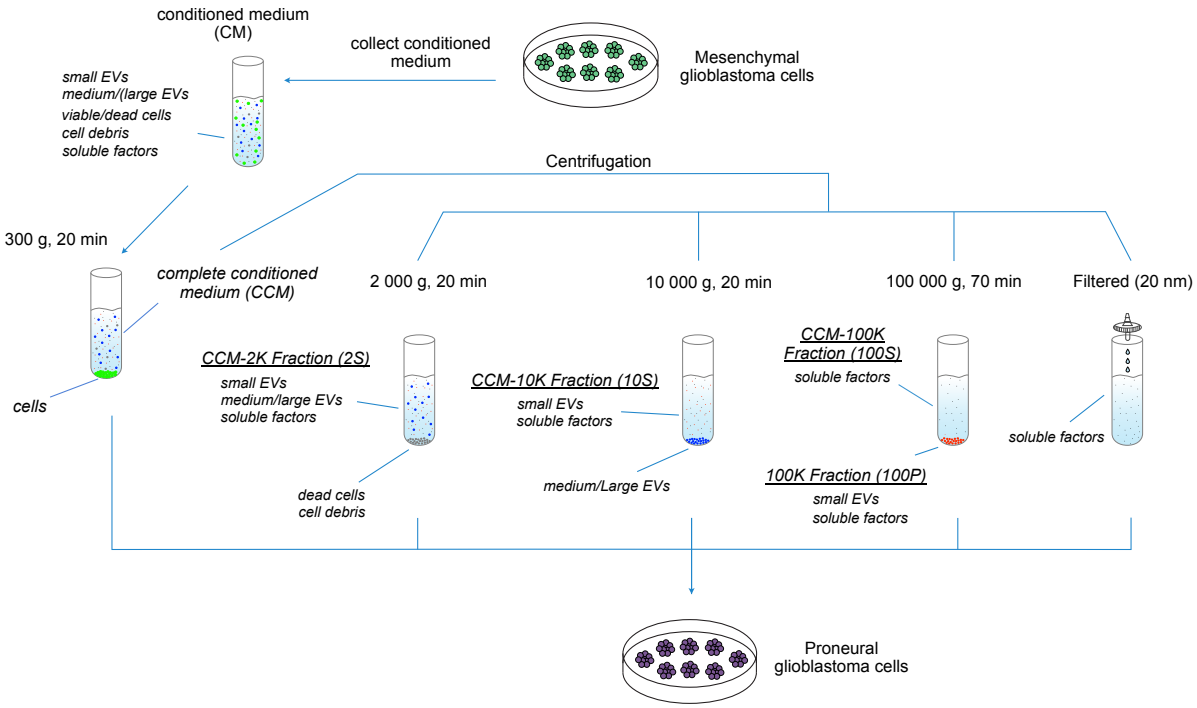

Figure 12. The fractionation of complete conditioned medium by ultracentrifugation and filtering

Proneural cells treated with the mesenchymal supernatant were centrifuged at 2000 g and 10000 g, called 2S and 10S fractions, respectively, showed an increase in CD44 expression, comparable with the one obtained when treated with the complete conditioned medium (CCM). Interestingly, this effect was abrogated when small extracellular vesicles (sEVs) were depleted from the supernatant by 100 000 g centrifugation (100S) and filtering with membrane filters (pore size, 20 nm), suggesting that sEVs may contain important factors that drives the increase in CD44 positivity. Supportively, treating PN cells with the sEVs-enriched fraction (100P) also resulted in the increase of CD44 abundance, which was not observed when they were exposed to the soluble factors-enriched fraction (Filtered). The flow cytometry results of NCH421 (PN) cells treated with the different fractions of NCH705 (MES) and NCH711d (MES) conditioned medium were indicated in **Figure 13** and **Supplementary Figure 1**, respectively.

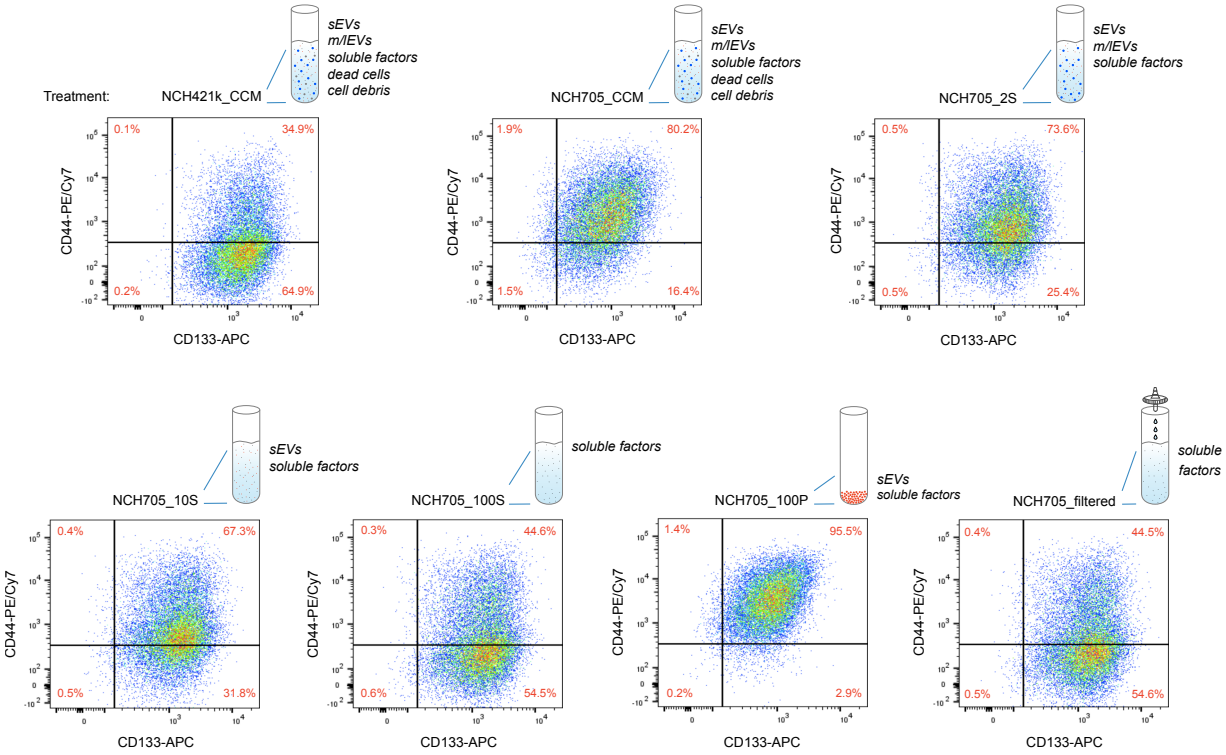

Figure 13. Flow cytometry results of PN cells treated with different fractions of MES conditioned medium

NCH421k cells (PN) were treated with the different fractions of NCH705 (MES) conditioned medium, and the expression of GSCs surface markers (CD133 and CD44) was measured by flow cytometry. NCH421k complete conditioned medium (NCH421k_CCM) was used as a control. CCM, complete conditioned medium; 2S, supernatant after 2000 g; 10S, supernatant after 10 000 g; 100S, supernatant after 100 000 g; 100P, pellet after 100 000 g centrifugation; Filtered, supernatant filtered with membrane filter (pore size, 20 nm).

3.3 Separation, Characterization and Trafficking of sEVs

Noting again that treatment with sEVs-enriched fraction of mesenchymal conditioned medium resulted in the increase of CD44 abundance in the recipient cells, subsequent experiments focused on the detailed characterization of sEVs. Firstly, GSCs-derived sEVs were separated using differential ultracentrifugation (dUC) followed by OptiPrep™ density cushion (**Figure 14A),** and their size distribution was assessed by nanoparticle tracking analysis (NTA). The separated sEVs had a size distribution of ~170-200 nm, consistent with sEVs (**Figure 14B**). Protein content-based characterization of sEVs by western blotting revealed the high expression of sEVs markers CD138, ALIX, ENO1, TSG10, and CD9 (**Figure 14C, left**). To attribute the specificity of the study to small extracellular vesicles (sEVs) subtype, the absence (or depletion) of markers (GM130, Lamin B1, and Cytochrome C), which are associated to other intracellular compartments than plasma membrane and endosome was verified. In addition, the depletion of potential co-isolate RPLP0 (a ribosomal protein) indicated the high degree of purity of sEVs preparations (**Figure 14C, right**).

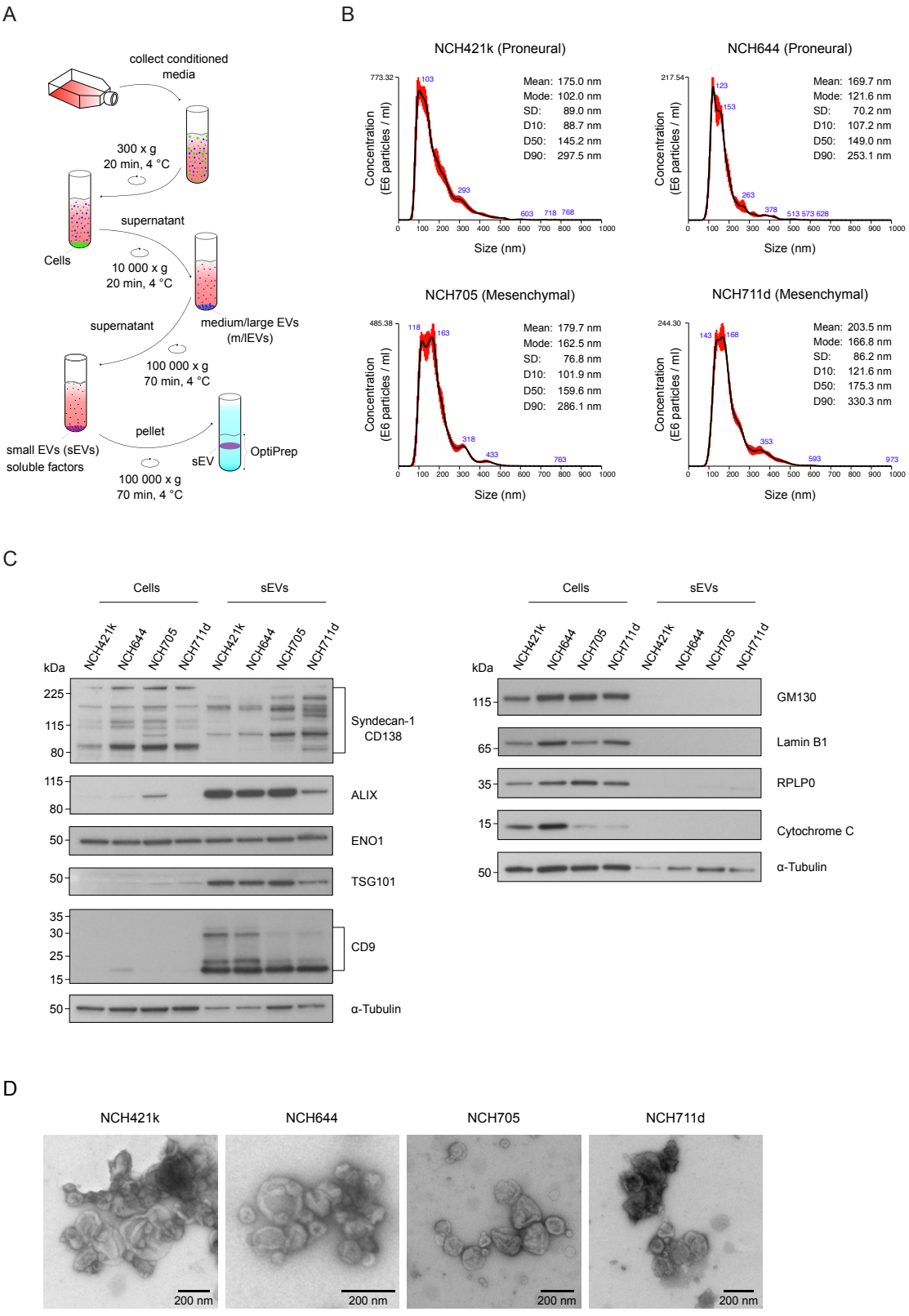

Figure 14. Separation and characterization of small extracellular vesicles (sEVs)

(legend continued on next page)

(A) Separation of sEVs using differential ultracentrifugation (dUC) followed by OptiPrep™ density cushion.
(B) Nanoparticle tracking analysis (NTA) of sEVs released from NCH421k, NCH644, NCH705, and NCH711d cells.
(C) Western blots of NCH421k, NCH644, NCH705, and NCH711d whole-cell lysate and sEVs. Equal amount of proteins were loaded on SDS-PAGE, and membranes were blotted with the antibodies indicated.
(D) Negative-stain transmission electron microscopy (TEM) of NCH421k, NCH644, NCH705, and NCH711d sEVs.

Finally, negative-stain transmission electron micrographs revealed the size (<200 nm) and cup-shaped morphology of sEVs, further supporting the high degree of purity and the specific analysis of sEVs (**Figure 14D**).

To monitor the uptake of sEVs by GSCs, mesenchymal GSCs (NCH705) were genetically engineered with a lentiviral vector expressing palmitoylated tdTomato (PalmtdTomato), which allows the labelling of extracellular vesicle membranes. Subsequently, PalmtdTomato labelled sEVs were isolated from the PalmtdTomato tagged NCH705 cells, following the protocol described in methods section. Similarly, proneural NCH421k cells were also stably transduced with a lentiviral construct encoding palmitoylated EGFP (PalmGFP) for better discrimination of the cell population truly internalized the labelled sEVs. Afterwards, NCH421k-PalmGFP cells were treated with the NCH705-PalmtdTomato-sEVs, and the uptake was traced overtime using flow cytometry. **Figure 15** demonstrates the overtime increase of tdTomato-positivity in recipient cells, revealing the time-dependent uptake of sEVs. Here, PBS treated NCH421k-PalmGFP cells were used as a negative control.

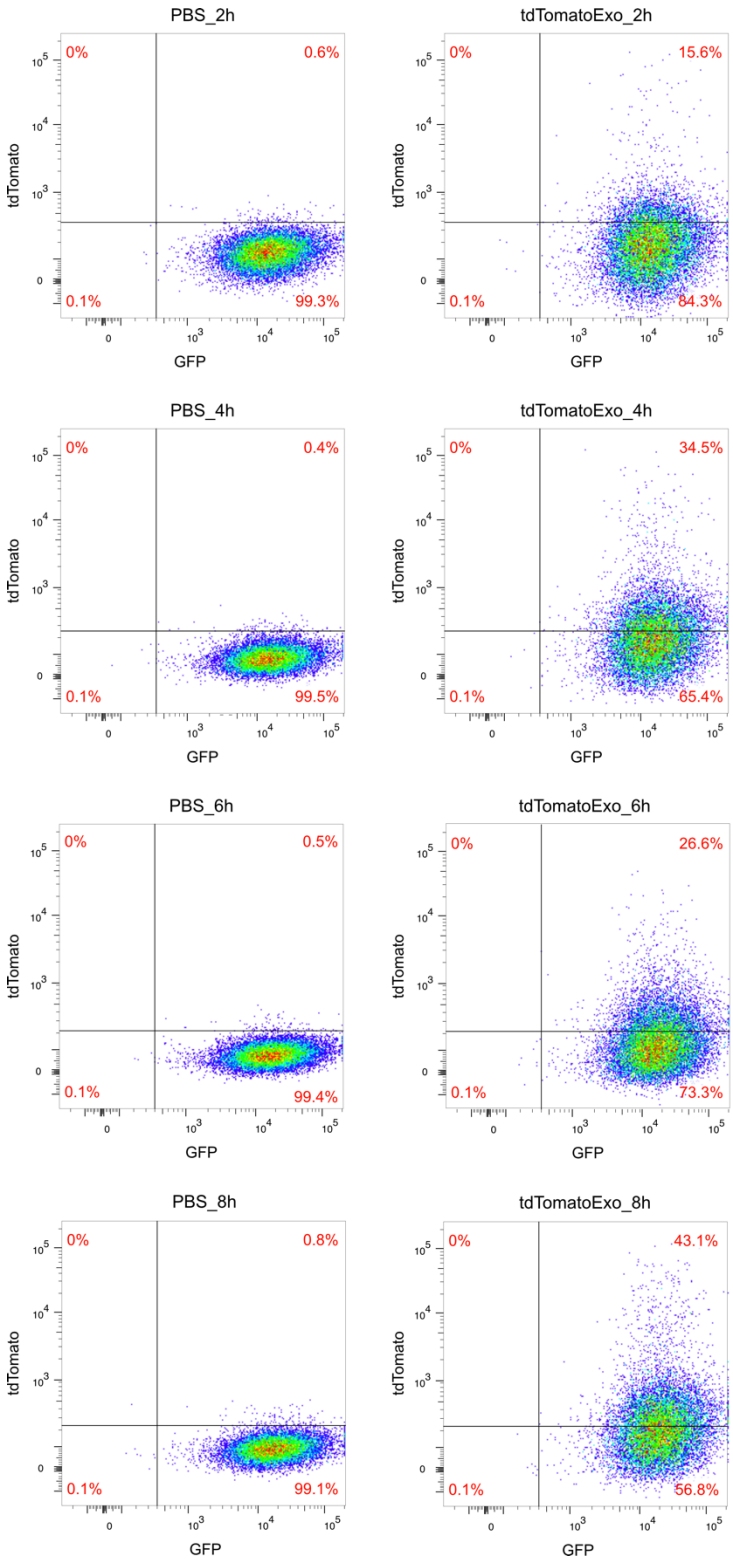

Figure 15. Flow cytometry results showing time-dependent uptake of sEVs

NCH421k-PalmGFP cells (recipient) were treated with the sEVs isolated from NCH705-PalmtdTomato (donor), and sEVs uptake was monitored every 2 hours for 8 hours. PBS treated cells were used as a control.

In addition to flow cytometric detection, the internalization of sEVs by recipient cells has also been visualized with confocal microscopy. Firstly, sEVs separated from NCH705 cells were stained with the fluorescent lipophilic dye PKH26, and their internalization by NCH421k-PalmGFP cells was monitored by confocal microscopy (**Figure 16**). Taken together, these data suggest that GSCs from proneural and mesenchymal subtypes can effectively exchange the sEVs, which might eventually contribute to the increased heterogeneity of glioblastoma.

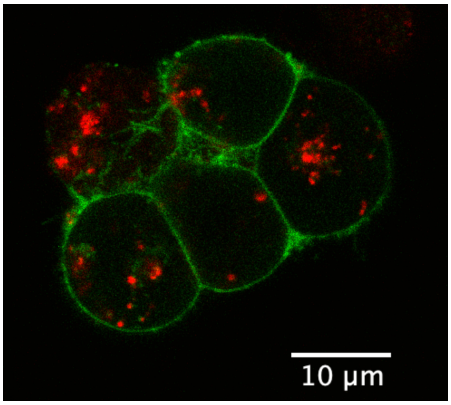

Figure 16. Visualization of sEVs uptake by confocal microscopy

Proneural NCH421k cells, stably transduced with PalmGFP encoding vector, were treated with PKH26 labelled mesenchymal sEVs (NCH705-PKH26-sEVs).

3.4 Proteome Profiling of GSCs and GSCs-derived sEVs

Given that glioblastoma is a very aggressive tumor with extremely high heterogeneity, and that tumor secreted small extracellular vesicles could be a key factor in increased heterogeneity and plasticity, the protein content of GSCs-derived sEVs, together with their respective cell lines, has been investigated by liquid chromatography-mass spectrometry (LC-MS).

3.4.1 Mass spectrometry-based analysis of GSCs and GSC-derived sEVs allowed the identification of several proteins

The analysis of mass spectrometry data was carried out by MaxQuant (version 1.6.14.0). In total of ~37000-47000 and ~16000-21000 peptides could have been identified in whole-cell lysates and sEVs, respectively, by MSMS based on an FDR cutoff of 0.01 on peptide level. Mock sEVs isolation (sEVs isolated from cell-free conditioned medium) was used as a negative control for the sEVs samples, and only 677 peptides have been identified (**Figure 17A**). In total of 7017 different proteins could have been detected in whole-cell lysate and sEVs samples, and from those 6445 different ones have been identified with at least 2 unique peptides. Finally, the quantification was performed using a label free quantification approach based on the MaxLFQ algorithm, and a total of 6985 different proteins were quantified (**Figure 17B**).

A

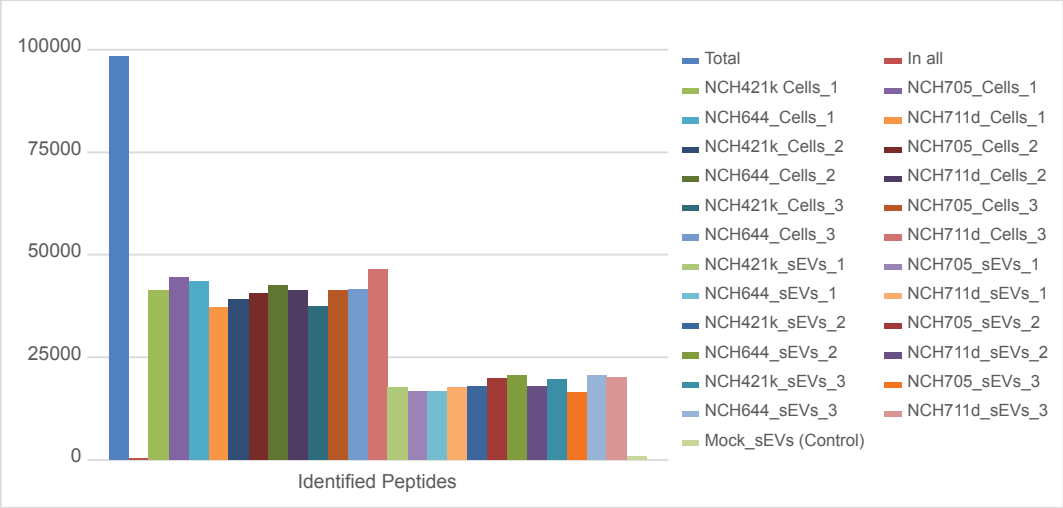

B

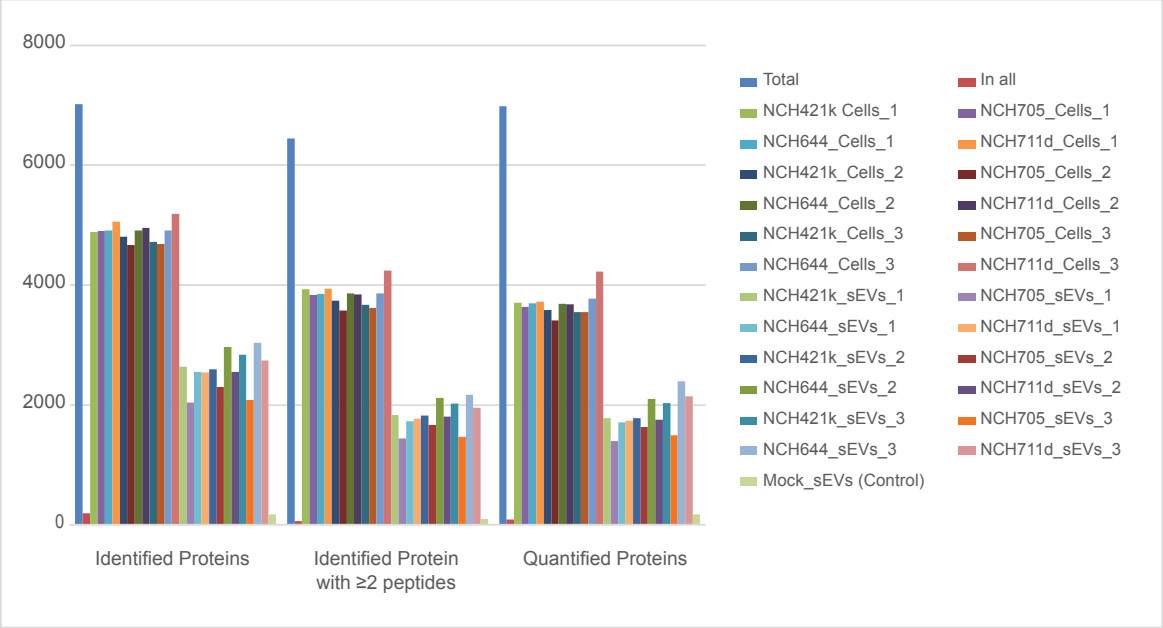

Figure 17. An overview showing identification and quantification numbers on peptide and protein level

(A) Bar graph showing the total number of peptides identified in each sample (n=3, biological replicates)
(B) Bar graphs demonstrating the total number of identified proteins (left), proteins identified with at least 2 unique peptides (middle), and quantified proteins (right). (n=3, biological replicates)

3.4.2 Small extracellular vesicles (sEVs), compared with their respective cell lines, harbor distinct subsets of proteins, which differ from subtype to subtype

To evaluate the similarities and differences in the proteome profile of these cells and sEVs, principal component analysis (PCA) was performed. As shown in **Figure 18A**, sEVs clearly cluster together and segregated away from their respective cell lines. In addition, PCA showed a clear cluster separation of the proneural (NCH421k and NCH644) and mesenchymal (NCH705 and NCH711d) sEVs, which was also revealed for the cell samples. All biological replicates of sEVs and cell samples cluster tightly together, suggesting the high reproducibility of sEVs separation, sample preparation, and robust MS quantification. To point out clusters of proteins and sEVs/cells samples with consistent behavior, log transformed LFQ values have been z-score-normalized, and the hierarchical clustering has been generated with Euclidean distance and Ward's D2 clustering. Subsequently, the relative LFQ intensities across the samples have allowed to visualize the subtype specific clusters of proteins in sEVs and cells (**Figure 18B**). In line with PCA results, unsupervised hierarchical clustering of the Pearson correlations also illustrated the separation of sEVs and cell samples in a subtype-dependent manner. The high Pearson correlation coefficients between the biological replicates further revealed the high reproducibility of MS data (**Figure 18C**). Collectively, these data imply that GSCs-derived sEVs, compared with their respective cell lines, are loaded with distinct sets of proteins, and that proteome of glioblastoma sEVs differ from subtype to subtype, which might contribute to heterogenous nature of the disease.

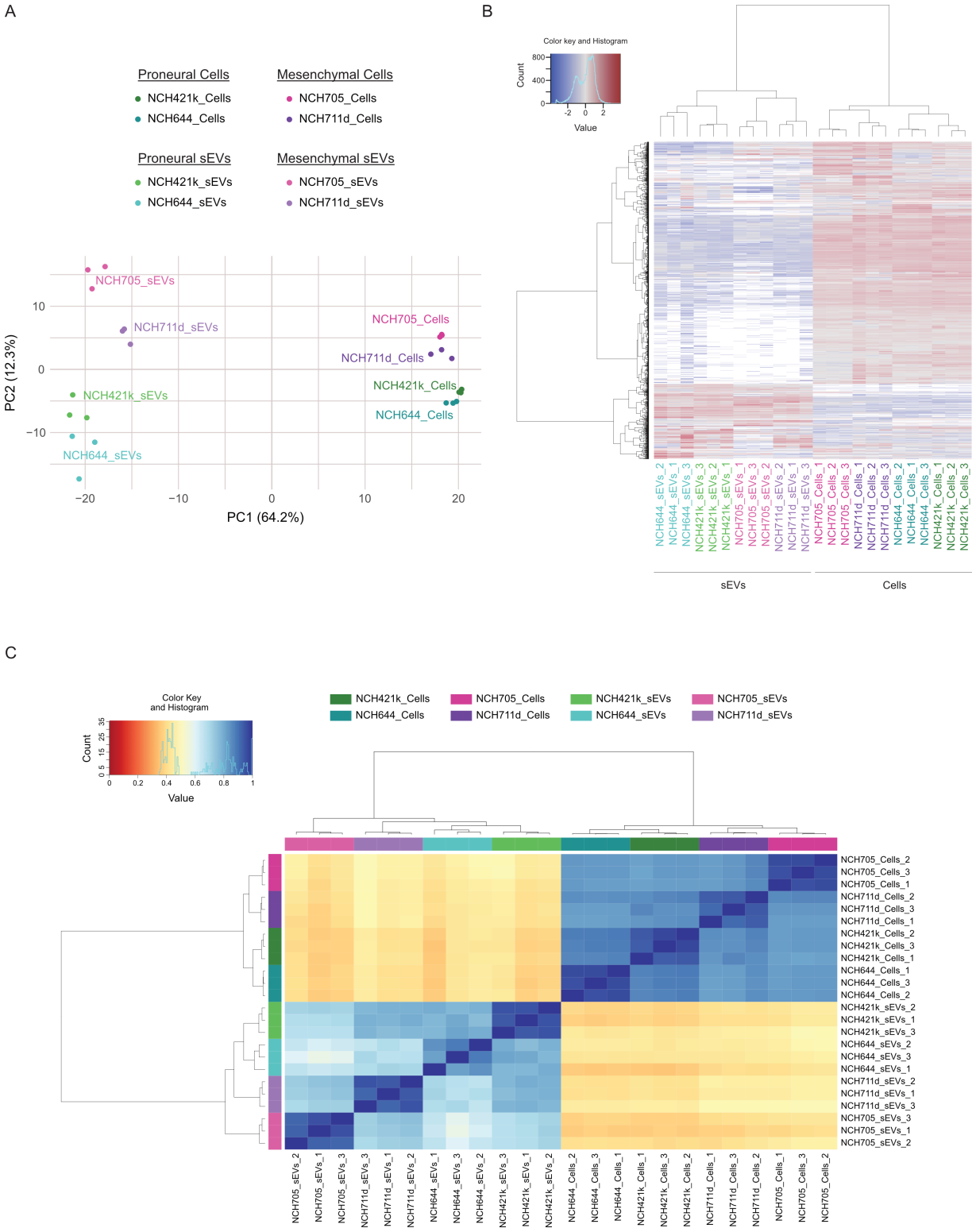

Figure 18. Proteomic profiling of GSCs and GSCs-derived sEVs

Principal Component Analysis (A), unsupervised hierarchical clustering of the Pearson correlations (B), and hierarchical clustering heatmap (C) of proteomic MS data sets. (n=3 biological replicates).

To verify whether sEVs proteins identified in this study have also been previously associated with the extracellular vesicles, MS data was cross-referenced with the publicly available extracellular vesicles proteome databases (Vesiclepedia and ExoCarta). Initially, proteins listed in these two databases were sorted according to the identification method (“mass spectrometry”) and species (“Homo sapiens”), and the sorted list was used as a reference to evaluate the degree of match with the glioblastoma sEVs. Venn diagrams in **Figure 19A** highlight proteins identified in GSCs-derived sEVs and proteins reported in extracellular vesicle protein databases-Vesiclepedia and ExoCarta. In this direction, it has been demonstrated that the majority of GSCs-derived sEVs proteins identified in this study have been previously reported to be expressed in extracellular vesicles, further verifying the efficient sEVs isolation. In addition, several proteins, which have not been previously reported by other studies to be present in EVs have also been uniquely identified in GSCs-derived sEVs, emerging as having strong potential as circulating biomarkers for glioblastoma diagnosis. To have a closer look at the proteins identified in GSC-derived sEVs and listed in vesicle proteome datasets, upset plot of all intersections (excluding the empty ones) has been generated by using UpSetR v1.4.0 R package. In line with Venn diagrams, upset plot also visualizes the overlapping proteins among the GSCs-derived sEVs and vesicle proteome datasets, together with the ones uniquely identified in each set, further confirming the high quality of sEVs isolation, and revealing the heterogenous nature of the proteome across sEVs produced by different glioblastoma stem cells (**Figure 19B**).

A

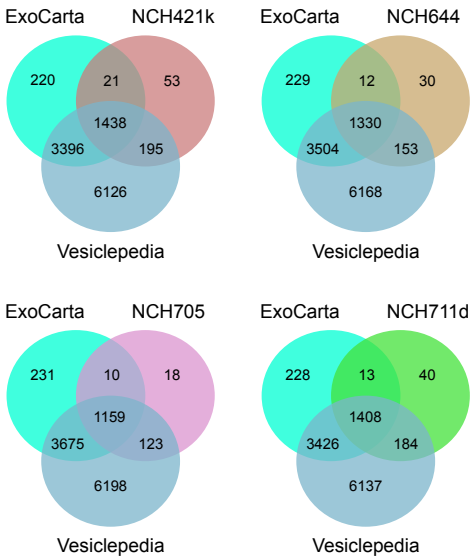

B

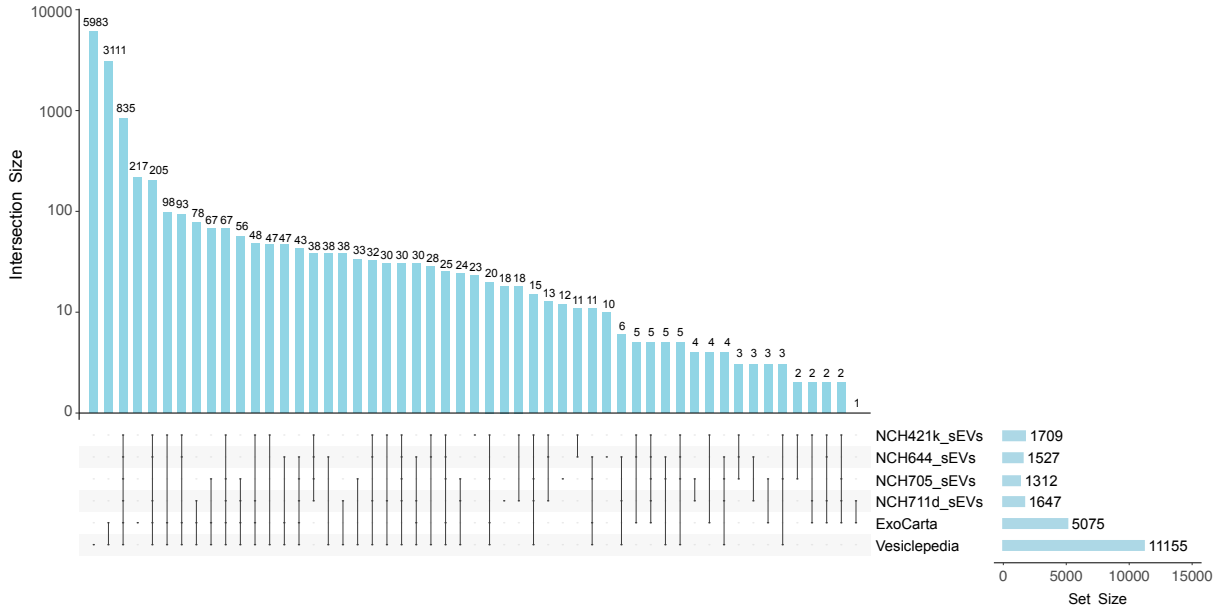

Figure 19. Qualitative and quantitative analysis of identified sEVs proteins by using publicly available datasets

(A) Venn diagram showing the number of proteins identified in the sEVs samples compared with the proteins listed in the Vesiclepedia and Exocarta databases.
(B) Upset plot indicating the number of unique and shared proteins found in GSCs-derived sEVs and vesicle proteome datasets (Vesiclepedia and ExoCarta). The total set size in each data group was shown at the bottom right of the plot. Interconnected circles in the matrix indicate the intersecting proteins.

In order to identify the differentially abundant proteins in each group, iBAQ values of proteins identified both in sEVs and whole-cell lysates (WCLs) were first quantile normalized and the relative abundance of proteins were compared statistically. **Figure 20** represents the volcano plots showing the distribution of statistical significance ($-\log_{10}$ adjusted p-val) and fold change ($\log_2$FC) for the proteins quantified both in sEVs and WCLs. For simplicity, only top 5 hits with the highest fold change were highlighted in red (increased) and blue (decreased). In total of 181, 118, 80, and 85 significantly abundant (adjusted p-value < 0.001 and $\log_2$FC > 4) proteins have been identified in NCH421, NCH644, NCH705, and NCH711d sEVs, respectively, while 506, 676, 626, and 584 proteins have been detected in low abundance (adjusted p-value < 0.001 and $\log_2$FC < -4) in these sEVs samples compared with their respective cell lines. The detailed lists of proteins (Top 50, adjusted p-value<0.001 and $\log_2$FC > 4), which are enriched in NCH421k, NCH644, NCH705, and NCH711d sEVs are shown in **Supplementary Table 1-4**. In addition, the comparison of mesenchymal and proneural sEVs revealed the enrichment of Annexin A1 (*ANXA1*), Annexin A2 (*ANXA2*), Neuropilin-1 (*NRP1*), DBH-like monooxygenase protein 1 (*MOXD1*), Integrin alpha-5 (*ITGA5*), Endoglin (*ENG*), Integrin alpha-3 (*ITGA3*), CD109 antigen (*CD109*), Integrin beta-4 (*ITGB4*), Matrix metalloproteinase-14 (*MMP14*), Spectrin beta chain, non-erythrocytic 1 (*SPTBN1*), and Trophoblast glycoprotein (*TPBG*) in mesenchymal sEVs. Besides, Annexin A1 (*ANXA1*), Transgelin-2 (*TAGLN2*), Annexin A2 (*ANXA2*), Retinal dehydrogenase 1 (*ALDH1A1*), Plasma membrane calcium-transporting ATPase 4 (*ATP2B4*), NADPH: adrenodoxin oxidoreductase, mitochondrial (*FDXR*), Prelamin-A/C (*LMNA*), Laminin subunit gamma-1 (*LAMC1*), and Kinesin heavy chain isoform 5C (*KIF5C*) proteins have been determined to be enriched in mesenchymal GSCs in comparison to proneural GSCs. The lists of proteins that are enriched in mesenchymal sEVs and cells (in comparison to proneural sEVs and cells, respectively) are provided in **Supplementary Table 5-6**.

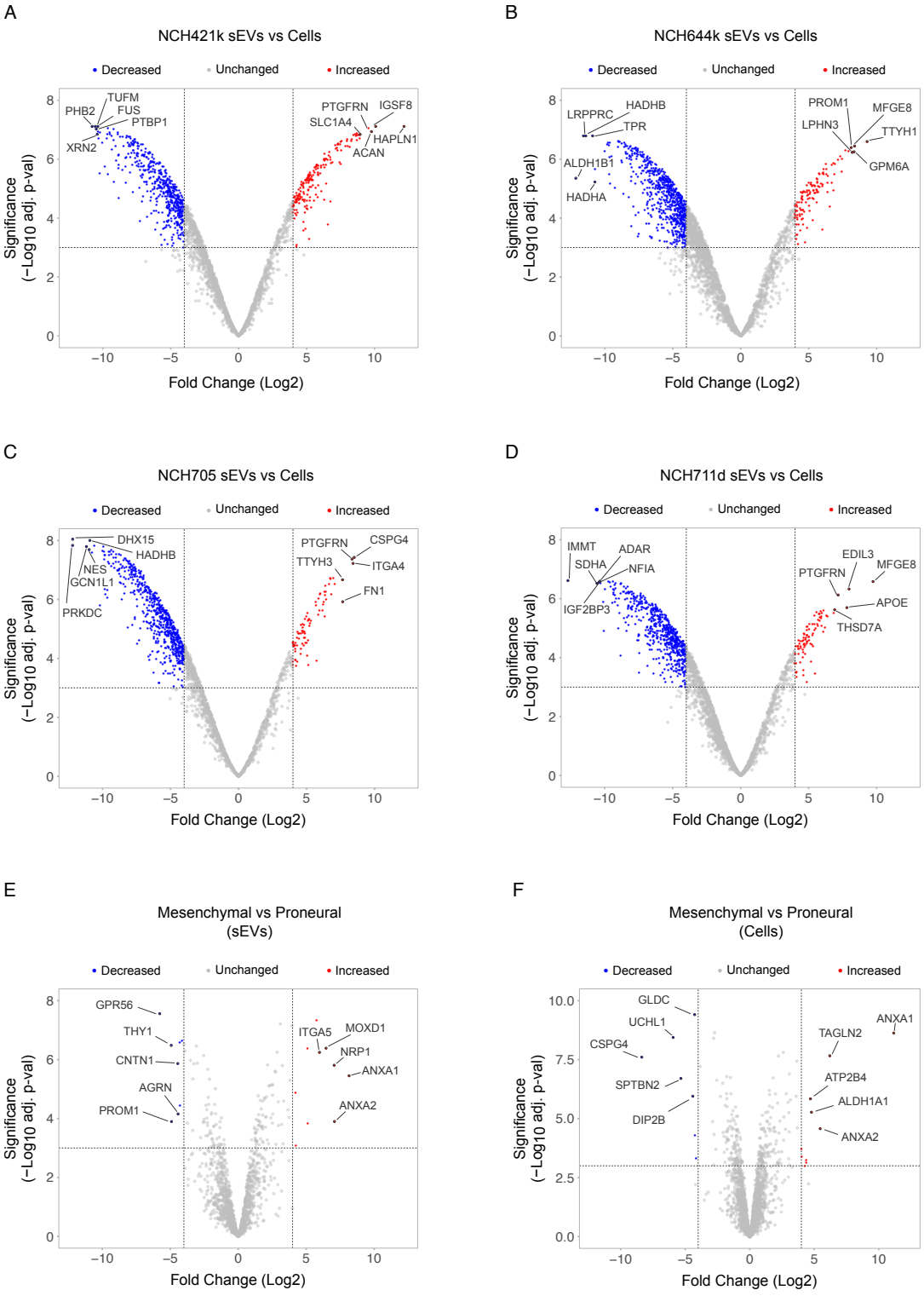

Figure 20. Volcano plots of quantified proteins in sEVs and whole-cell lysates

Volcano plots are showing the differentially expressed proteins between sEVs and whole-cell lysates in NCH421k (A), NCH644 (B), NCH705 (C), and NCH711 (D). MES versus PN sEVs and cells comparisons were depicted in (E) and (F), respectively. The horizontal and vertical dashed lines indicate the thresholds of adjusted p-value of 0.001 (-log10 adjusted p-value:3) and fold change of ± 16 (|Log2FC|=4), respectively.

Furthermore, to check whether GSCs-derived sEVs retain their subtype characteristics, GSEA was run by using the Verhaak glioblastoma subtype signatures[43], and demonstrated that MES sEVs, compared with PN sEVs, were highly enriched in proteins associated with the mesenchymal subtype of glioblastoma (**Figure 21, left**). The negative enrichment of proneural subtype related gene set in MES sEVs (**Figure 21, right**) also supported the fact that sEVs produced from GSCs retain their subtype characteristics and suggested a possible mechanism that glioblastoma cells exploit to feed neighboring cells (showing different characteristics), with the proteins, which could participate to heterogeneity of tumor cells and contribute to the aggressive nature of glioblastoma.

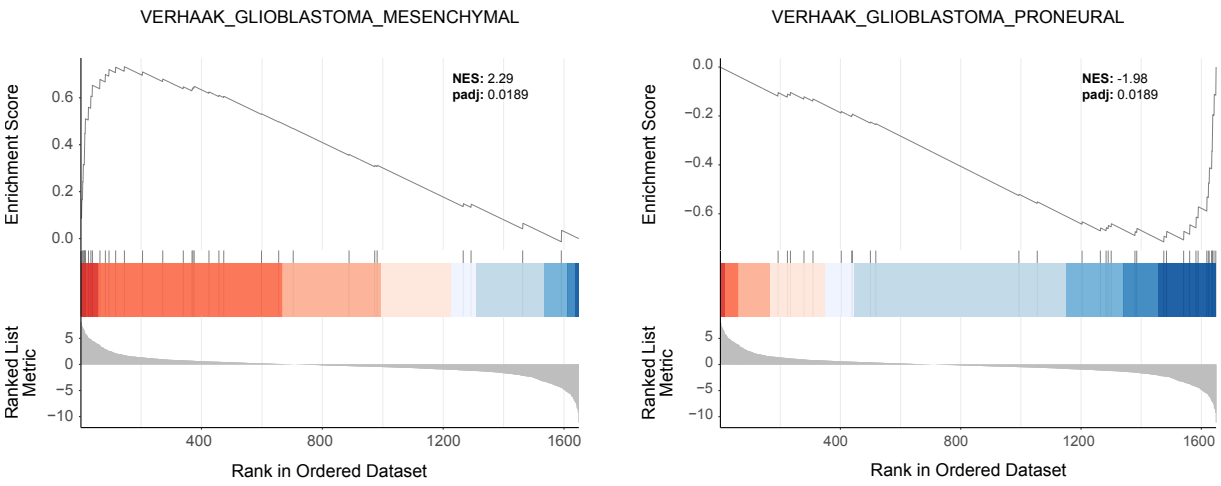

Figure 21. Gene set enrichment analysis (GSEA) of proteins differentially expressed in MES_sEVs compared to PN_sEVs

To gain functional insight into the proteome of sEVs, relative abundance of proteins in sEVs and their respective cell line was compared, and the biological and functional properties of identified proteins were characterized by Gene Ontology (GO) enrichment analysis. GO analysis of biological processes for differentially abundant proteins in sEVs has showed significant enrichment of biological programs associated with the cell-cell/matrix adhesion, transmembrane transport, cell-cell communication, and extracellular matrix organization, which were in line with well-recognized roles of sEVs, further verifying the successful and efficient separation of sEVs. Interestingly, many other biological processes involving amino acid, carboxylic acid, and organic acid transmembrane transport, amino acid import and organic anion transport have also been identified to be enriched in each sEVs samples in comparison to their respective whole cell lysates, suggesting the critical involvement of tumor-secreted sEVs in metabolic pathways and fatty acid metabolism. In addition to the biological processes/pathways related to cell-cell/matrix adhesion, cell-cell communication, transmembrane transport, and cellular metabolism, the enrichment of cancer promoting pathways, such as integrin-mediated signaling pathway, also reveals the contribution of GSC-derived sEVs to aggressiveness of glioblastoma (**Figure 21**).

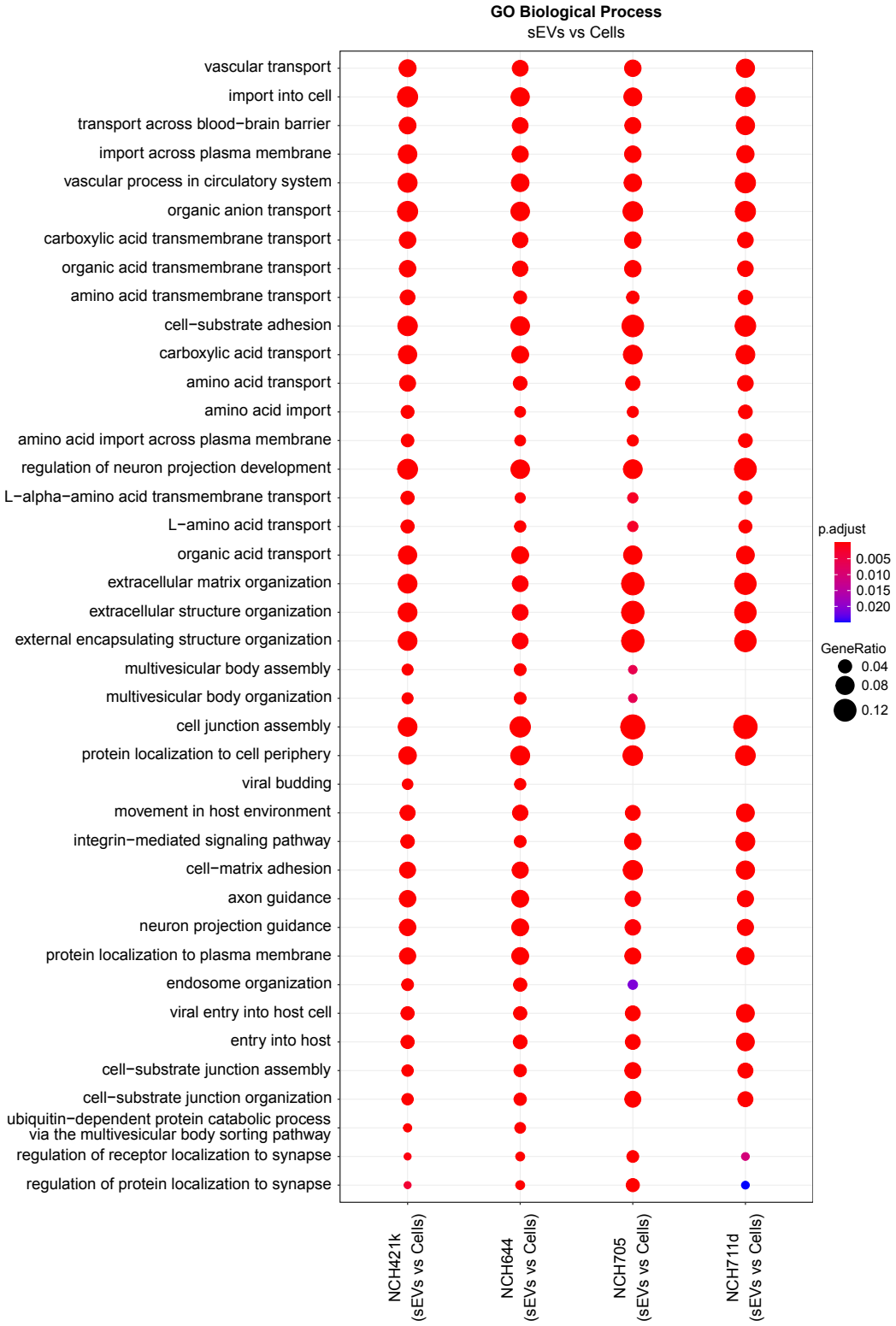

Figure 22. Gene ontology (GO) analysis (biological process) of proteins enriched in sEVs in comparison to their respective cell lines

Dot plot showing the GO biological process analysis of differentially abundant proteins (sEVs vs Cells, adj. pval < 0.001 and $\log_2$FC > 4) in sEVs. The plot was generated using Top 20 biological process terms of each comparison.

Moreover, the analysis of molecular functions also indicated the enrichment of proteins associated with growth factor and cytokine binding (i.e., “growth factor binding”, “insulin-like growth factor I binding”, transforming growth factor beta binding”, “cytokine binding”) in sEVs, further supporting the potential role of sEVs in glioblastoma cell proliferation and aggressiveness (**Supplementary Figure 2**). As expected, GO analysis of cellular components for the proteins enriched in sEVs demonstrated their association with plasma membrane, cell surface, adhesion, and endosome related cellular component terms, which was in line with the biogenesis and mechanisms of secretion of sEVs (**Supplementary Figure 3**).

3.5 Metabolomic profiling of GSCs and GSC-derived sEVs

The first observations on altered cellular metabolism in tumor cells were made nearly a century ago by Otto Warburg who showed the elevated consumption of glucose by tumor cells compared with the nonproliferating normal cells[151]. Advances in biochemical and molecular biological tools over the past decades have drastically increased our knowledge of the mechanisms, molecular and cellular players involved and functional consequences of this changes. Cancer-associated metabolic alterations can now be broadly divided into six hallmarks, which are (1) the deregulation in glucose and amino acids uptake, (2) adaptations to use different modes of nutrient acquisition, (3) reprogramming of intracellular metabolism such as increased usage of Glycolysis/TCA Cycle intermediates for biosynthesis/NADH production, (4) elevated demand for nitrogen, (5) changes in metabolite-driven gene regulation, and (6) reprogramming of metabolic interactions with the normal cells in tumor microenvironment[152]. Like most cancer cells, glioblastoma cells can also rewire their cellular metabolism to sustain their survival, growth, proliferation, invasion, and therapeutic resistance. In this direction, this part of the study focuses on the potential role of glioblastoma-derived small extracellular vesicles (sEVs), in coordination with the tumor cells, in rewiring cellular metabolism to support the cellular plasticity and heterogeneity, which could eventually result in an increased aggressiveness of the disease and resistance to conventional therapies.

3.5.1 Identification of metabolites in GSCs and GSCs-derived sEVs and their relative abundance in different subtypes

Emerging evidences suggest that an altered tumor metabolism is a defining hallmark of glioblastoma, and that metabolic reprogramming contributes to the plasticity, heterogeneity, and therapeutic resistance of glioblastoma cells[153–155]. Glioblastoma cells, like most cancer cells, can interact with each other and with the normal cells in their vicinity by exchanging diverse range of metabolites via the direct secretion/uptake of these metabolites and/or extracellular vesicles. In this regard, it is relevant to profile the metabolome of glioblastoma cells together with their biological messengers (small-extracellular vesicles in this study) to better understand the role of metabolic dysregulation in glioblastoma plasticity, heterogeneity, and therapy resistance.

To this end, Gas Chromatography-Mass Spectrometry (GC-MS) based metabolite screening of sEVs and glioblastoma cells allowed the identification of several metabolites that are implicated in essential metabolic pathways, suggesting their crucial role in cell viability and metabolic reprogramming of glioblastoma cells. The number of metabolites detected in proneural (NCH421k and NCH644) and mesenchymal (NCH705 and NCH711d) sEVs, together with the GSCs lines they are derived from were depicted with Venn diagrams in **Figure 23A**. A total of 55 and 42 metabolites were detected in proneural NCH421k and NCH644 sEVs, respectively, and a total of 34 and 38 metabolites were identified in mesenchymal NCH705 and NCH711d sEVs, respectively.

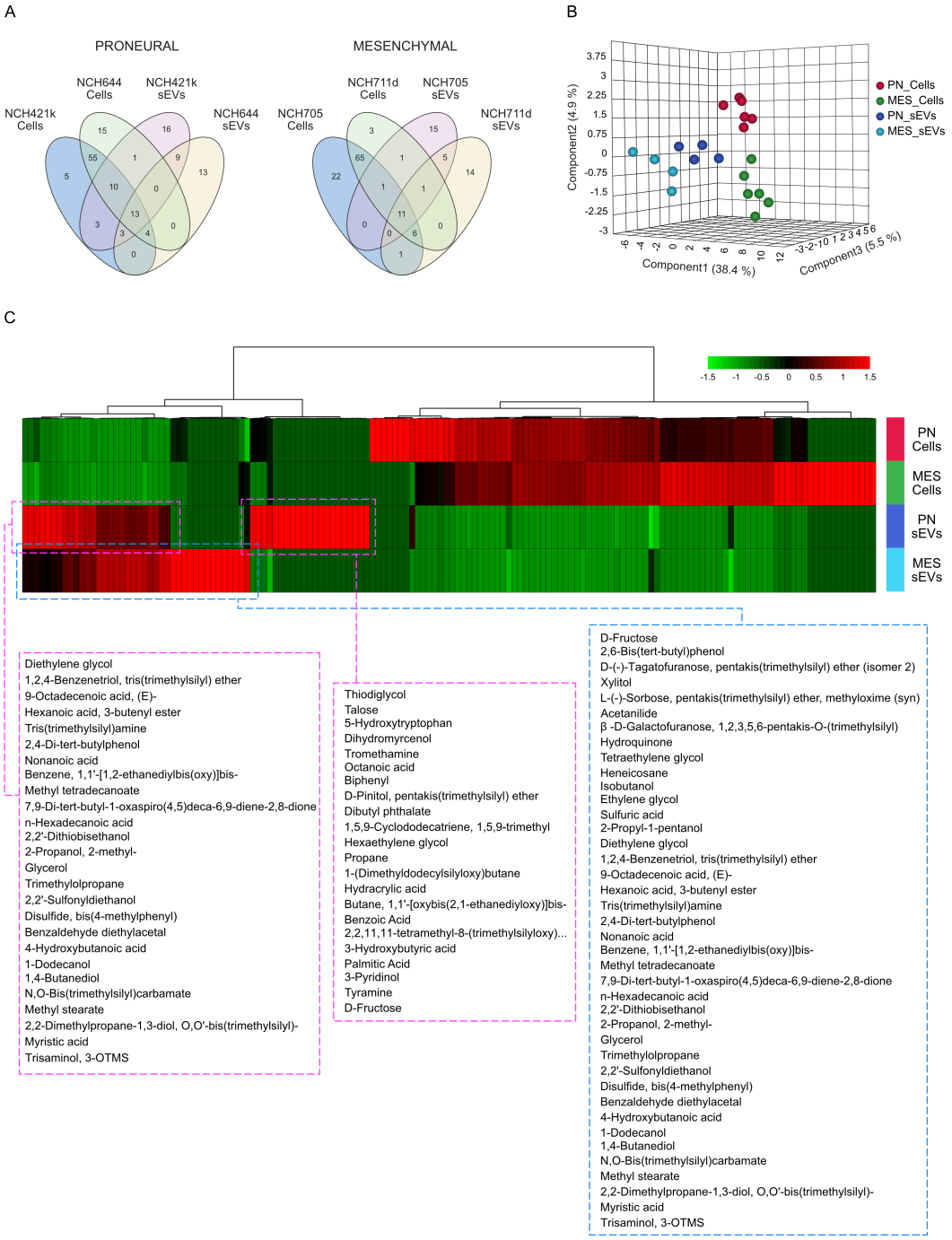

Figure 23. Metabolomic profiling of GSCs and GSCs-derived sEVs

(A) Venn diagrams showing the number of metabolites identified in proneural (left) and mesenchymal (right) cells/sEVs samples.
(B) The 3D partial least squares discriminant analysis (PLS-DA) score plot of the cells and sEVs classified into subtypes. Red: proneural cells; Green: mesenchymal cells; Blue: proneural sEVs; Turquoise: mesenchymal sEVs.
(C) The hierarchical clustering heatmap of metabolites identified in proneural/mesenchymal cells and sEVs. Distance measure: Euclidean, Clustering algorithm: Ward. For simplicity, only top 150 metabolites are shown here. Dashed magenta and blue boxes indicate the metabolites that are differentially abundant in proneural and mesenchymal sEVs respectively as compared with the corresponding cell lines.

In addition, unsurprisingly, many more metabolites were detected both in proneural and in mesenchymal cells as compared to their respective sEVs. Furthermore, 3D partial least squares discriminant analysis (PLS-DA) score plot showed that the first three components discriminate the cells and sEVs in a subtype-dependent manner, suggesting unique profiles of metabolites in between sEVs and their respective cell lines (**Figure 23B**). Finally, the overall metabolome profile of proneural and mesenchymal cells/sEVs was visualized as a heatmap as shown in **Figure 23C**. For simplicity the heatmap only shows the top 150 metabolites, and from those the ones that have higher discriminatory potential in PN-sEVs versus PN-Cells and MES-sEVs versus MES-Cells comparisons were listed in dashed magenta and blue boxes, respectively.

3.5.2 Investigation of metabolic pathways associated with the metabolites identified in GSCs and GSCs-derived sEVs

To investigate the biologically meaningful patters, which were significantly enriched in these metabolomic datasets, Metabolite Set Enrichment Analysis (MSEA) was performed by using over-representation analysis (ORA) approach. Over-representation analysis verifies whether a certain metabolite set is represented more than anticipated by chance within the metabolite list provided. To this end, 84 metabolic sets (based on KEGG human metabolic pathways) were used as a metabolite set library, and biologically important metabolic patterns were identified both in cells and sEVs samples. **Figure 24** shows the MSEA results with the most enriched metabolic sets in the GSCs and GSCs-derived sEVs. MSEA revealed that metabolites associated with the “galactose metabolism” are commonly enriched in NCH421k, NCH644, NCH705, and NCH711d sEVs. NCH421k and NCH711d sEVs have also been shown to be enriched for other sugar related metabolic pathway namely “fructose and mannose metabolism”. Furthermore, the enrichment of metabolites related to “starch and sucrose metabolism” has been also demonstrated in NCH711d sEVs. Amino acid related metabolic pathways such as “alanine, aspartate, glutamate metabolism” and “arginine biosynthesis” were also among the ones significantly enriched in NCH421k-derived sEVs. In addition, “butanoate metabolism” has been revealed as enriched commonly in NCH421k and NCH644 sEVs. The enrichment of above-mentioned amino acid and sugar related metabolic pathways has also been observed in the cells that sEVs are derived from, supporting the idea that sEVs are a “fingerprint” of their parent cells. Moreover, “aminoacyl-tRNA”, “valine, leucine and isoleucine”, “phenylalanine, tyrosine and tryptophan”, “pantothenate and CoA” biosynthesis pathways and “glutathione”, “glyoxylate and dicarboxylate”, and “D-Glutamine and D-glutamate” metabolism associated metabolite sets were also found to be enriched in all GSCs used.

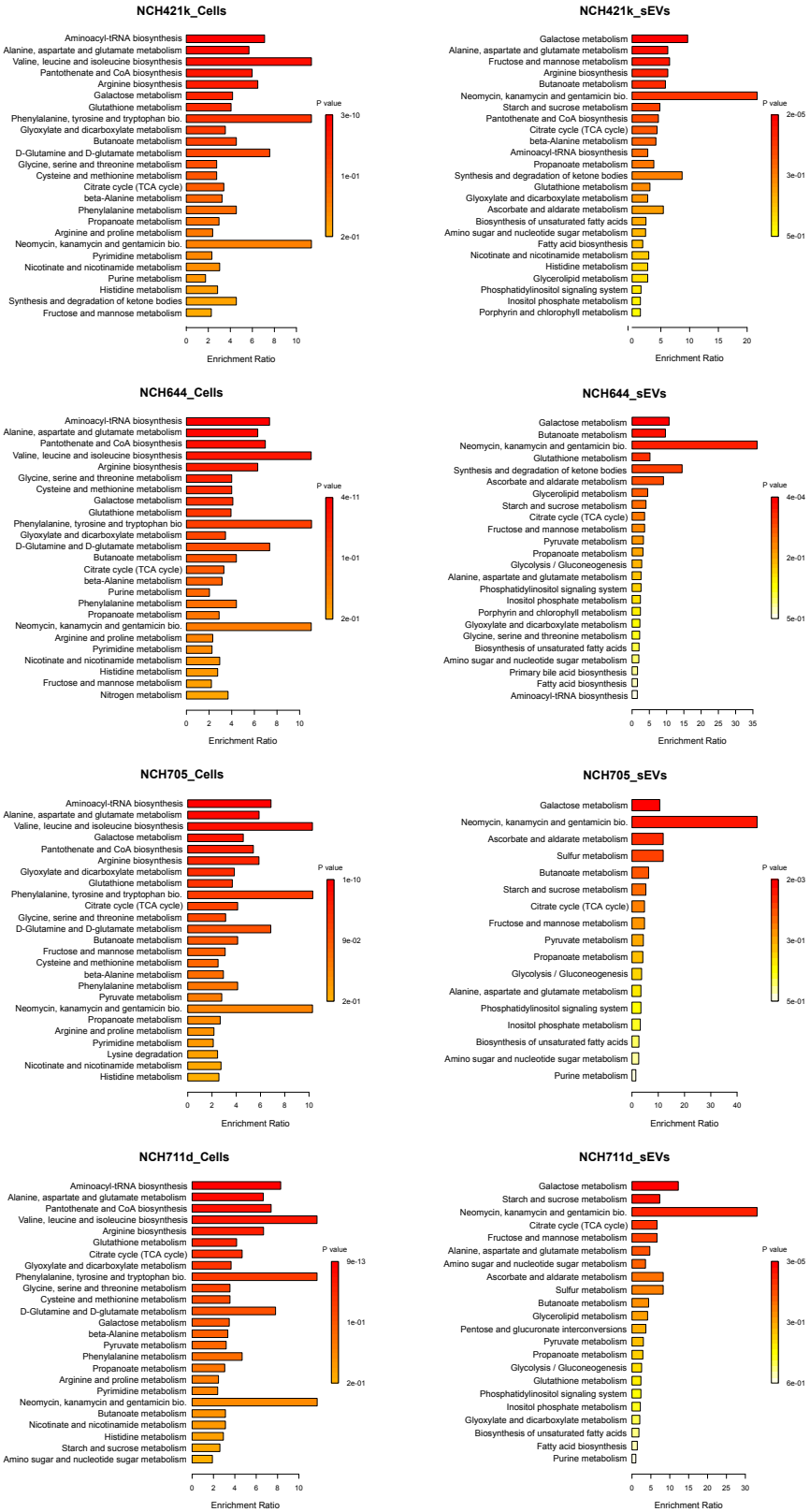

Figure 24. Metabolite Set Enrichment Analysis (MSEA) showing the most enriched metabolic sets in cells and sEVs

Finally, MSEA was performed for the metabolites detected in proneural and mesenchymal sEVs/cells to check whether there is any subtype-specific enrichment of metabolite sets (**Figure 25)**. Whereas PN sEVs are enriched for metabolites involved in galactose, butanoate and glutathione metabolism and neomycin, kanamycin, gentamicin biosynthesis, MES sEVs are only found to be rich in metabolites related to galactose metabolism and neomycin, kanamycin, gentamicin biosynthesis. Additionally, it has been revealed that PN and MES cells share many metabolites and are enriched for similar metabolite sets.

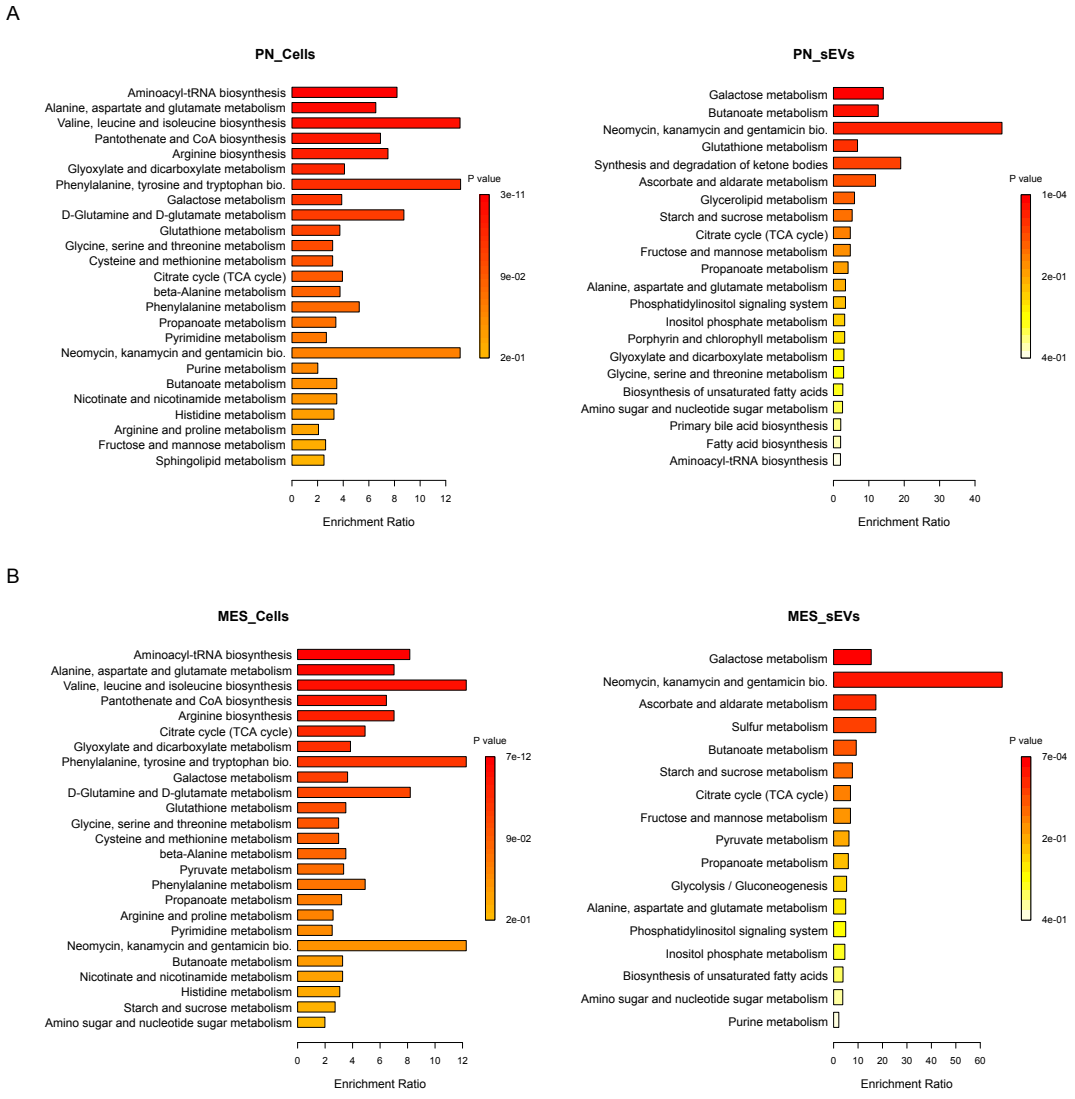

Figure 25. Metabolite Set Enrichment Analysis (MSEA) showing the subtype dependent enrichment of metabolic sets in PN and MES cells/sEVs

3.6 Fatty acid profiling of GSCs and GSC-derived sEVs

After the observations done by Otto Warburg on preferential increase of aerobic glycolysis in cancer cells, it has long been thought that cancer cells primarily use glucose for energy production. However, cancer cells also metabolize many other substances, including amino acids and fatty acids, for their cellular maintenance[156]. In addition to the dependence of cancer cells on aerobic glycolysis, recent studies have demonstrated that fatty acid metabolism also play a crucial role in tumorigenesis. Prabhu et al. have revealed that fatty acid oxidation is one of the key drivers of progression from low-grade gliomas into high-grade glioblastomas[157]. Supportively, Lin et al. have demonstrated the presence of enzymes involved in fatty acid oxidation within human glioblastoma tissues, and showed that the inhibition of fatty acid oxidation diminished tumor growth and prolonged survival in vivo[158]. Furthermore, the dependence of glioblastoma cells on fatty acid metabolism has also been nicely shown by Duman et al. by uncovering that reduced expression of acyl-CoA-binding protein (ACBP), a protein that mediates fatty acid oxidation, led to tumor senescence, and prolonged the survival of experimental animals[159]. Collectively, these data suggest that fatty acid metabolism is crucial for glioblastoma cells to maintain their viability and proliferation and could be used as a therapeutic target for the treatment of glioblastoma. Considering also that exosomes are reservoirs of saturated and unsaturated fatty acids and serve as a transporter for fatty acids[160–162], this part of the study focused on profiling of fatty acids in glioblastoma small extracellular vesicles and their respective source cells to better understand their role in and contribution to glioblastoma heterogeneity and plasticity.

3.6.1 Identification of fatty acids in GSCs and GSCs-derived sEVs and their relative abundance in different subtypes

Considering the above-mentioned roles of fatty acid metabolism in glioblastoma cell maintenance and the potential contribution of sEVs in establishing glioblastoma associated cellular mechanisms, the fatty acid content of GSCs-derived sEVs, together with their source cell lines, was assessed using Gas Chromatography-Mass Spectrometry (GC-MS).

Figure 26A shows the 2-D scores plot of selected components (Component 1 and Component 2) and reveals a clear separation between the cells and sEVs, thereby indicating the divergence of fatty acid metabolism between the two groups. The 2-D scores plot also demonstrates a cluster separation of the proneural (NCH421k and NCH644) and mesenchymal (NCH705 and NCH711d) cells. On the other hand, the obvious clustering and separation between proneural and mesenchymal sEVs have not been observed. Interestingly, hierarchical clustering heatmap of fatty acids (**Figure 26B**) revealed that cholesterol and many of the saturated fatty acids, namely arachidic acid, behenic acid, stearic acid, palmitic acid, and lignoceric acid were specifically enriched in sEVs compared with their respective cell lines. On the contrary, monounsaturated (palmitoleic acid, elaidic acid, myristoleic acid, erucic acid, and nervonic acid) and polyunsaturated (cis-4,7,10,13,16,19-DHA, arachidonic acid, eicosatrienoic acid, and

cis-5,8,11,14,17-EPA) fatty acids were specifically enriched in GSCs, further indicating the difference in the fatty acid composition of GSCs and their respective sEVs.

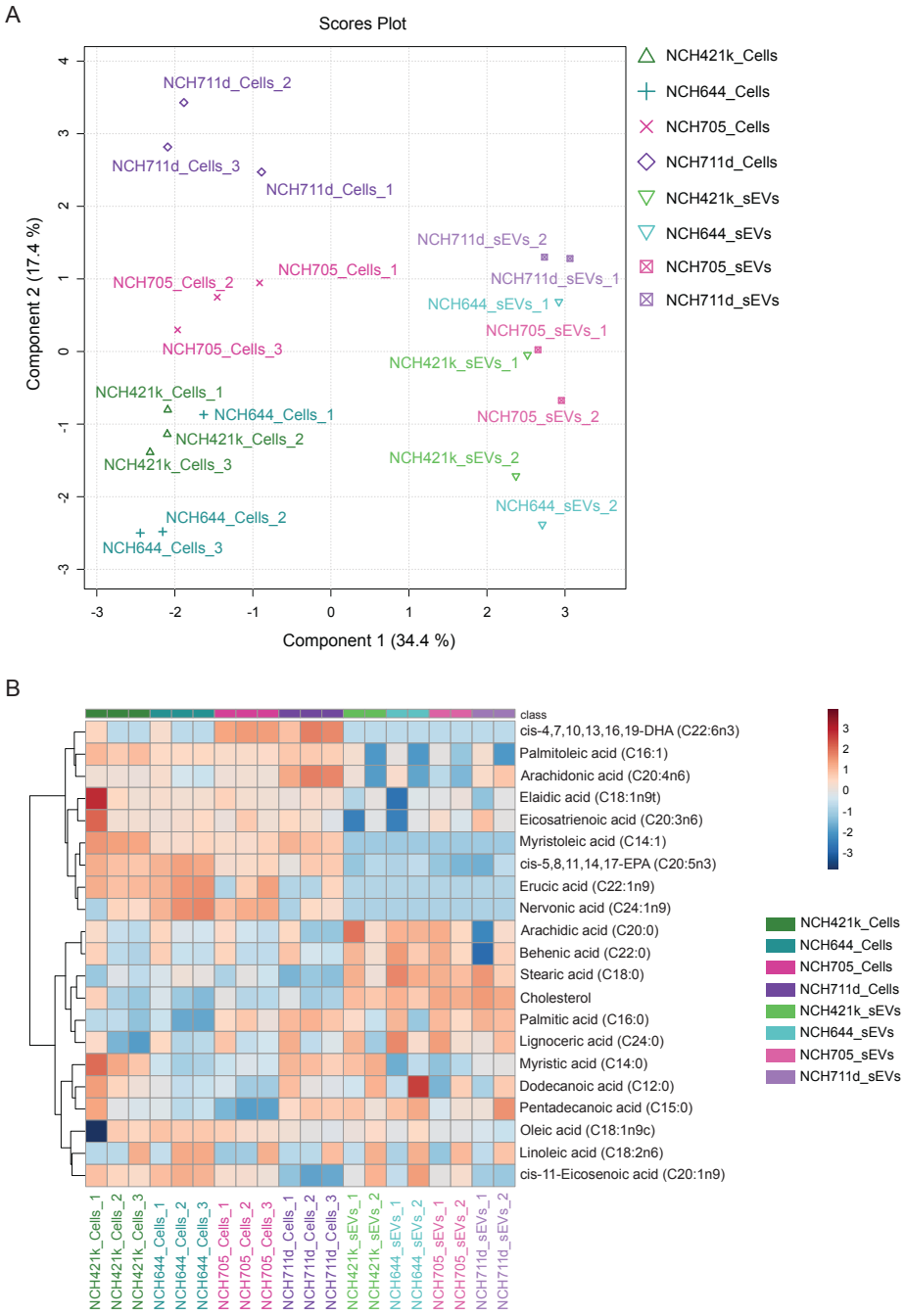

Figure 26. Fatty acid analysis of GSCs and GSCs-derived sEVs

(A) The 2-D score plot (Component 1 and Component 2) using the Sparse Partial Least Squares-Discriminant Analysis (sPLS-DA) of fatty acids.
(B) The hierarchical clustering heatmap of fatty acids in GSCs and sEVs. Distance measure: Euclidean, Clustering algorithm: Ward

The correlation heatmap of fatty acid data also indicates that the abundance of saturated fatty acids is positively correlated with each other and negatively correlated with the unsaturated fatty acids as depicted in **Figure 27**.

Taken together, these data clearly demonstrate that GSCs and their sEVs are enriched for a distinct set of fatty acids, which might contribute to the increased heterogeneity and aggressiveness of glioblastoma cells by exchanging crucial fatty acids via sEVs.

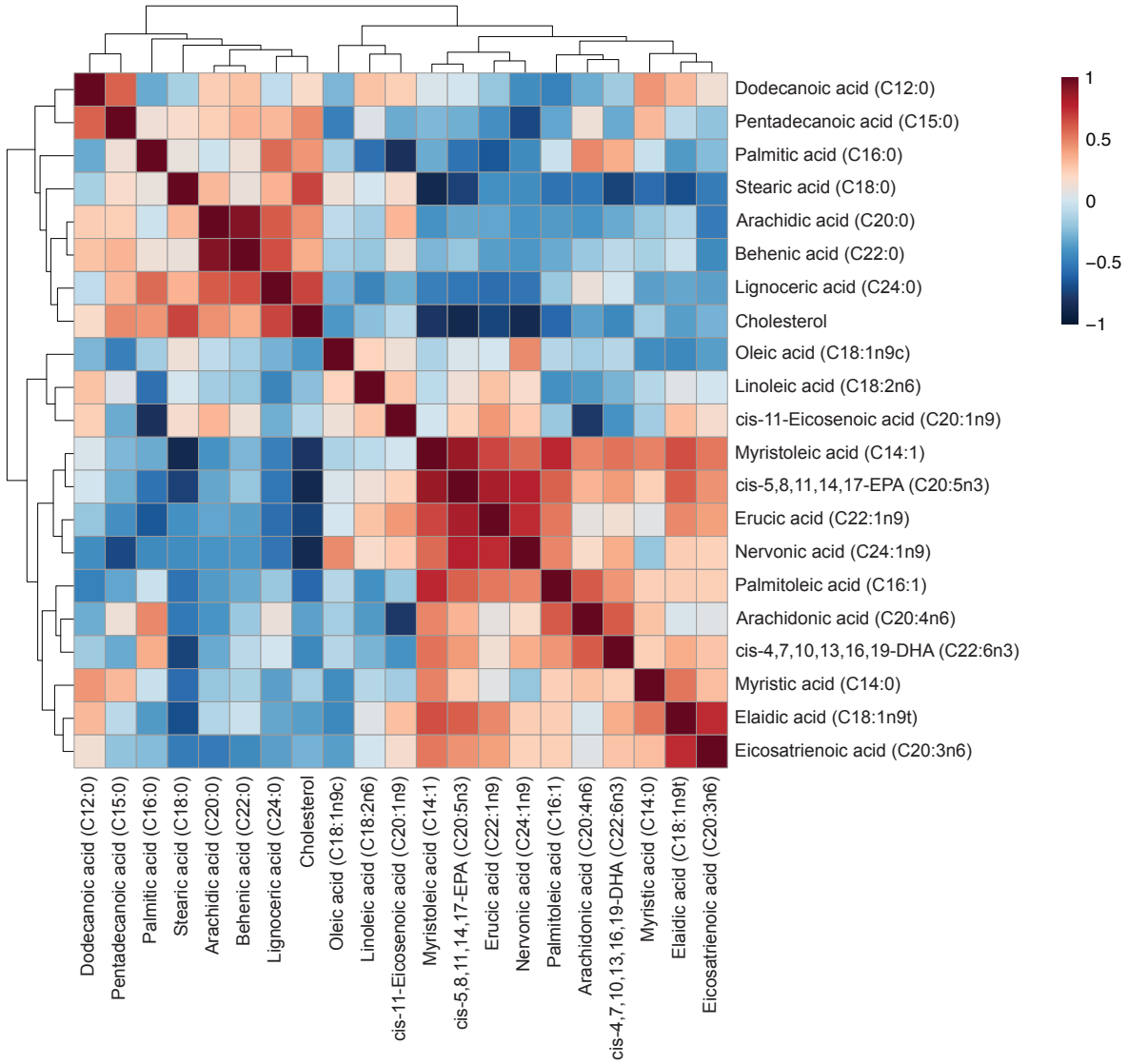

Figure 27. Correlation heatmap of fatty acids

The overall correlation heatmap of fatty acids generated by MetaboAnalyst 5.0 software. Pearson correlation coefficient was used in distance measure. Colors are representing the Pearson's coefficient of correlation. Red and blue depict positive and negative correlation, respectively.

To identify the key fatty acids that significantly discriminate the cells and sEVs in a subtype-dependent manner (i.e., PN_Cells vs PN_sEVs and MES_Cells vs MES_sEVs), Partial Least Squares-Discriminant analysis (PLS-DA), a supervised multivariate statistical analysis method, has been performed. Like Principal Component Analysis (PCA), which is an unsupervised statistical analysis approach, PLS-DA is also based on dimensionality reduction; however, different from PCA, the PLS-DA uses group labels of samples to identify the main features that maximize the differences between the groups. Firstly, to estimate the predictive ability of the model, cross validation (CV) method was employed by implementing Leave One Out Cross-Validation (LOOCV), and R^2 and Q^2 values were calculated. Accordingly, 5 components-model (having high values of R^2 and Q^2) that could clearly discriminate the groups has been selected as a good-fit model for the classification and data stability (**Figure 28A**). In addition, to test the significance of group discrimination, a permutation test was conducted using the optimal number of components obtained by cross validation. Separation distance (B/W ratio) was used as test statistics for measuring the group discrimination, with the permutation number of 100. The highlighted red bar is close to the right side of the distribution, which means that group separation can be considered as statistically significant (**Figure 28B**).

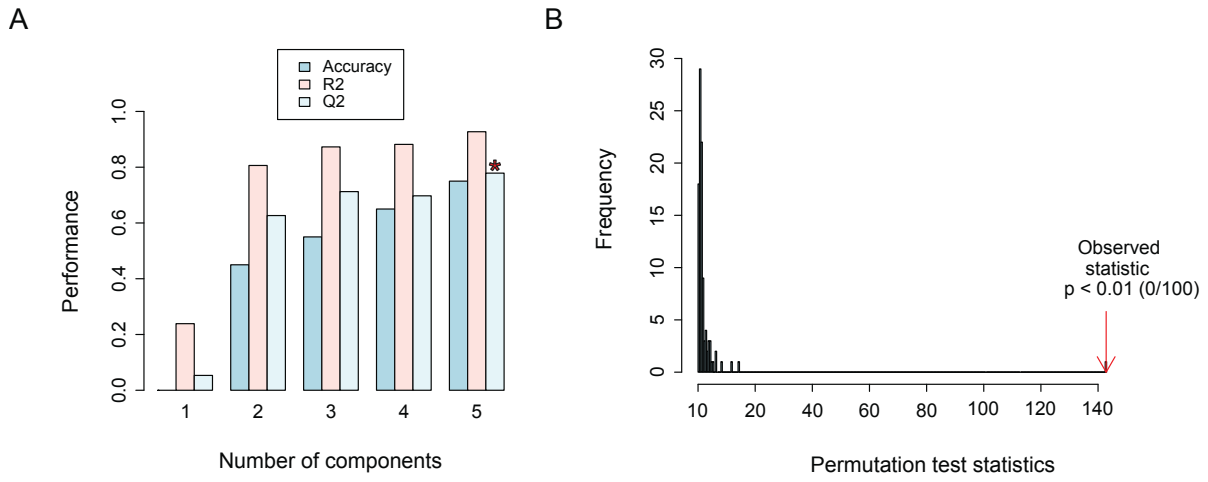

Figure 28. PLS-DA classification and model validation

(A) PLS-DA classification using different number of components. The red asterisk shows the best classifier. Cross Validation (CV) method: Leave One Out Cross-Validation (LOOCV), Maximum components searched: 5, Performance measure: Q^2

(B) PLS-DA model validation by permutation tests based on Separation distance (B/W). The p-value based on permutation is $p < 0.01$ (0/100).

To estimate the discriminatory power of each individual fatty acid, Variable Importance in Projection (VIP) analysis was performed, and the fatty acids having VIP score above 1 were considered as important parameter for the class separation (**Figure 29**).

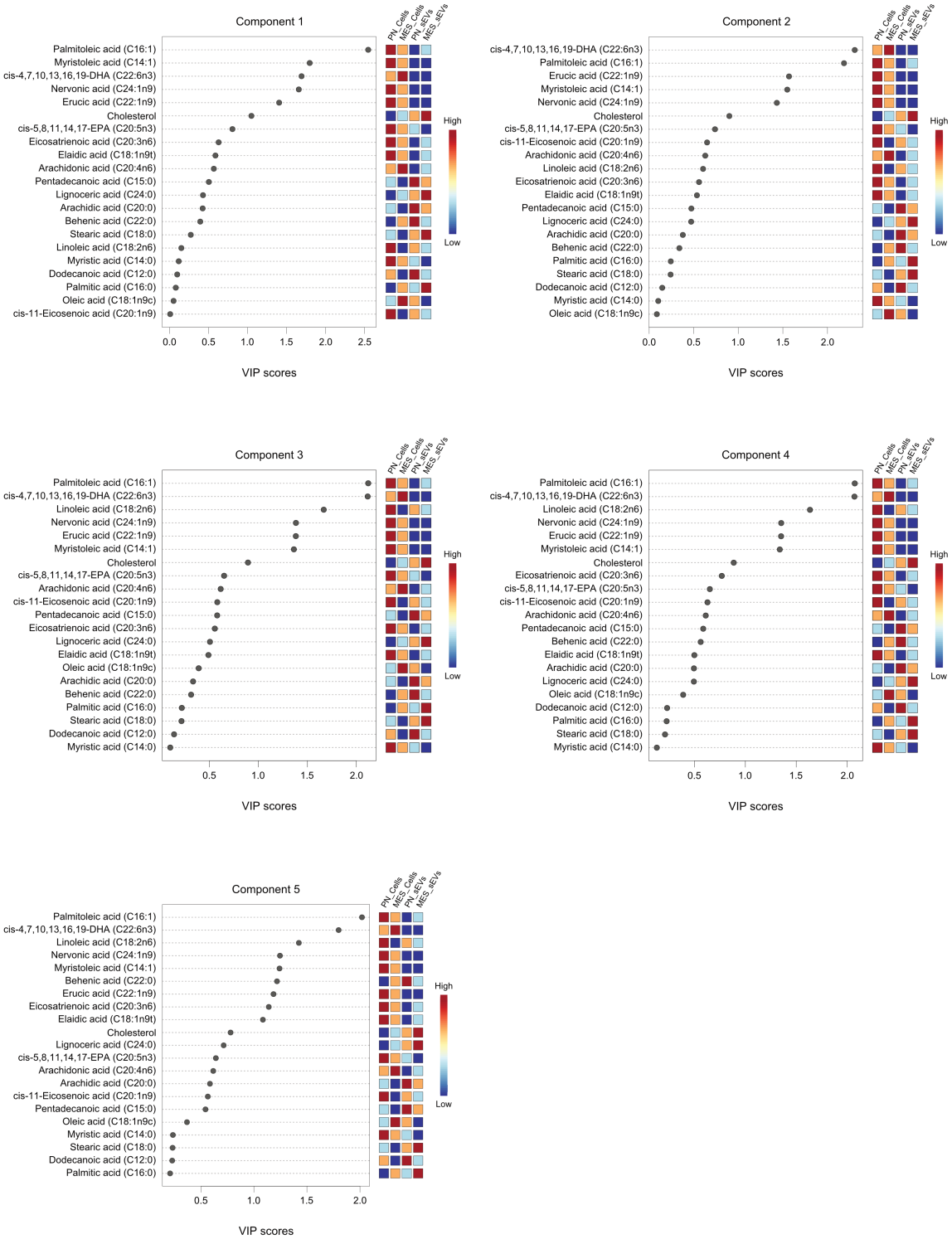

Figure 29. Variable Importance in Projection (VIP) scores showing the important features identified by PLS-DA

Plots showing VIP rank-scores of quantified fatty acids calculated for each component (1-5). The colored boxes indicate the relative abundance of the corresponding fatty acid.

Table 3 summarizes the VIP scores for Component 1-5. As indicated, Palmitoleic acid (C16:1), Myristoleic acid (C14:1), cis-4,7,10,13,16,19-DHA (C22:6n3), Nervonic acid (C24:1n9) and Erucic acid (C22:1n9) have been determined with VIP scores above 1 for all components.

Table 3. Variable Importance in Projection (VIP) scores of each fatty acid

	Comp. 1	Comp. 2	Comp. 3	Comp. 4	Comp. 5
C16:1	2.5454	2.1853	2.1205	2.0740	2.0193
C14:1	1.7960	1.5489	1.3623	1.3382	1.2413
C22:6n3	1.6916	2.3056	2.1151	2.0709	1.7991
C24:1n9	1.6562	1.4322	1.3833	1.3522	1.2456
C22:1n9	1.4043	1.5685	1.3823	1.3511	1.1847
Cholesterol	1.0492	0.8991	0.8941	0.8864	0.7796
C20:5n3	0.8062	0.7384	0.6506	0.6519	0.6407
C20:3n6	0.6293	0.5595	0.5559	0.7692	1.1399
C18:1n9t	0.5881	0.5360	0.4910	0.4999	1.0845
C20:4n6	0.5676	0.6293	0.6157	0.6115	0.6161
C15:0	0.5041	0.4733	0.5800	0.5870	0.5429
C24:0	0.4290	0.4711	0.5064	0.4952	0.7142
C20:0	0.4247	0.3779	0.3342	0.4957	0.5849
C22:0	0.3938	0.3389	0.3139	0.5621	1.2176
C18:0	0.2723	0.2405	0.2161	0.2123	0.2326
C18:2n6	0.1515	0.6050	1.6670	1.6346	1.4237
C14:0	0.1183	0.1021	0.1014	0.1315	0.2355
C12:0	0.0987	0.1469	0.1404	0.2324	0.2288
C16:0	0.0806	0.2427	0.2193	0.2278	0.2089
C18:1n9c	0.0519	0.0862	0.3915	0.3902	0.3682
C20:1n9	0.0086	0.6497	0.5813	0.6288	0.5651

Finally, to identify the fatty acids that are associated with the sEVs/cells in a subtype-dependent manner, normalized intensities of fatty acids were compared with each other within the same subtype, and the results were visualized as box plots. For simplicity, **Figure 30** only demonstrates the fatty acids that show statistical significance in at least one comparison. For instance, stearic acid (C18:0) and cholesterol were detected high in both PN and MES sEVs compared to PN and MES cells, respectively. On the other hand, palmitic acid (C16:0) was enriched only in PN sEVs compared with their parental PN cells.

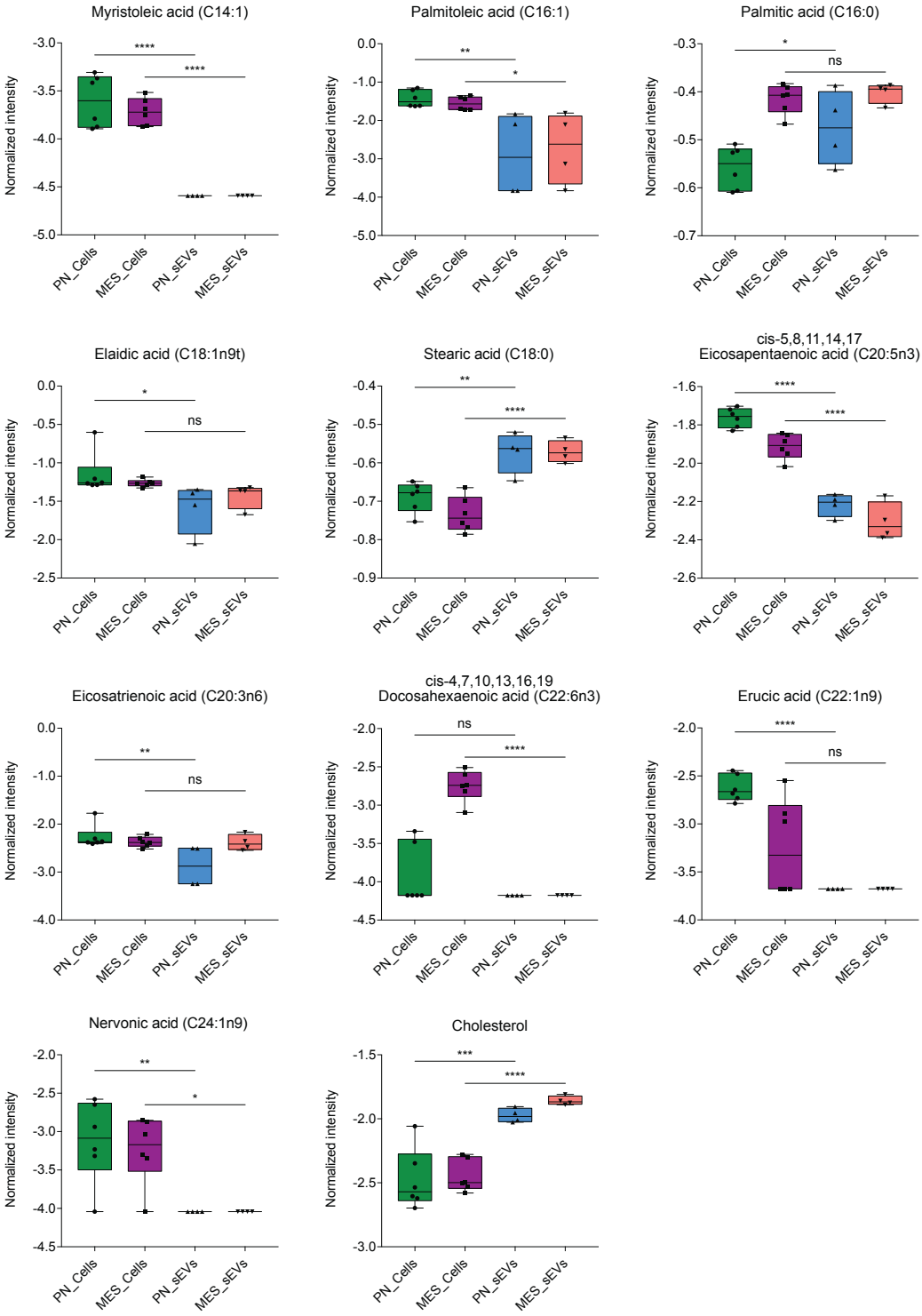

Figure 30. Box plots showing the relative abundance of fatty acids in proneural and mesenchymal sEVs/cells

The intensities of fatty acids were transformed by generalized logarithm transformation and statistically compared by one-way ANOVA. The significance was indicated as follows: * p<0.05, ** p<0.01, *** p<0.001, ***p<0.0001

3.7 Small RNA profiling of GSCs and GSC-derived sEVs

In addition to proteins, metabolites, and fatty acids, glioblastoma cells have also been shown to transfer different RNA species to closely surrounding and distant cells via extracellular vesicles, resulting in the phenotypic changes of recipient cells. Numerous RNA species including microRNA (miRNA), transfer RNA (tRNA), small nucleolar RNA (snoRNA), Y RNA, vault RNA (vRNA), mitochondrial RNA (mtRNA), long non-coding RNA (lncRNA) and mRNA have been previously detected in human glioblastoma stem cells[124,163]. Supportively, Van der Vos et al. have demonstrated that glioblastoma derived extracellular vesicles transfer high level of miR-451 and miR-21 to microglia, causing a decrease in miR-451/miR-21 target *c-Myc* mRNA[144].

Given that the change of small RNAs between glioblastoma cells and cells of tumor microenvironment via extracellular vesicles might promote tumor progression and disease aggressiveness, this part of the project particularly focused on the characterization of small RNA species of glioblastoma-derived sEVs, which allow us to reveal the diversity of RNAs that can potentially be exchanged between tumor cells, resulting eventually in increased cell plasticity and heterogeneity of glioblastoma cells. In that respect, small RNA sequencing of GSCs-derived sEVs and parent cells was carried out and the results are depicted in **Figure 31**. Accordingly, principal component analysis showed the distinct pattern of small RNAs between sEVs and their parental cells. In addition, subtype-dependent separation of small RNA profiles has also been revealed both in sEVs and parent cells (**Figure 31A**). The percent distribution of different RNA species (**Figure 31B)** indicated that the vast majority of reads obtained from sEVs samples aligned to protein coding regions (62.1%, 81.7%, 57.4% and 82.2% for NCH421k, NCH644, NCH705 and NCH711d sEVs, respectively). In addition, whereas lincRNA was the second most abundant RNA type represented in NCH421k, NCH644, and NCH711d sEVs (31.8%, 9.4% and 7.5%, respectively), lincRNAs were only represented less than 1% in NCH705 sEVs. Mitochondrial RNAs (MtRNAs) were also detected in NCH421k, NCH644, NCH705, and NCH711d sEVs (0.3.%, 3.8.%, 1.7% and 5.3%, respectively). Unexpectedly, miRNAs, snRNAs and snoRNAs were found to be extremely low in all sEVs samples used. On the other hand, snoRNAs represented 4.9%, 6.0%, 2.2% and 3.3% in NCH421k, NCH644, NCH705, and NCH711d cells, respectively, while MtRNAs were present in 3.0%, 6.3%, 1.0% and 6.0%. Finally, rRNA was the most abundant RNA species detected in all GSCs. (57.5%-82.2%). However, the analysis of smRNA sequencing datasets revealed a lot of duplicate reads (over 80% in all samples) at low read counts, which suggests very low library complexity and makes the data unreliable for comparative analysis.

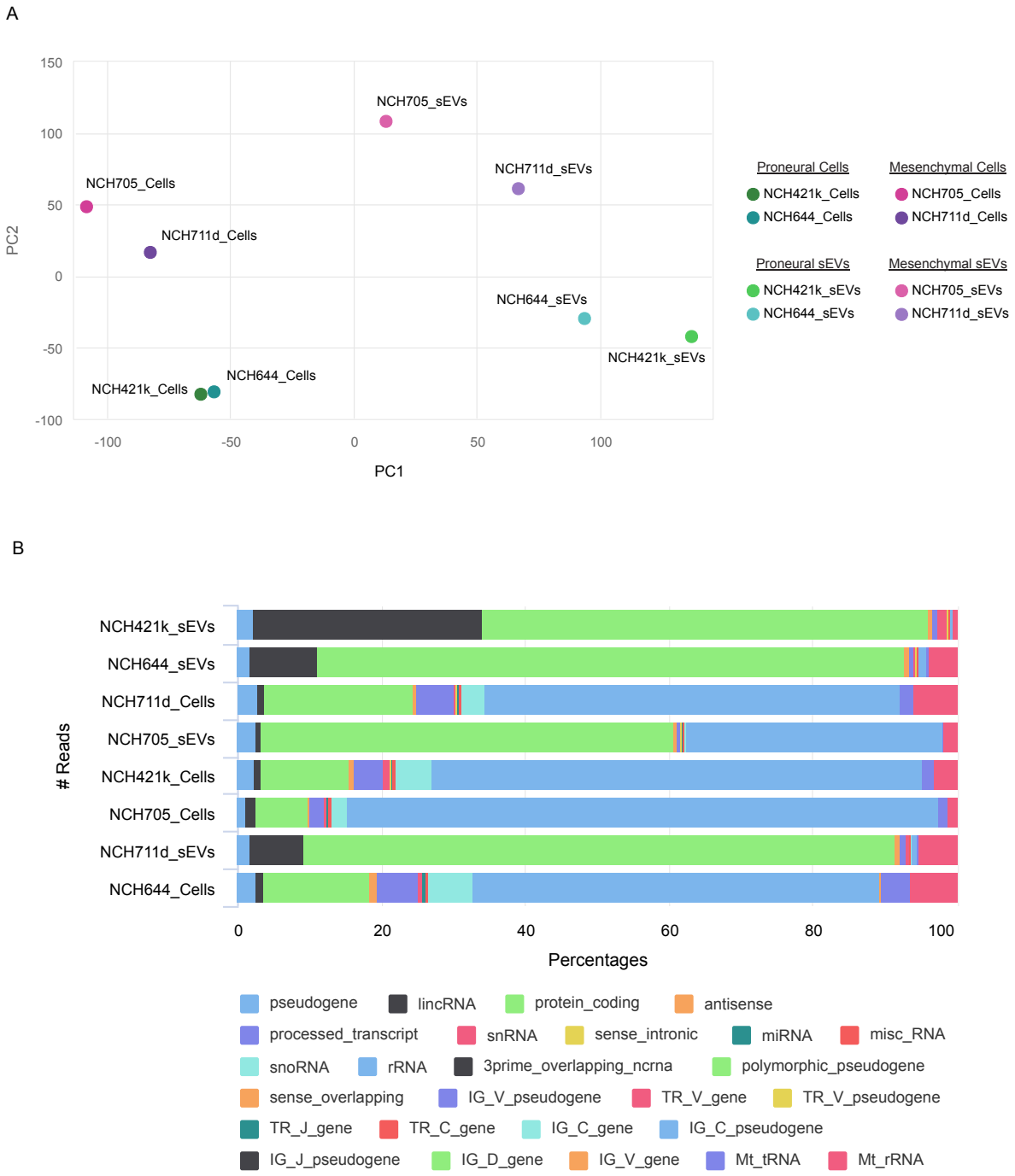

Figure 31. Small RNA sequencing of GSCs-derived sEVs and their parent cells

(A) Principal component analysis of small RNA sequencing data.
(B) Percentages of RNA reads mapping to different genomic features for sEVs and cell samples.

4. Discussion

Glioblastoma is the most common and lethal primary brain tumor of central nervous system, which is accounting for approximately half of primary malignant brain tumors. Despite the intensive treatment modalities including maximal safe surgery, irradiation and chemotherapy, the complete eradication of glioblastoma is still extremely challenging[36,37]. Many cell-intrinsic and cell-extrinsic factors such as genomic instability, changes in the gene expression, clonal evolution of tumor cells, epigenetic deregulation, and complex interactions between the tumor cells and neighboring stromal cells within the tumor stroma contribute to the aggressive nature of glioblastoma[45,46,49–52]. Over the past decades, several studies have focused on above mentioned factors to uncover the molecular and cellular outcomes of these alterations on aggressiveness and therapeutic resistance of glioblastoma. From those, tumor heterogeneity is one the most extensively studied aspect of glioblastoma, and still holds a lot to be discovered. Given that glioblastoma is an extremely aggressive tumor with the high level of intratumoral and intertumoral heterogeneity, and that glioblastoma cells intensively interact with each other to maintain their cellular function and increased aggressiveness, the contribution of glioblastoma-derived small extracellular vesicles (sEVs) to glioblastoma heterogeneity and plasticity was investigated by profiling their protein, metabolite, fatty acid, and small RNA contents, together with the cell lines they are sourced from.

To examine the role of small extracellular vesicles mediated delivery of proteins, metabolites, fatty acids, and small RNAs in glioblastoma heterogeneity, cell plasticity and aggressiveness, first patient-derived glioblastoma stem cells (NCH421k, NCH644, NCH705 and NCH711d) were classified into proneural and mesenchymal subtypes by comparing their gene expression profile with the published glioblastoma subtype signatures. It has been previously shown that glioblastoma stem cells are highly plastic and can transition from one subtype to another one dynamically, which is the phenomenon named as proneural-to-mesenchymal transition in glioblastoma[164]. This epithelial-to-mesenchymal like transition of glioblastoma cells raised the question whether sEVs from different glioblastoma subtypes contribute to the plastic and highly heterogenous nature of glioblastoma cells, making it extremely challenging to eradicate. To this end, using well characterized proneural (NCH421k and NCH644) and mesenchymal (NCH705 and NCH711d) GSC lines allowed us to better reveal the complex composition of glioblastoma sEVs, suggesting a highly regulated and efficient way of exchanging critical biomolecules (i.e., proteins, metabolites, fatty acids, small RNAs etc.) between the transcriptionally different subtypes of glioblastoma stem cells. Considering the well-known transition (PN-to-MES transition) and interactions between proneural and mesenchymal GSCs, in this project, only proneural and mesenchymal GSCs were used; however, the potential contribution of sEVs derived from classical (CL) subtype of glioblastoma to increased cell plasticity and heterogeneity cannot be excluded.

Previous studies in the functional and biological roles of GSCs-derived sEVs primarily focused on the interaction between glioblastoma and tumor microenvironment cells, revealing the modulation of tumor microenvironment (TME) via the secreted biomolecules in the form of extracellular vesicles. Supportively, the biological and functional consequences of exchanging certain cargos between tumor and surrounding normal cells via sEVs, such as increased tumor cell proliferation/growth, enhanced tumor viability and elevated migration/invasion capacity, have also been demonstrated in different cancer entities. However, cell-to-cell communication and trafficking of vesicular cargos between transcriptionally different glioblastoma cell populations have been sparsely investigated. Here in this project, it has been exhibited that PN GSCs treated with the complete conditioned medium of MES GSCs increased the CD44 abundance, which is a well-established mesenchymal marker in glioblastoma cells, thus giving a hint towards a potential transfer of soluble and/or vesicular factors between different subtypes of glioblastoma stem cells (GSCs). The fractionation/depletion of MES conditioned medium (Figure 13 and Supplementary Figure 1), together with flow cytometry (Figure 15) and confocal microscopy (Figure 16) based approaches further supported that GSC-derived sEVs can successfully be transferred from one subtype to another one.

Given that GSCs-derived sEVs can be internalized by other tumor cells, and that the uptake of tumor-derived sEVs could result in phenotypic changes in recipient cells, subsequent experiments first focused on establishing reliable sEVs separation and characterization techniques prior to profiling of protein, metabolite, fatty acid, and smRNA contents of GSC-secreted sEVs. Several studies have already uncovered that culturing conditions of cells, such as seeding density, incubation time, culture volume, and type of culture vessels (conventional cell culture dishes/flasks or bioreactor systems) have a great impact on biological and functional properties of extracellular vesicles. Furthermore, the effect of extracellular vesicle separation methods on physical and biological properties of exosomes has been reported repeatedly in many studies[165–168]. Considering the availability of different EV separation techniques including ultracentrifugation (UC), size-exclusion chromatography (SEC), immunoaffinity (IA) capture, ultrafiltration (UF) and precipitation, the optimal separation methods should be selected considering the scientific aim and downstream applications[61,169,170]. To this end, in this project, culturing conditions of GSCs, details of conditioned medium harvesting, specifications of sEVs separation method used, and the steps of sEVs characterization were clearly reported for the reliability and reproducibility of the results.

Over the past decades, tumor-derived sEVs have emerged as critical regulators of cell communication between cancer and the surrounding cells, and several studies focused on their biological and function role in cancer initiation, progression, metastasis, and therapy resistance[149]. Most particularly, along with the advances in mass spectrometry, proteomic studies in EVs have elucidated various roles of tumor-derived sEVs in different cancer entities, including glioblastoma[171,172]. However, protein content of sEVs derived from transcriptionally different subpopulation of glioblastoma stem cells and their contribution to

increased heterogeneity, plasticity and aggressiveness of glioblastoma cells have been sparsely investigated so far. Here, it has been clearly shown that GSCs-derived sEVs are enriched, as compared to the cells they are derived from, in proteins associated with the transmembrane transport of amino acids, carboxylic acids, and organic acids, making them useful sources of molecular mediators required for amino acid and fatty acid metabolism, which have been shown to be altered in glioblastoma. As amino acids are important components of energy metabolism, biosynthetic support, redox balance, and homeostasis, they are crucial for cancer cell viability and growth[173]. From those, glutamine is the most intriguing amino acid for rapidly proliferating cancer cells as it participates in tricarboxylic acid (TCA) cycle for mitochondrial ATP production[174]. It has been demonstrated that glutamine is also used in the biosynthesis of glutathione (GSH), nucleotides, and nonessential amino acids, and its deprivation limits cancer cell growth and triggers cell death in many cancers, including glioblastoma[174–177]. Glioblastoma cells have been shown to take up high amounts of glutamine as a source of α-ketoglutarate to support anaplerosis (replenishing TCA cycle intermediates), to generate ATP and reactive oxygen species (ROS) scavengers[174]. In addition, Restall et al. have demonstrated that GSCs expressing low level of astrocytic glutamate transporters (EAAT1 and EAAT2) are dependent on glutaminase (GLS) to maintain their intracellular glutamate level, and that depletion of GLS induces the amino acid deprivation response (AADR) pathway and cell death in GSCs[178]. In addition to glutamine, tumor promoting role of branched-chain amino acids (BCAAs), namely leucine, isoleucine, and valine, in glioblastoma has been uncovered by Tönjes et al. with the findings that inhibition of BCAA catabolic enzyme branched-chain amino acid transaminase 1 (BCAT1) reduced the growth of glioblastoma cells *in vivo*[179]. Furthermore, the dependence of glioblastoma cells on essential amino acid methionine to maintain their survival, proliferation, colony formation has also been demonstrated by Palanichamy et al. in 2016[180]. Like amino acid metabolism, the synthesis and catabolism of fatty acids (carboxylic acids with long aliphatic chains) are also deregulated in glioblastoma. The high expression of fatty acid synthesis genes fatty acid synthetase (FAS) and acetyl-CoA carboxylase (ACC) have been detected in glioblastoma and is associated with poor patient survival[181,182]. Moreover, Duman et al. have clearly demonstrated the dependence of glioblastoma cells on fatty acid metabolism by discovering tumor promoting role of acyl-CoA-binding protein (ACBP) in sustaining fatty acid oxidation in glioblastoma[159].

Interestingly in this project, several SLC (solute carrier)-type transporters, a family of proteins responsible for the transport of small molecules into cells, have been detected in GSCs-derived sEVs, including the ones belonging SLC1, SLC6, SLC7, and SLC38 families, which are considered as main transporters for glutamine. Besides, BCAT1 has also been identified in all triplicate samples of NCH421k and NCH705 sEVs, but not in NCH644 and NCH711d sEVs. In line with the previous studies showing elevated fatty acid metabolism and high expression of fatty acid synthetase (FAS) in glioblastoma cells, here GSCs-derived sEVs (NCH421k, NCH644, NCH705, and NCH711d sEVs, in all replicates) have also been found to harbor fatty acid synthetase, as well as acetyl-CoA carboxylase 1 (except NCH705 sEVs). Furthermore, acyl-CoA-binding protein (ACBP) has also been detected in all sEVs samples used

in our mass spectrometry-based proteome profiling. Collectively, these data indicate that sEVs are not just “cellular garbage bins”, but are convenient sources of proteins (i.e., transporters and metabolic enzymes) that GSCs might exploit to fuel their metabolic machineries, which ultimately results in tumor progression and aggressiveness. Given that GSCs-derived sEVs contain a wide range of proteins associated with the transport of amino acids, carboxylic acids, and organic acids, they can also be considered as an escape route for different subpopulation of glioblastoma cells in stress conditions, by exchanging these biomolecules to maintain their tumor-associated cellular activities.

In addition to the proteins that play a role in cellular metabolism of glioblastoma, proteins associated with the growth factor binding, such as insulin-like growth factor I (IGF1-) and transforming growth factor beta (TGF-β) binding, have also been identified in this study. It has been previously shown in various studies that several signaling pathways, for instance RTK/RAS/PI3K signalling, are deregulated in glioblastoma. These signalling pathways are often initiated by the binding of growth factors, such as epidermal growth factor (EGF), basic fibroblast growth factor (bFGF), vascular endothelial growth factor (VEGF), platelet-derived growth factor (PDGF), insulin-like growth factor (IGF), and transforming growth factor beta (TGF-β) to their receptors[183]. The enrichment of proteins that facilitate the binding of growth factors to their respective receptors in sEVs also suggest that GSCs-derived sEVs contribute to the pathogenesis and progression of glioblastoma by facilitating the initiation of key signaling pathways commonly deregulated in malignant gliomas.

In this study, it has also been demonstrated by GSEA using previously published glioblastoma subtype signatures[43] that GSCs-derived sEVs retain the subtype characteristics of their respective cell lines. In addition to potential contribution of this retained proteome profile to glioblastoma heterogeneity and plasticity by exchanging different sets of proteins between transcriptionally different cell populations, it also makes GSCs-derived sEVs potential biomarkers for the subtype classification of glioblastoma cells.

In line with the proteome profiling, metabolomic profiling of GSCs and GSCs-derived sEVs has also indicated that sEVs are loaded with the metabolites, which could be utilized by GSCs to fuel their highly active biosynthesis and energy metabolism. Recently, Sharpe et al. have demonstrated the expression of sugar transporters (Glut3 and Glut14, galactose transporters) and the metabolic remodeling in glioblastoma cells to use alternative nutrients for their growth and proliferation. Accordingly, they revealed that glioblastoma cells scavenge galactose from the extracellular space and metabolize it at physiological glucose concentrations by means of Leloir and pentose phosphate pathways, allowing them to use an alternative source of energy[184]. In line with these findings, metabolomic profiling of GSCs-derived sEVs in our study unveiled the enrichment of metabolites associated with the galactose metabolism, suggesting the role of tumor secreted sEVs in fuelling glioblastoma cells to enhance their ability to use alternative energy pathways to sustain their viability and proliferation. Supportively, the enrichment of fructose and mannose metabolism (another sugar related metabolic pathway) associated

metabolites has also been shown in NCH421k and NCH711d sEVs. Furthermore, NCH711d sEVs have been found to be enriched in metabolites functioning in starch and sucrose metabolism, further revealing the support of sEVs in glioblastoma energy metabolism. Moreover, in conjunction with proteome profiling, metabolite screening of GSCs-derived sEVs identified the presence of metabolites related to alanine, aspartate, glutamate metabolism and arginine biosynthesis in NCH421k-derived sEVs. The metabolites taking a part in carboxylic acid metabolism, namely butanoate metabolism here, have also been detected in NCH421k and NCH644 sEVs. Collectively, these data imply that GSCs-derived sEVs not only provide proteins facilitating the transport of amino acids and carboxylic acids to recipient cells, but also supply them with the metabolites that are used in amino acid and carboxylic acid metabolism, indicating their dual role in cellular metabolism of glioblastoma.

In addition to proteins and metabolites, emerging evidence have also uncovered tumor promoting roles of fatty acids in different cancer entities. For instance, the exposure of oral squamous cell carcinoma (OSCC) cells to palmitic acid results in robust increase in the percentage of $CD36^{+}$ metastasis-initiating cells, followed by high frequency of lymph node and lung metastases[185]. Similarly, palmitic acid has also been shown to promote the metastasis of gastric cancer cells through AKT/GSK-3β/β-catenin signaling pathway[186]. Interestingly, erythrocyte fatty acid monitoring in cancer patients indicated that high level of palmitic acid is associated with the colorectal cancer, breast cancer, advanced squamous cell lung carcinoma (SCC), lung adenocarcinoma (ADC) and small cell lung cancer (SCLC)[187]. In addition to increased level of palmitic acid in different human malignancies, significantly higher levels of stearic acid and cholesterol have also been found in breast and prostate cancers[188,189]. In breast cancer, the elevated level of stearic acid was found in tumor tissues compared with the adjacent normal tissues[189]. Furthermore, the high level of cholesterol in lipid rafts has been shown to promote tumor growth and diminish apoptosis in prostate cancer xenografts[190]. Moreover, the examination of superenhancer landscape of glioblastoma stem cells unveiled the epigenetic upregulation of ELOVL2 (elongation of very-long-chain fatty acids-like 2), a critical polyunsaturated fatty-acid synthesis enzyme[191]. ELOVL2 is responsible for the conversion of arachidonic acid (C20:4 AA) and eicosapentaenoic acid (C20:5 EPA) to the longer chain polyunsaturated fatty acids (LC-PUFAs) docosapentaenoic acid (C22:5 DPA) and docosahexaenoic acid (C22:6 DHA). Also, Gimple et al. elegantly discovered that GSCs use PUFA synthesis to maintain their membrane integrity, and that ELOVL2 is essential for the EGFR localization and signaling in glioblastoma cells. The inhibition of ELOVL2 was shown disrupted GSC proliferation and self-renewal and promoted apoptosis, further emphasizing the critical role of ELOVL2 in GSC maintenance[191]. In addition to GSCs, elevated level of PUFAs including arachidonic acid (20:4 n-6), dihomo-gamma-linolenic acid (20:3 n-6), docosapentaenoic acid (22:5 n-6), adrenic acid (22:4 n-6), alpha-linolenic acid (18:3 n-3), eicosapentaenoic acid (20:5 n-3), eicosatetraenoic acid (20:4 n-3), and docosahexaenoic acid (22:6 n-3) has also been determined in colorectal cancer tissues as compared to normal colorectal mucosa[192].

Given the above-mentioned functions of fatty acids in cancer and considering our findings that sEVs-derived proteins and metabolites potentially contribute glioblastoma aggressiveness, fatty acid content of GSCs-derived sEVs (reservoirs of fatty acids) and the potential roles of sEVs-derived fatty acids in glioblastoma cell plasticity, heterogeneity, and cellular metabolism have also been studied in this project. Interestingly, it has been unveiled that GSCs-derived sEVs, compared to their respective cell lines, were rich in saturated fatty acids (arachidic acid, behenic acid, stearic acid, palmitic acid, and lignoceric acid), whereas parent cells were enriched in monounsaturated (palmitoleic acid, elaidic acid, myristoleic acid, erucic acid, and nervonic acid) and polyunsaturated fatty acids (cis-4,7,10,13,16,19-DHA, arachidonic acid, eicosatrienoic acid, and cis-5,8,11,14,17-EPA), suggesting that loading of saturated fatty acids into sEVs might be a tightly regulated process. However, biological, functional, and structural reasons behind the preferential loading of saturated fatty acids into GSCs-derived sEVs remain highly elusive. On the other hand, in line with the proteomics and metabolomics data showing the enrichment of proteins and metabolites associated with the carboxylic acid transport and metabolism, profiling of fatty acids (carboxylic acids with long aliphatic chains) of GSCs-derived sEVs further revealed their importance in fueling tumor cells.

Finally, to shed some light on the role of sEVs-derived small RNAs in glioblastoma heterogeneity and aggressiveness, small RNA sequencing of GSCs-derived sEVs (together with their parent cells) was carried out using SMART (Switching Mechanism at the 5’ end of RNA Template) technology for library preparation. Even though high-throughput small RNA sequencing of GSCs and GSCs-derived sEVs revealed the subtype-dependent separation of small RNA profiles of cells and sEVs and identified some small RNA species in cells and sEVs samples, getting very low number of unique reads for different RNA species made the data not reliable for comparative analysis. The analysis of sequencing reads (data now shown) revealed over 80% duplications in all samples used, resulting in very low representation of RNAs. Considering the low complexity and representation, library preparation conditions should be optimized for the samples obtained from glioblastoma cells. In this direction, increasing the amount of starting material, optimization of number of PCR cycles, and implementing efficient size-selection steps could help to generate high quality sequencing libraries.

In conclusion, this study provided insights for the complexity of GSCs-derived sEVs by revealing their protein, metabolite, fatty acid, and smRNA contents, and demonstrated the potential contribution of GSCs-derived sEVs to the plasticity, heterogeneity, and aggressiveness of glioblastoma.

Future Perspectives

Despite the intense effort of developing new treatment modalities, complete eradication of glioblastoma is still extremely challenging. The inevitable relapse of glioblastoma is mainly attributed to the persistence of brain tumor initiating cells or glioblastoma stem cells (GSCs) in this context. The increased intratumoral and intertumoral heterogeneity of glioblastoma is considered as a major hurdle for the effective treatment of the disease. Several studies have revealed the sources of glioblastoma tumor heterogeneity and plasticity; however, the roles tumor-secreted sEVs have been sparsely investigated so far. Here, this project has provided valuable insights into heterogenous nature of glioblastoma by profiling protein, metabolite, fatty acid, and smRNA contents of GSCs and their sEVs.

To better understand the role and importance of sEVs mediated cell-to-cell communication in glioblastoma heterogeneity, cell plasticity, and cellular maintenance, further studies should focus on above discussed pathways and cellular processes that glioblastoma cells could exploit to maintain their malignant properties. Studies focusing on the inhibition and/or deprivation of the proteins, metabolites, and fatty acids playing direct or indirect roles in amino acid, carboxylic acid, and organic acid related pathways could pave the way of discovering novel targets, facilitating to develop new treatment modalities. Considering that this study emphasized the complexity of GSCs-derived sEVs and showed their potential contribution to increased heterogeneity of glioblastoma by transferring a wide range of biomolecules associated with the malignant pathways and cellular processes, future investigations on blocking tumor-derived sEVs biogenesis, secretion, and uptake could open a new avenue for glioblastoma therapy. Given that sEVs are also crucial for normal cells to maintain their homeostasis and cell communications, tumor-derived sEVs specific blocking approaches should be considered.

5. References

1. Lapointe, S., Perry, A. & Butowski, N. A. Primary brain tumours in adults. *Lancet* **392**, 432–446 (2018).

2. Louis, D. N. *et al.* The 2021 WHO Classification of Tumors of the Central Nervous System: a summary. *Neuro. Oncol.* (2021) doi:10.1093/neuonc/noab106.

3. Ostrom, Q. T. *et al.* CBTRUS Statistical Report: Primary Brain and Other Central Nervous System Tumors Diagnosed in the United States in 2013-2017. *Neuro. Oncol.* **22**, iv1–iv96 (2020).

4. Weller, M. *et al.* Glioma. *Nat. Rev. Dis. Prim.* **1**, 15017 (2015).

5. Aquilanti, E., Miller, J., Santagata, S., Cahill, D. P. & Brastianos, P. K. Updates in prognostic markers for gliomas. *Neuro. Oncol.* **20**, vii17–vii26 (2018).

6. Dang, L. *et al.* Cancer-associated IDH1 mutations produce 2-hydroxyglutarate. *Nature* **462**, 739–744 (2009).

7. Flavahan, W. A. *et al.* Insulator dysfunction and oncogene activation in IDH mutant gliomas. *Nature* **529**, 110–114 (2016).

8. Turcan, S. *et al.* IDH1 mutation is sufficient to establish the glioma hypermethylator phenotype. *Nature* **483**, 479–483 (2012).

9. Lu, C. *et al.* IDH mutation impairs histone demethylation and results in a block to cell differentiation. *Nature* **483**, 474–478 (2012).

10. Rohle, D. *et al.* An inhibitor of mutant IDH1 delays growth and promotes differentiation of glioma cells. *Science* **340**, 626–630 (2013).

11. Hartmann, C. *et al.* Type and frequency of IDH1 and IDH2 mutations are related to astrocytic and oligodendroglial differentiation and age: a study of 1,010 diffuse gliomas. *Acta Neuropathol.* **118**, 469–474 (2009).

12. Yan, H. *et al.* IDH1 and IDH2 mutations in gliomas. *N. Engl. J. Med.* **360**, 765–773 (2009).

13. Hartmann, C. *et al.* Patients with IDH1 wild type anaplastic astrocytomas exhibit worse prognosis than IDH1-mutated glioblastomas, and IDH1 mutation status accounts for the unfavorable prognostic effect of higher age: implications for classification of gliomas. *Acta Neuropathol.* **120**, 707–718 (2010).

14. Bettegowda, C. *et al.* Mutations in CIC and FUBP1 contribute to human oligodendroglioma. *Science* **333**, 1453–1455 (2011).

15. van den Bent, M. J. *et al.* Adjuvant procarbazine, lomustine, and vincristine chemotherapy in newly diagnosed anaplastic oligodendroglioma: long-term follow-up of EORTC brain tumor group study 26951. *J. Clin. Oncol. Off. J. Am. Soc. Clin. Oncol.* **31**, 344–350 (2013).

16. Jenkins, R. B. *et al.* A t(1;19)(q10;p10) mediates the combined deletions of 1p and 19q and predicts a better prognosis of patients with oligodendroglioma. *Cancer Res.* **66**, 9852–9861 (2006).

17. Zawlik, I. *et al.* Promoter methylation and polymorphisms of the MGMT gene in glioblastomas: a population-based study. *Neuroepidemiology* **32**, 21–29 (2009).

18. Hegi, M. E. *et al.* MGMT gene silencing and benefit from temozolomide in glioblastoma. *N. Engl.*

J. Med. **352**, 997–1003 (2005).

19. Hegi, M. E. *et al.* Correlation of O6-methylguanine methyltransferase (MGMT) promoter methylation with clinical outcomes in glioblastoma and clinical strategies to modulate MGMT activity. *J. Clin. Oncol. Off. J. Am. Soc. Clin. Oncol.* **26**, 4189–4199 (2008).

20. Deaton, A. M. & Bird, A. CpG islands and the regulation of transcription. *Genes Dev.* **25**, 1010–1022 (2011).

21. Nazemalhosseini Mojarad, E., Kuppen, P. J., Aghdaei, H. A. & Zali, M. R. The CpG island methylator phenotype (CIMP) in colorectal cancer. *Gastroenterol. Hepatol. from bed to bench* **6**, 120–128 (2013).

22. Noushmehr, H. *et al.* Identification of a CpG Island Methylator Phenotype that Defines a Distinct Subgroup of Glioma. *Cancer Cell* **17**, 510–522 (2010).

23. Trybek, T., Kowalik, A., Góźdź, S. & Kowalska, A. Telomeres and telomerase in oncogenesis. *Oncol. Lett.* **20**, 1015–1027 (2020).

24. Eckel-Passow, J. E. *et al.* Glioma Groups Based on 1p/19q, IDH, and TERT Promoter Mutations in Tumors. *N. Engl. J. Med.* **372**, 2499–2508 (2015).

25. Killela, P. J. *et al.* TERT promoter mutations occur frequently in gliomas and a subset of tumors derived from cells with low rates of self-renewal. *Proc. Natl. Acad. Sci. U. S. A.* **110**, 6021–6026 (2013).

26. Brennan, C. W. *et al.* The Somatic Genomic Landscape of Glioblastoma. *Cell* **155**, 462–477 (2013).

27. Ceccarelli, M. *et al.* Molecular Profiling Reveals Biologically Discrete Subsets and Pathways of Progression in Diffuse Glioma. *Cell* **164**, 550–563 (2016).

28. Wen, P. Y. & Kesari, S. Malignant gliomas in adults. *N. Engl. J. Med.* **359**, 492–507 (2008).

29. Felsberg, J. *et al.* Epidermal Growth Factor Receptor Variant III (EGFRvIII) Positivity in EGFR-Amplified Glioblastomas: Prognostic Role and Comparison between Primary and Recurrent Tumors. *Clin. cancer Res. an Off. J. Am. Assoc. Cancer Res.* **23**, 6846–6855 (2017).

30. Li, J., Liang, R., Song, C., Xiang, Y. & Liu, Y. Prognostic significance of epidermal growth factor receptor expression in glioma patients. *Onco. Targets. Ther.* **11**, 731–742 (2018).

31. Ellison, D. W. *et al.* cIMPACT-NOW update 4: diffuse gliomas characterized by MYB, MYBL1, or FGFR1 alterations or BRAF(V600E) mutation. *Acta neuropathologica* vol. 137 683–687 (2019).

32. Vuong, H. G. *et al.* BRAF Mutation is Associated with an Improved Survival in Glioma-a Systematic Review and Meta-analysis. *Mol. Neurobiol.* **55**, 3718–3724 (2018).

33. Mackay, A. *et al.* Integrated Molecular Meta-Analysis of 1,000 Pediatric High-Grade and Diffuse Intrinsic Pontine Glioma. *Cancer Cell* **32**, 520-537.e5 (2017).

34. Meyronet, D. *et al.* Characteristics of H3 K27M-mutant gliomas in adults. *Neuro. Oncol.* **19**, 1127–1134 (2017).

35. Karremann, M. *et al.* Diffuse high-grade gliomas with H3 K27M mutations carry a dismal prognosis independent of tumor location. *Neuro. Oncol.* **20**, 123–131 (2018).

36. Ostrom, Q. T. *et al.* CBTRUS Statistical Report: Primary Brain and Other Central Nervous System Tumors Diagnosed in the United States in 2012-2016. *Neuro. Oncol.* **21**, v1–v100 (2019).

37. Thakkar, J. P. *et al.* Epidemiologic and Molecular Prognostic Review of Glioblastoma. *Cancer Epidemiol. Biomarkers & Prev.* **23**, 1985 LP – 1996 (2014).

38. Ohgaki, H. & Kleihues, P. The Definition of Primary and Secondary Glioblastoma. *Clin. Cancer Res.* **19**, 764 LP – 772 (2013).

39. Ohgaki, H. & Kleihues, P. Genetic Pathways to Primary and Secondary Glioblastoma. *Am. J. Pathol.* **170**, 1445–1453 (2007).

40. McLendon, R. *et al.* Comprehensive genomic characterization defines human glioblastoma genes and core pathways. *Nature* **455**, 1061–1068 (2008).

41. Zheng, S., Chheda, M. G. & Verhaak, R. G. W. Studying a complex tumor: potential and pitfalls. *Cancer J.* **18**, 107–114 (2012).

42. Phillips, H. S. *et al.* Molecular subclasses of high-grade glioma predict prognosis, delineate a pattern of disease progression, and resemble stages in neurogenesis. *Cancer Cell* **9**, 157–173 (2006).

43. Verhaak, R. G. W. *et al.* Integrated Genomic Analysis Identifies Clinically Relevant Subtypes of Glioblastoma Characterized by Abnormalities in PDGFRA, IDH1, EGFR, and NF1. *Cancer Cell* **17**, 98–110 (2010).

44. Wang, Q. *et al.* Tumor Evolution of Glioma-Intrinsic Gene Expression Subtypes Associates with Immunological Changes in the Microenvironment. *Cancer Cell* **32**, 42-56.e6 (2017).

45. Lawson, D. A., Kessenbrock, K., Davis, R. T., Pervolarakis, N. & Werb, Z. Tumour heterogeneity and metastasis at single-cell resolution. *Nat. Cell Biol.* **20**, 1349–1360 (2018).

46. Qazi, M. A. *et al.* Intratumoral heterogeneity: pathways to treatment resistance and relapse in human glioblastoma. *Ann. Oncol.* **28**, 1448–1456 (2017).

47. Dagogo-Jack, I. & Shaw, A. T. Tumour heterogeneity and resistance to cancer therapies. *Nat. Rev. Clin. Oncol.* **15**, 81–94 (2018).

48. Sun, X. & Yu, Q. Intra-tumor heterogeneity of cancer cells and its implications for cancer treatment. *Acta Pharmacol. Sin.* **36**, 1219–1227 (2015).

49. Patel, A. P. *et al.* Single-cell RNA-seq highlights intratumoral heterogeneity in primary glioblastoma. *Science* **344**, 1396–1401 (2014).

50. Little, S. E. *et al.* Receptor tyrosine kinase genes amplified in glioblastoma exhibit a mutual exclusivity in variable proportions reflective of individual tumor heterogeneity. *Cancer Res.* **72**, 1614–1620 (2012).

51. Francis, J. M. *et al.* EGFR variant heterogeneity in glioblastoma resolved through single-nucleus sequencing. *Cancer Discov.* **4**, 956–971 (2014).

52. Meyer, M. *et al.* Single cell-derived clonal analysis of human glioblastoma links functional and genomic heterogeneity. *Proc. Natl. Acad. Sci.* **112**, 851 LP – 856 (2015).

53. Kim, H. *et al.* Whole-genome and multisector exome sequencing of primary and post-treatment glioblastoma reveals patterns of tumor evolution. *Genome Res.* **25**, 316–327 (2015).

54. Kim, J. *et al.* Spatiotemporal Evolution of the Primary Glioblastoma Genome. *Cancer Cell* **28**, 318–328 (2015).

55. Laperriere, N., Zuraw, L. & Cairncross, G. Radiotherapy for newly diagnosed malignant glioma in

adults: a systematic review. *Radiother. Oncol.* **64**, 259–273 (2002).

56. Stupp, R. *et al.* Radiotherapy plus Concomitant and Adjuvant Temozolomide for Glioblastoma. *N. Engl. J. Med.* **352**, 987–996 (2005).

57. Hart, M. G., Garside, R., Rogers, G., Stein, K. & Grant, R. Temozolomide for high grade glioma. *Cochrane database Syst. Rev.* **2013**, CD007415–CD007415 (2013).

58. Stupp, R. *et al.* Effects of radiotherapy with concomitant and adjuvant temozolomide versus radiotherapy alone on survival in glioblastoma in a randomised phase III study: 5-year analysis of the EORTC-NCIC trial. *Lancet Oncol.* **10**, 459–466 (2009).

59. Weller, M. *et al.* EANO guideline for the diagnosis and treatment of anaplastic gliomas and glioblastoma. *Lancet Oncol.* **15**, e395–e403 (2014).

60. Weller, M., Cloughesy, T., Perry, J. R. & Wick, W. Standards of care for treatment of recurrent glioblastoma--are we there yet? *Neuro. Oncol.* **15**, 4–27 (2013).

61. Théry, C. *et al.* Minimal information for studies of extracellular vesicles 2018 (MISEV2018): a position statement of the International Society for Extracellular Vesicles and update of the MISEV2014 guidelines. *J. Extracell. Vesicles* **7**, 1535750 (2018).

62. Möller, A. & Lobb, R. J. The evolving translational potential of small extracellular vesicles in cancer. *Nat. Rev. Cancer* **20**, 697–709 (2020).

63. van Niel, G., D'Angelo, G. & Raposo, G. Shedding light on the cell biology of extracellular vesicles. *Nat. Rev. Mol. Cell Biol.* **19**, 213–228 (2018).

64. Mathieu, M., Martin-Jaular, L., Lavieu, G. & Théry, C. Specificities of secretion and uptake of exosomes and other extracellular vesicles for cell-to-cell communication. *Nat. Cell Biol.* **21**, 9–17 (2019).

65. Takahashi, A. *et al.* Exosomes maintain cellular homeostasis by excreting harmful DNA from cells. *Nat. Commun.* **8**, 15287 (2017).

66. Kahlert, C. & Kalluri, R. Exosomes in tumor microenvironment influence cancer progression and metastasis. *J. Mol. Med. (Berl).* **91**, 431–437 (2013).

67. Cocozza, F., Grisard, E., Martin-Jaular, L., Mathieu, M. & Théry, C. SnapShot: Extracellular Vesicles. *Cell* **182**, 262-262.e1 (2020).

68. Kalluri, R. & LeBleu, V. S. The biology, function, and biomedical applications of exosomes. *Science* **367**, (2020).

69. Yáñez-Mó, M. *et al.* Biological properties of extracellular vesicles and their physiological functions. *J. Extracell. Vesicles* **4**, 27066 (2015).

70. Hurley, J. H. ESCRT complexes and the biogenesis of multivesicular bodies. *Curr. Opin. Cell Biol.* **20**, 4–11 (2008).

71. Baietti, M. F. *et al.* Syndecan–syntenin–ALIX regulates the biogenesis of exosomes. *Nat. Cell Biol.* **14**, 677–685 (2012).

72. Stuffers, S., Sem Wegner, C., Stenmark, H. & Brech, A. Multivesicular Endosome Biogenesis in the Absence of ESCRTs. *Traffic* **10**, 925–937 (2009).

73. Trajkovic, K. *et al.* Ceramide triggers budding of exosome vesicles into multivesicular endosomes. *Science* **319**, 1244–1247 (2008).

74. Gulbins, E. & Kolesnick, R. Raft ceramide in molecular medicine. *Oncogene* **22**, 7070–7077 (2003).

75. Zerial, M. & McBride, H. Rab proteins as membrane organizers. *Nat. Rev. Mol. Cell Biol.* **2**, 107–117 (2001).

76. Seabra, M. C., Mules, E. H. & Hume, A. N. Rab GTPases, intracellular traffic and disease. *Trends Mol. Med.* **8**, 23–30 (2002).

77. Ostrowski, M. *et al.* Rab27a and Rab27b control different steps of the exosome secretion pathway. *Nat. Cell Biol.* **12**, 19–30 (2010).

78. Savina, A., Fader, C. M., Damiani, M. T. & Colombo, M. I. Rab11 promotes docking and fusion of multivesicular bodies in a calcium-dependent manner. *Traffic* **6**, 131–143 (2005).

79. Messenger, S. W., Woo, S. S., Sun, Z. & Martin, T. F. J. A Ca2+-stimulated exosome release pathway in cancer cells is regulated by Munc13-4. *J. Cell Biol.* **217**, 2877–2890 (2018).

80. Hsu, C. *et al.* Regulation of exosome secretion by Rab35 and its GTPase-activating proteins TBC1D10A-C. *J. Cell Biol.* **189**, 223–232 (2010).

81. Gross, J. C., Chaudhary, V., Bartscherer, K. & Boutros, M. Active Wnt proteins are secreted on exosomes. *Nat. Cell Biol.* **14**, 1036–1045 (2012).

82. Ruiz-Martinez, M. *et al.* YKT6 expression, exosome release, and survival in non-small cell lung cancer. *Oncotarget* **7**, 51515–51524 (2016).

83. Koles, K. *et al.* Mechanism of evenness interrupted (Evi)-Exosome Release at synaptic boutons. *J. Biol. Chem.* **287**, 16820–16834 (2012).

84. Hyenne, V. *et al.* RAL-1 controls multivesicular body biogenesis and exosome secretion. *J. Cell Biol.* **211**, 27–37 (2015).

85. Wei, Y. *et al.* Pyruvate kinase type M2 promotes tumour cell exosome release via phosphorylating synaptosome-associated protein 23. *Nat. Commun.* **8**, 14041 (2017).

86. Verweij, F. J. *et al.* Quantifying exosome secretion from single cells reveals a modulatory role for GPCR signaling. *J. Cell Biol.* **217**, 1129–1142 (2018).

87. Sedgwick, A. E. & D'Souza-Schorey, C. The biology of extracellular microvesicles. *Traffic* **19**, 319–327 (2018).

88. Granger, E., McNee, G., Allan, V. & Woodman, P. The role of the cytoskeleton and molecular motors in endosomal dynamics. *Semin. Cell Dev. Biol.* **31**, 20–29 (2014).

89. Mathieu, M., Martin-Jaular, L., Lavieu, G. & Théry, C. Specificities of secretion and uptake of exosomes and other extracellular vesicles for cell-to-cell communication. *Nat. Cell Biol.* **21**, 9–17 (2019).

90. Wiklander, O. P. B., Brennan, M. Á., Lötvall, J., Breakefield, X. O. & EL Andaloussi, S. Advances in therapeutic applications of extracellular vesicles. *Sci. Transl. Med.* **11**, eaav8521 (2019).

91. Morelli, A. E. *et al.* Endocytosis, intracellular sorting, and processing of exosomes by dendritic cells. *Blood* **104**, 3257–3266 (2004).

92. Leiss, M., Beckmann, K., Girós, A., Costell, M. & Fässler, R. The role of integrin binding sites in fibronectin matrix assembly in vivo. *Curr. Opin. Cell Biol.* **20**, 502–507 (2008).

93. Purushothaman, A. *et al.* Fibronectin on the Surface of Myeloma Cell-derived Exosomes Mediates Exosome-Cell Interactions. *J. Biol. Chem.* **291**, 1652–1663 (2016).

94. Sung, B. H., Ketova, T., Hoshino, D., Zijlstra, A. & Weaver, A. M. Directional cell movement through tissues is controlled by exosome secretion. *Nat. Commun.* **6**, 7164 (2015).

95. Melo, S. A. *et al.* Glypican-1 identifies cancer exosomes and detects early pancreatic cancer. *Nature* **523**, 177–182 (2015).

96. Bruno, S. *et al.* Mesenchymal stem cell-derived microvesicles protect against acute tubular injury. *J. Am. Soc. Nephrol.* **20**, 1053–1067 (2009).

97. Kwok, Z. H., Wang, C. & Jin, Y. Extracellular Vesicle Transportation and Uptake by Recipient Cells: A Critical Process to Regulate Human Diseases. *Processes* vol. 9 (2021).

98. Escrevente, C., Keller, S., Altevogt, P. & Costa, J. Interaction and uptake of exosomes by ovarian cancer cells. *BMC Cancer* **11**, 108 (2011).

99. Mulcahy, L. A., Pink, R. C. & Carter, D. R. F. Routes and mechanisms of extracellular vesicle uptake. *J. Extracell. vesicles* **3**, 10.3402/jev.v3.24641 (2014).

100. Batlle, E. & Clevers, H. Cancer stem cells revisited. *Nat. Med.* **23**, 1124–1134 (2017).

101. Singh, S. K. *et al.* Identification of human brain tumour initiating cells. *Nature* **432**, 396–401 (2004).

102. Chen, J. *et al.* A restricted cell population propagates glioblastoma growth after chemotherapy. *Nature* **488**, 522–526 (2012).

103. Liau, B. B. *et al.* Adaptive Chromatin Remodeling Drives Glioblastoma Stem Cell Plasticity and Drug Tolerance. *Cell Stem Cell* **20**, 233-246.e7 (2017).

104. Bao, S. *et al.* Glioma stem cells promote radioresistance by preferential activation of the DNA damage response. *Nature* **444**, 756–760 (2006).

105. Wang, J. *et al.* Notch promotes radioresistance of glioma stem cells. *Stem Cells* **28**, 17–28 (2010).

106. Rheinbay, E. *et al.* An aberrant transcription factor network essential for Wnt signaling and stem cell maintenance in glioblastoma. *Cell Rep.* **3**, 1567–1579 (2013).

107. Vlashi, E. *et al.* Metabolic state of glioma stem cells and nontumorigenic cells. *Proc. Natl. Acad. Sci. U. S. A.* **108**, 16062–16067 (2011).

108. Abou-Antoun, T. J., Hale, J. S., Lathia, J. D. & Dombrowski, S. M. Brain Cancer Stem Cells in Adults and Children: Cell Biology and Therapeutic Implications. *Neurotherapeutics* **14**, 372–384 (2017).

109. Fanelli, G. N., Naccarato, A. G. & Scatena, C. Recent Advances in Cancer Plasticity: Cellular Mechanisms, Surveillance Strategies, and Therapeutic Optimization. *Front. Oncol.* **10**, 569 (2020).

110. Boumahdi, S. & de Sauvage, F. J. The great escape: tumour cell plasticity in resistance to targeted therapy. *Nat. Rev. Drug Discov.* **19**, 39–56 (2020).

111. Shibue, T. & Weinberg, R. A. EMT, CSCs, and drug resistance: the mechanistic link and clinical implications. *Nat. Rev. Clin. Oncol.* **14**, 611–629 (2017).

112. Jin, X. *et al.* Frizzled 4 Regulates Stemness and Invasiveness of Migrating Glioma Cells

Established by Serial Intracranial Transplantation. *Cancer Res.* **71**, 3066 LP – 3075 (2011).

113. Lu, K. V *et al.* VEGF inhibits tumor cell invasion and mesenchymal transition through a MET/VEGFR2 complex. *Cancer Cell* **22**, 21–35 (2012).

114. Kahlert, U. D. *et al.* Activation of canonical WNT/β-catenin signaling enhances in vitro motility of glioblastoma cells by activation of ZEB1 and other activators of epithelial-to-mesenchymal transition. *Cancer Lett.* **325**, 42–53 (2012).

115. Sharma, S. V *et al.* A chromatin-mediated reversible drug-tolerant state in cancer cell subpopulations. *Cell* **141**, 69–80 (2010).

116. Ravindran Menon, D. *et al.* A stress-induced early innate response causes multidrug tolerance in melanoma. *Oncogene* **34**, 4448–4459 (2015).

117. Touil, Y. *et al.* Colon cancer cells escape 5FU chemotherapy-induced cell death by entering stemness and quiescence associated with the c-Yes/YAP axis. *Clin. cancer Res. an Off. J. Am. Assoc. Cancer Res.* **20**, 837–846 (2014).

118. Jin, X. *et al.* Targeting glioma stem cells through combined BMI1 and EZH2 inhibition. *Nat. Med.* **23**, 1352–1361 (2017).

119. Bastola, S. *et al.* Glioma-initiating cells at tumor edge gain signals from tumor core cells to promote their malignancy. *Nat. Commun.* **11**, 4660 (2020).

120. Minata, M. *et al.* Phenotypic Plasticity of Invasive Edge Glioma Stem-like Cells in Response to Ionizing Radiation. *Cell Rep.* **26**, 1893-1905.e7 (2019).

121. Puchalski, R. B. *et al.* An anatomic transcriptional atlas of human glioblastoma. *Science (80-.).* **360**, 660 LP – 663 (2018).

122. Dominiak, A., Chełstowska, B., Olejarz, W. & Nowicka, G. Communication in the Cancer Microenvironment as a Target for Therapeutic Interventions. *Cancers (Basel).* **12**, 1232 (2020).

123. Dranoff, G. Cytokines in cancer pathogenesis and cancer therapy. *Nat. Rev. Cancer* **4**, 11–22 (2004).

124. Skog, J. *et al.* Glioblastoma microvesicles transport RNA and proteins that promote tumour growth and provide diagnostic biomarkers. *Nat. Cell Biol.* **10**, 1470–1476 (2008).

125. Al-Nedawi, K. *et al.* Intercellular transfer of the oncogenic receptor EGFRvIII by microvesicles derived from tumour cells. *Nat. Cell Biol.* **10**, 619–624 (2008).

126. Ricklefs, F. L. *et al.* Immune evasion mediated by PD-L1 on glioblastoma-derived extracellular vesicles. *Sci. Adv.* **4**, eaar2766 (2018).

127. Maas, S. L. N., Breakefield, X. O. & Weaver, A. M. Extracellular Vesicles: Unique Intercellular Delivery Vehicles. *Trends Cell Biol.* **27**, 172–188 (2017).

128. Zomer, A. *et al.* In Vivo Imaging Reveals Extracellular Vesicle-Mediated Phenocopying of Metastatic Behavior. *Cell* **161**, 1046–1057 (2015).

129. Luga, V. *et al.* Exosomes Mediate Stromal Mobilization of Autocrine Wnt-PCP Signaling in Breast Cancer Cell Migration. *Cell* **151**, 1542–1556 (2012).

130. Hoshino, A. *et al.* Tumour exosome integrins determine organotropic metastasis. *Nature* **527**, 329–335 (2015).

131. Mu, W., Rana, S. & Zöller, M. Host matrix modulation by tumor exosomes promotes motility and invasiveness. *Neoplasia* **15**, 875–887 (2013).

132. Sedgwick, A. E., Clancy, J. W., Olivia Balmert, M. & D'Souza-Schorey, C. Extracellular microvesicles and invadopodia mediate non-overlapping modes of tumor cell invasion. *Sci. Rep.* **5**, 14748 (2015).

133. Clancy, J. W. *et al.* Regulated delivery of molecular cargo to invasive tumour-derived microvesicles. *Nat. Commun.* **6**, 6919 (2015).

134. Hoshino, D. *et al.* Exosome Secretion Is Enhanced by Invadopodia and Drives Invasive Behavior. *Cell Rep.* **5**, 1159–1168 (2013).

135. Hanahan, D. & Weinberg, R. A. Hallmarks of cancer: the next generation. *Cell* **144**, 646–674 (2011).

136. Zomer, A. & van Rheenen, J. Implications of Extracellular Vesicle Transfer on Cellular Heterogeneity in Cancer: What Are the Potential Clinical Ramifications? *Cancer Res.* **76**, 2071–2075 (2016).

137. Quail, D. F. & Joyce, J. A. The Microenvironmental Landscape of Brain Tumors. *Cancer Cell* **31**, 326–341 (2017).

138. Al-Nedawi, K., Meehan, B., Kerbel, R. S., Allison, A. C. & Rak, J. Endothelial expression of autocrine VEGF upon the uptake of tumor-derived microvesicles containing oncogenic EGFR. *Proc. Natl. Acad. Sci. U. S. A.* **106**, 3794–3799 (2009).

139. Kucharzewska, P. *et al.* Exosomes reflect the hypoxic status of glioma cells and mediate hypoxia-dependent activation of vascular cells during tumor development. *Proc. Natl. Acad. Sci. U. S. A.* **110**, 7312–7317 (2013).

140. Webber, J. P. *et al.* Differentiation of tumour-promoting stromal myofibroblasts by cancer exosomes. *Oncogene* **34**, 290–302 (2015).

141. Graeber, M. B., Scheithauer, B. W. & Kreutzberg, G. W. Microglia in brain tumors. *Glia* **40**, 252–259 (2002).

142. Noy, R. & Pollard, J. W. Tumor-associated macrophages: from mechanisms to therapy. *Immunity* **41**, 49–61 (2014).

143. de Vrij, J. *et al.* Glioblastoma-derived extracellular vesicles modify the phenotype of monocytic cells. *Int. J. Cancer* **137**, 1630–1642 (2015).

144. van der Vos, K. E. *et al.* Directly visualized glioblastoma-derived extracellular vesicles transfer RNA to microglia/macrophages in the brain. *Neuro. Oncol.* **18**, 58–69 (2016).

145. Gao, Y. *et al.* Metastasis Organotropism: Redefining the Congenial Soil. *Dev. Cell* **49**, 375–391 (2019).

146. Chen, W., Hoffmann, A. D., Liu, H. & Liu, X. Organotropism: new insights into molecular mechanisms of breast cancer metastasis. *npj Precis. Oncol.* **2**, 4 (2018).

147. Peinado, H. *et al.* Melanoma exosomes educate bone marrow progenitor cells toward a pro-metastatic phenotype through MET. *Nat. Med.* **18**, 883–891 (2012).

148. Costa-Silva, B. *et al.* Pancreatic cancer exosomes initiate pre-metastatic niche formation in the liver. *Nat. Cell Biol.* **17**, 816–826 (2015).

149. Becker, A. *et al.* Extracellular Vesicles in Cancer: Cell-to-Cell Mediators of Metastasis. *Cancer Cell* **30**, 836–848 (2016).

150. Xia, J. & Wishart, D. S. Using MetaboAnalyst 3.0 for Comprehensive Metabolomics Data Analysis. *Curr. Protoc. Bioinforma.* **55**, 14.10.1-14.10.91 (2016).

151. Warburg, O., Wind, F. & Negelein, E. THE METABOLISM OF TUMORS IN THE BODY. *J. Gen. Physiol.* **8**, 519–530 (1927).

152. Pavlova, N. N. & Thompson, C. B. The Emerging Hallmarks of Cancer Metabolism. *Cell Metab.* **23**, 27–47 (2016).

153. Agnihotri, S. & Zadeh, G. Metabolic reprogramming in glioblastoma: the influence of cancer metabolism on epigenetics and unanswered questions. *Neuro. Oncol.* **18**, 160–172 (2016).

154. Bi, J. *et al.* Altered cellular metabolism in gliomas — an emerging landscape of actionable co-dependency targets. *Nat. Rev. Cancer* **20**, 57–70 (2020).

155. Marin-Valencia, I. *et al.* Analysis of tumor metabolism reveals mitochondrial glucose oxidation in genetically diverse human glioblastomas in the mouse brain in vivo. *Cell Metab.* **15**, 827–837 (2012).

156. Strickland, M. & Stoll, E. A. Metabolic Reprogramming in Glioma . *Frontiers in Cell and Developmental Biology* vol. 5 43 (2017).

157. Prabhu, A. H. *et al.* Integrative cross-platform analyses identify enhanced heterotrophy as a metabolic hallmark in glioblastoma. *Neuro. Oncol.* **21**, 337–347 (2019).

158. Lin, H. *et al.* Fatty acid oxidation is required for the respiration and proliferation of malignant glioma cells. *Neuro. Oncol.* **19**, 43–54 (2017).

159. Duman, C. *et al.* Acyl-CoA-Binding Protein Drives Glioblastoma Tumorigenesis by Sustaining Fatty Acid Oxidation. *Cell Metab.* **30**, 274-289.e5 (2019).

160. Haraszti, R. A. *et al.* High-resolution proteomic and lipidomic analysis of exosomes and microvesicles from different cell sources. *J. Extracell. vesicles* **5**, 32570 (2016).

161. Record, M., Subra, C., Silvente-Poirot, S. & Poirot, M. Exosomes as intercellular signalosomes and pharmacological effectors. *Biochem. Pharmacol.* **81**, 1171–1182 (2011).

162. Subra, C. *et al.* Exosomes account for vesicle-mediated transcellular transport of activatable phospholipases and prostaglandins[S]. *J. Lipid Res.* **51**, 2105–2120 (2010).

163. Wei, Z. *et al.* Coding and noncoding landscape of extracellular RNA released by human glioma stem cells. *Nat. Commun.* **8**, 1145 (2017).

164. Bhat, K. P. L. *et al.* Mesenchymal Differentiation Mediated by NF-κB Promotes Radiation Resistance in Glioblastoma. *Cancer Cell* **24**, 331–346 (2013).

165. Stranska, R. *et al.* Comparison of membrane affinity-based method with size-exclusion chromatography for isolation of exosome-like vesicles from human plasma. *J. Transl. Med.* **16**, 1 (2018).

166. Lobb, R. J. *et al.* Optimized exosome isolation protocol for cell culture supernatant and human plasma. *J. Extracell. Vesicles* **4**, 27031 (2015).

167. Konoshenko, M. Y., Lekchnov, E. A., Vlassov, A. V & Laktionov, P. P. Isolation of Extracellular Vesicles: General Methodologies and Latest Trends. *Biomed Res. Int.* **2018**, 8545347 (2018).

168. Palviainen, M. *et al.* Metabolic signature of extracellular vesicles depends on the cell culture conditions. *J. Extracell. vesicles* **8**, 1596669 (2019).

169. Zhang, Y. *et al.* Exosome: A Review of Its Classification, Isolation Techniques, Storage, Diagnostic and Targeted Therapy Applications. *Int. J. Nanomedicine* **15**, 6917–6934 (2020).

170. Liangsupree, T., Multia, E. & Riekkola, M.-L. Modern isolation and separation techniques for extracellular vesicles. *J. Chromatogr. A* **1636**, 461773 (2021).

171. Bandu, R., Oh, J. W. & Kim, K. P. Mass spectrometry-based proteome profiling of extracellular vesicles and their roles in cancer biology. *Exp. Mol. Med.* **51**, 1–10 (2019).

172. Ricklefs, F. *et al.* Extracellular vesicles from high-grade glioma exchange diverse pro-oncogenic signals that maintain intratumoral heterogeneity. *Cancer Res.* **76**, 2876–2881 (2016).

173. Lieu, E. L., Nguyen, T., Rhyne, S. & Kim, J. Amino acids in cancer. *Exp. Mol. Med.* **52**, 15–30 (2020).

174. Yoo, H. C., Yu, Y. C., Sung, Y. & Han, J. M. Glutamine reliance in cell metabolism. *Exp. Mol. Med.* **52**, 1496–1516 (2020).

175. Qing, G. *et al.* ATF4 regulates MYC-mediated neuroblastoma cell death upon glutamine deprivation. *Cancer Cell* **22**, 631–644 (2012).

176. Chen, L. & Cui, H. Targeting Glutamine Induces Apoptosis: A Cancer Therapy Approach. *International Journal of Molecular Sciences* vol. 16 (2015).

177. Obara-Michlewska, M. & Szeliga, M. Targeting Glutamine Addiction in Gliomas. *Cancers* vol. 12 (2020).

178. Restall, I. J. *et al.* Brain Tumor Stem Cell Dependence on Glutaminase Reveals a Metabolic Vulnerability through the Amino Acid Deprivation Response Pathway. *Cancer Res.* **80**, 5478 LP – 5490 (2020).

179. Tönjes, M. *et al.* BCAT1 promotes cell proliferation through amino acid catabolism in gliomas carrying wild-type IDH1. *Nat. Med.* **19**, 901–908 (2013).

180. Palanichamy, K. *et al.* Methionine and Kynurenine Activate Oncogenic Kinases in Glioblastoma, and Methionine Deprivation Compromises Proliferation. *Clin. Cancer Res.* **22**, 3513 LP – 3523 (2016).

181. Taïb, B. *et al.* Lipid accumulation and oxidation in glioblastoma multiforme. *Sci. Rep.* **9**, 19593 (2019).

182. Zhao, W. *et al.* Fatty acid synthase: a novel target for antiglioma therapy. *Br. J. Cancer* **95**, 869–878 (2006).

183. Tanaka, S., Louis, D. N., Curry, W. T., Batchelor, T. T. & Dietrich, J. Diagnostic and therapeutic avenues for glioblastoma: no longer a dead end? *Nat. Rev. Clin. Oncol.* **10**, 14–26 (2013).

184. Sharpe, M. A. *et al.* The Leloir Cycle in Glioblastoma: Galactose Scavenging and Metabolic Remodeling. *Cancers (Basel).* **13**, (2021).

185. Pascual, G. *et al.* Targeting metastasis-initiating cells through the fatty acid receptor CD36. *Nature* **541**, 41–45 (2017).

186. Pan, J. *et al.* CD36 mediates palmitate acid-induced metastasis of gastric cancer via AKT/GSK-3β/β-catenin pathway. *J. Exp. Clin. Cancer Res.* **38**, 52 (2019).

187. Sánchez-Rodríguez, P., Rodríguez, M. C. & Sánchez-Yagüe, J. Identification of potential erythrocyte phospholipid fatty acid biomarkers of advanced lung adenocarcinoma, squamous cell lung carcinoma, and small cell lung cancer. *Tumour Biol. J. Int. Soc. Oncodevelopmental Biol. Med.* **36**, 5687–5698 (2015).

188. Hager, M. H., Solomon, K. R. & Freeman, M. R. The role of cholesterol in prostate cancer. *Curr. Opin. Clin. Nutr. Metab. Care* **9**, 379–385 (2006).

189. Azordegan, N. *et al.* Carcinogenesis alters fatty acid profile in breast tissue. *Mol. Cell. Biochem.* **374**, 223–232 (2013).

190. Zhuang, L., Kim, J., Adam, R. M., Solomon, K. R. & Freeman, M. R. Cholesterol targeting alters lipid raft composition and cell survival in prostate cancer cells and xenografts. *J. Clin. Invest.* **115**, 959–968 (2005).

191. Gimple, R. C. *et al.* Glioma Stem Cell–Specific Superenhancer Promotes Polyunsaturated Fatty-Acid Synthesis to Support EGFR Signaling. *Cancer Discov.* **9**, 1248 LP – 1267 (2019).

192. Mika, A. *et al.* Preferential uptake of polyunsaturated fatty acids by colorectal cancer cells. *Sci. Rep.* **10**, 1954 (2020).

6. Publications

Alhalabi, O. T., Fletcher, M., Hielscher, T., Kessler, T., **Lokumcu, T.,** Baumgartner, U., Wittmann, E., Schlue, S., Göttmann, M., Rahman, S., Hai, L., Hansen-Palmus, L., Puccio, L., Nakano, I., Herold-Mende, C., Day, B. W., Wick, W., Sahm, F., Phillips, E., & Goidts, V. (2021). A novel patient stratification strategy to enhance the therapeutic efficacy of dasatinib in glioblastoma. *Neuro-oncology*, noab158. Advance online publication. https://doi.org/10.1093/neuonc/noab158

Oran, D. C., **Lokumcu, T.**, Inceoglu, Y., Akolpoglu, M. B., Albayrak, O., Bal, T., Kurtoglu, M., Erkan, M., Can, F., Bagci-Onder, T., & Kizilel, S. (2019). Engineering human stellate cells for beta cell replacement therapy promotes *in vivo* recruitment of regulatory T cells. *Materials today. Bio*, *2*, 100006. https://doi.org/10.1016/j.mtbio.2019.100006

Kaya-Aksoy, E., Cingoz, A., Senbabaoglu, F., Seker, F., Sur-Erdem, I., Kayabolen, A., **Lokumcu, T.**, Sahin, G. N., Karahuseyinoglu, S., & Bagci-Onder, T. (2019). The pro-apoptotic Bcl-2 family member Harakiri (HRK) induces cell death in glioblastoma multiforme. *Cell death discovery*, *5*, 64. https://doi.org/10.1038/s41420-019-0144-z

7. Appendix

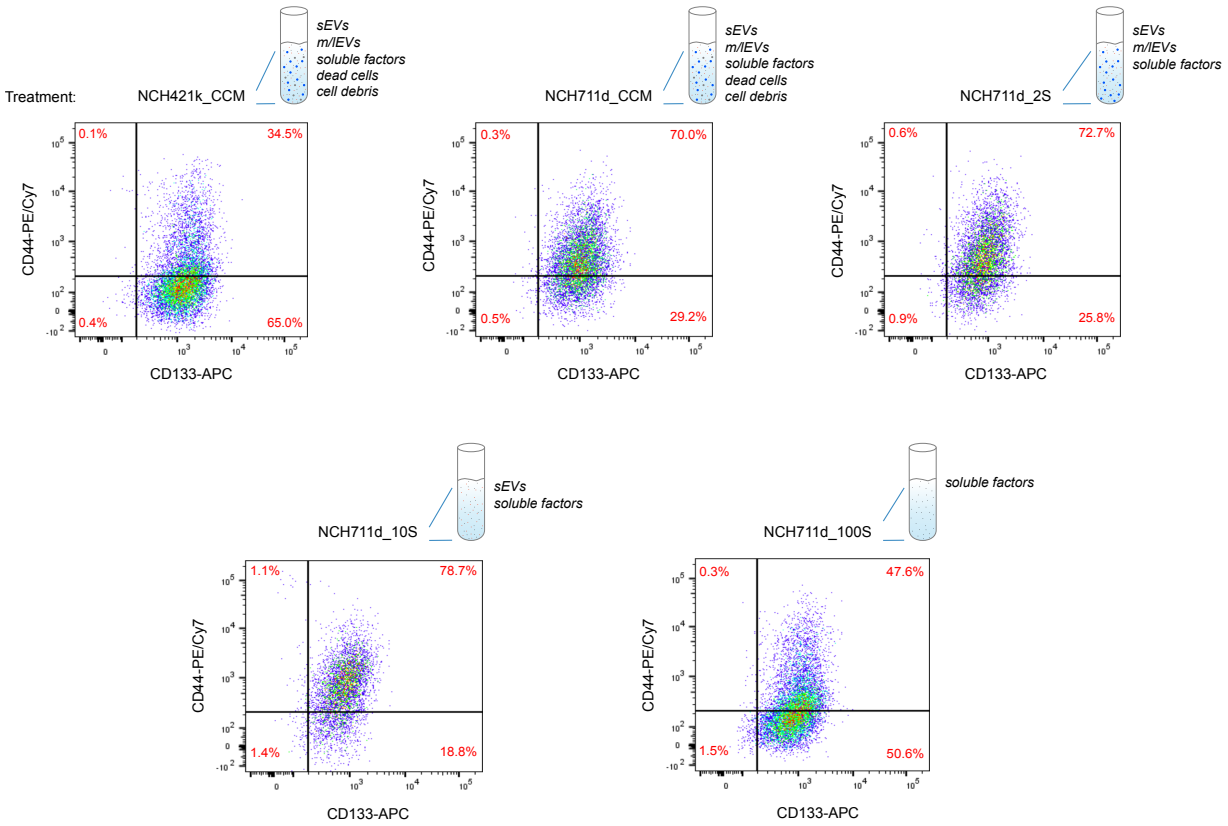

Supplementary Figure 1. Flow cytometry results of PN cells treated with different fractions of MES conditioned medium

NCH421k cells (PN) were treated with the different fractions of NCH711d (MES) conditioned medium, and the expression of GSCs surface markers (CD133 and CD44) was measured by flow cytometry. NCH421k complete conditioned medium (NCH421k_CCM) was used as a control. CCM, complete conditioned medium; 2S, supernatant after 2000 g; 10S, supernatant after 10 000 g; 100S, supernatant after 100 000 g; 100P, pellet after 100 000 g centrifugation; Filtered, supernatant filtered with membrane filter (pore size, 20 nm).

Supplementary Table 1. The list of proteins (Top 50) enriched in NCH421k sEVs compared to parental cells

The relative abundance of identified proteins was statistically compared for differences between sEVs and parental cells, and Top 50 hits (adj. pval < 0.001, $log_2FC > 4$) were listed below. The hits were ranked according to log_2FC.

Gene names	Log_2 (Fold_Change)	adj_pval	-log10 (adj_pval)
HAPLN1	12.201	7.55E-08	7.122
IGSF8	10.121	7.55E-08	7.122
ACAN	9.808	1.13E-07	6.946
PTGFRN	9.587	8.66E-08	7.063
SLC1A4	8.971	1.42E-07	6.849
HTRA1	8.946	1.93E-07	6.715
PCDH15	8.924	1.52E-07	6.817
ITGA6	8.824	1.49E-07	6.828
HSPG2	8.746	1.25E-07	6.902
GPC4	8.732	2.27E-07	6.644
PLXNA1	8.715	1.45E-07	6.839
CACNA2D1	8.677	1.53E-07	6.816
MFGE8	8.611	1.37E-07	6.863
SDCBP	8.486	1.45E-07	6.839
PROM1	8.351	2.10E-07	6.677
ADGRL2	8.315	2.41E-07	6.618
SLC44A2	8.206	3.73E-07	6.428
GPM6A	8.067	3.55E-07	6.450
CD81	8.020	2.05E-07	6.689
SLC39A10	7.998	2.32E-07	6.634
CPS1	7.902	3.57E-07	6.447
BCAN	7.606	2.33E-07	6.633
CD9	7.583	5.01E-07	6.301
ITGA2	7.557	2.50E-07	6.602
DIP2A	7.547	1.41E-06	5.850

NT5E	7.496	3.08E-07	6.511
ATP1A2	7.457	1.21E-06	5.919
NCAN	7.353	2.93E-07	6.533
P2RX7	7.348	3.04E-07	6.517
SLC38A5	7.336	2.99E-07	6.525
LPHN3	7.317	5.05E-07	6.297
MAP4K4	7.270	3.92E-07	6.407
CD47	7.184	4.20E-07	6.376
ENPP1	7.160	3.19E-07	6.496
PLXNB1	6.931	1.21E-06	5.917
SLC29A1	6.842	1.32E-06	5.879
TTYH3	6.790	2.66E-05	4.575
ITFG3	6.787	1.04E-06	5.983
PCDH7	6.775	8.45E-07	6.073
SLC7A2	6.716	5.46E-07	6.263
SLC1A5	6.674	7.25E-07	6.140
SH3BP4	6.606	1.60E-04	3.796
TSPAN14	6.578	1.01E-06	5.996
CA14	6.490	6.61E-06	5.180
GPM6B	6.485	9.67E-07	6.015
ATP2B4	6.466	1.56E-06	5.808
RP2	6.431	9.69E-07	6.014
ATRN	6.354	1.13E-06	5.949
TNIK	6.350	6.42E-07	6.192
NOTCH1	6.349	1.81E-06	5.743

Supplementary Table 2. The list of proteins (Top 50) enriched in NCH644 sEVs compared to parental cells

The relative abundance of identified proteins was statistically compared for differences between sEVs and parental cells, and Top 50 hits (adj. pval < 0.001, $log_2FC > 4$) were listed below. The hits were ranked according to log_2FC.

Gene names	Log_2 (Fold_Change)	adj_pval	-log10 (adj_pval)
TTYH1	9.333	2.45E-07	6.61
MFGE8	8.411	3.49E-07	6.46
GPM6A	8.373	5.47E-07	6.26
LPHN3	8.235	5.73E-07	6.24
PROM1	8.164	3.91E-07	6.41
SDCBP	7.976	5.10E-07	6.29
SDCBP	7.737	4.74E-07	6.32
ADAM10	7.482	9.43E-07	6.03
NOTCH1	7.460	2.51E-06	5.60
DIP2C	7.363	7.73E-07	6.11
EPHA3	7.195	9.97E-07	6.00
PLXNA1	6.966	1.42E-06	5.85
HTRA1	6.929	3.08E-06	5.51
SLC1A5	6.872	1.37E-06	5.86
SLIT1	6.872	1.11E-05	4.95
SLC29A1	6.744	5.97E-06	5.22
DAG1	6.734	1.48E-06	5.83
JUP	6.597	3.91E-05	4.41
CD9	6.453	3.61E-06	5.44
PTPRJ	6.434	6.21E-06	5.21
CSNK1G3	6.422	1.26E-05	4.90
ATP11C	6.347	3.26E-06	5.49
CD81	6.346	2.14E-06	5.67
ROBO1	6.295	1.41E-06	5.85
VPS28	6.141	3.15E-06	5.50

GPRC5B	6.123	2.08E-06	5.68
CD47	6.106	2.84E-06	5.55
ATRN	6.061	3.00E-06	5.52
PLXNA2	6.060	6.94E-06	5.16
ENPP6	6.055	8.05E-06	5.09
SLC38A1	6.045	2.33E-04	3.63
DAAM1	5.936	6.50E-06	5.19
ATP2B4	5.846	8.82E-06	5.05
TNIK	5.842	3.09E-06	5.51
PDCD6IP	5.797	2.97E-06	5.53
PLXNB1	5.744	8.23E-06	5.08
NT5E	5.732	1.28E-05	4.89
SLC9A3R2	5.678	4.59E-06	5.34
GPM6B	5.678	5.90E-06	5.23
STAM	5.667	6.09E-06	5.22
MAP4K4	5.658	1.09E-05	4.96
CEP55	5.650	1.27E-05	4.89
SLC7A2	5.637	4.32E-06	5.36
SLC19A1	5.629	2.84E-05	4.55
PTPRA	5.621	1.07E-05	4.97
EPB41L5	5.527	1.35E-05	4.87
ITGA6	5.509	8.24E-06	5.08
PCDH15	5.455	1.33E-05	4.88
NEDD4	5.447	7.57E-06	5.12
TSPAN7	5.406	2.23E-05	4.65

Supplementary Table 3. The list of proteins (Top 50) enriched in NCH705 sEVs compared to parental cells

The relative abundance of identified proteins was statistically compared for differences between sEVs and parental cells, and Top 50 hits (adj. pval < 0.001, $log_2FC > 4$) were listed below. The hits were ranked according to log_2FC.

Gene names	Log_2 (Fold_Change)	adj_pval	-log10 (adj_pval)
CSPG4	8.541	3.66E-08	7.44
ITGA4	8.452	5.84E-08	7.23
PTGFRN	8.376	4.17E-08	7.38
FN1	7.693	1.16E-06	5.93
TTYH3	7.679	2.11E-07	6.68
SDCBP	7.118	2.99E-07	6.52
MRGPRF	6.999	1.85E-07	6.73
ADAM10	6.860	6.52E-07	6.19
SLC44A2	6.802	1.97E-07	6.71
ITGA2	6.769	1.89E-07	6.72
ITGA3	6.689	2.99E-07	6.52
MME	6.479	9.52E-07	6.02
SLC44A1	6.435	5.53E-07	6.26
ENG	6.423	3.39E-07	6.47
NRP1	6.401	7.05E-07	6.15
EMILIN1	6.385	3.63E-06	5.44
DCHS1	6.360	5.32E-07	6.27
ACTR8	6.296	1.19E-06	5.93
SEMA3A	6.254	1.42E-06	5.85
KIRREL	6.213	2.37E-06	5.62
CAPN6	6.049	6.00E-07	6.22
ITGA7	6.030	6.54E-07	6.18
HTRA1	5.988	2.37E-06	5.63
SCARB1	5.923	8.95E-07	6.05
CD9	5.908	3.13E-06	5.50

CEP55	5.764	1.19E-04	3.92
LSAMP	5.726	1.58E-06	5.80
ITGB4	5.716	1.17E-06	5.93
ITGB5	5.347	5.11E-06	5.29
F3	5.301	6.44E-06	5.19
GNG12	5.260	7.48E-06	5.13
NT5E	5.225	4.54E-06	5.34
PTPRS	5.192	4.68E-06	5.33
LRRC17	5.168	1.63E-04	3.79
DIP2B	5.154	5.05E-06	5.30
DAG1	5.150	2.37E-05	4.63
ITGA6	5.110	2.86E-06	5.54
SLC29A1	5.087	7.63E-05	4.12
CD151	5.048	2.91E-05	4.54
CD81	5.028	3.71E-06	5.43
SLC5A3	4.965	2.89E-05	4.54
ENPP1	4.925	1.93E-05	4.72
TENM3	4.916	4.58E-06	5.34
GPC6	4.911	1.36E-05	4.87
GRPR	4.869	1.20E-05	4.92
SLC2A3	4.859	7.08E-06	5.15
ITFG3	4.857	1.95E-05	4.71
SYT1	4.841	3.61E-05	4.44
FREM2	4.777	1.15E-05	4.94
EFR3A	4.766	1.29E-05	4.89

Supplementary Table 4. The list of proteins (Top 50) enriched in NCH711d sEVs compared to parental cells

The relative abundance of identified proteins was statistically compared for differences between sEVs and parental cells, and Top 50 hits (adj. pval < 0.001, $log_2FC > 4$) were listed below. The hits were ranked according to log_2FC.

Gene names	Log_2 (Fold_Change)	adj_pval	-log10 (adj_pval)
MFGE8	9.771	2.56E-07	6.59
EDIL3	8.006	4.57E-07	6.34
APOE	7.848	1.96E-06	5.71
PTGFRN	7.209	7.32E-07	6.14
THSD7A	6.952	2.33E-06	5.63
DIP2B	6.895	2.98E-06	5.53
SLC1A4	6.426	3.92E-06	5.41
ITGB3	6.350	3.71E-06	5.43
ITFG3	6.238	9.17E-06	5.04
IGSF3	6.138	2.46E-06	5.61
CSPG4	6.120	1.28E-05	4.89
PVR	6.021	3.02E-06	5.52
PLXND1	5.986	8.20E-06	5.09
TENM3	5.964	3.98E-06	5.40
ITGA3	5.954	4.46E-06	5.35
SLC29A1	5.924	2.67E-06	5.57
ANO6	5.874	4.30E-06	5.37
CD9	5.851	3.10E-06	5.51
SYPL1	5.847	5.54E-06	5.26
FLVCR1	5.802	3.19E-06	5.50
NPR1	5.743	5.04E-06	5.30
ITGA5	5.720	8.39E-06	5.08
SDCBP	5.675	7.30E-06	5.14
DIP2C	5.606	2.84E-06	5.55
VANGL1	5.551	1.00E-05	5.00

SLC44A1	5.517	3.33E-04	3.48
CACNA2D1	5.479	6.90E-06	5.16
CD81	5.474	3.75E-06	5.43
PCDH7	5.467	1.15E-05	4.94
SCARB1	5.372	1.48E-05	4.83
CD47	5.370	3.94E-05	4.40
SLC7A2	5.323	7.27E-06	5.14
SLC1A5	5.315	1.68E-05	4.77
ADAMTS4	5.272	3.59E-05	4.44
SLC1A2	5.222	1.29E-04	3.89
CD109	5.177	3.26E-05	4.49
SDK2	5.094	7.23E-06	5.14
CD97	5.080	2.47E-05	4.61
ITGA6	5.078	1.07E-05	4.97
TGFBR3	5.061	1.89E-05	4.72
FN1	5.049	1.97E-05	4.71
CELSR2	4.956	8.58E-06	5.07
BAI1	4.932	1.72E-05	4.77
ADGRL2	4.927	2.62E-05	4.58
ZDHHC5	4.925	2.86E-05	4.54
TENM2	4.914	8.46E-06	5.07
PTPRA	4.907	1.12E-05	4.95
ADAM10	4.901	6.69E-04	3.17
SLC26A2	4.897	1.69E-05	4.77
SEMA3A	4.876	3.29E-05	4.48

Supplementary Table 5. The list of proteins enriched in mesenchymal sEVs (MES_sEVs) compared to proneural sEVs (PN_sEVs)

The relative abundance of proteins identified in MES_sEVs and PN_sEVs was statistically compared, and the ones with adj. pval < 0.001 and $log_2FC > 0$) were listed below. The hits were ranked according to log_2FC.

Gene names	Log_2 (Fold_Change)	adj_pval	-log10 (adj_pval)
ANXA1	8.192	3.46E-06	5.461
ANXA2	7.116	1.23E-04	3.910
NRP1	7.092	1.51E-06	5.820
MOXD1	6.498	3.98E-07	6.400
ITGA5	6.013	5.50E-07	6.260
ENG	5.796	4.50E-08	7.347
ITGA3	5.723	1.17E-09	8.931
CD109	5.162	1.41E-04	3.852
ITGB4	5.141	3.98E-07	6.400
MMP14	4.980	1.17E-09	8.931
SPTBN1	4.284	8.24E-04	3.084
TPBG	4.251	1.31E-05	4.884
CD44	3.941	7.22E-08	7.142
FN1	3.802	5.04E-06	5.297
FAM129A	3.744	9.18E-05	4.037
PLS3	3.661	5.08E-05	4.294
EPHA2	3.342	2.55E-05	4.593
SPTAN1	3.307	7.14E-04	3.146
VCL	3.246	1.60E-06	5.795
CPNE8	3.194	1.59E-04	3.800
CRYZ	3.098	6.12E-08	7.213
GBE1	2.955	1.73E-04	3.761
TMEM2	2.945	2.73E-05	4.563
ANTXR2	2.864	5.62E-07	6.250
CAPN6	2.778	7.51E-04	3.125

SLC2A3	2.746	2.61E-06	5.583
DPYSL3	2.705	2.49E-06	5.603
PVRL2	2.543	7.06E-05	4.151
ACTN4	2.528	7.18E-06	5.144
NDRG1	2.523	1.61E-05	4.793
ANXA5	2.508	1.43E-04	3.844
RALB	2.469	7.18E-06	5.144
FSCN1	2.396	9.54E-05	4.020
CAP1	2.326	7.59E-06	5.120
CUL2	2.249	7.82E-06	5.107
LDLR	2.224	7.18E-04	3.144
TPI1	2.161	1.51E-06	5.820
RRAS	2.131	5.34E-04	3.273
PSMD5	2.074	1.82E-05	4.739
ITGB1	2.053	8.72E-05	4.060
TSPAN9	2.016	8.91E-05	4.050
ROCK1	2.008	1.97E-04	3.706
TSN	1.951	2.19E-05	4.659
PLIN3	1.923	1.99E-05	4.702
PTPRG	1.834	6.63E-04	3.179
PSME1	1.797	2.29E-04	3.640
CDH2	1.787	7.59E-05	4.120
PROCR	1.786	5.98E-04	3.224
GSS	1.784	2.55E-05	4.593
SCRN1	1.776	1.79E-04	3.746
CNN3	1.752	1.97E-04	3.706
DPYSL2	1.725	2.02E-04	3.694
TXNRD1	1.690	4.69E-05	4.329
CCBL2	1.640	1.81E-04	3.741

YWHAB	1.634	4.88E-04	3.311
HLA-B	1.616	2.42E-05	4.616
GSTO1	1.606	1.33E-04	3.876
G6PD	1.541	7.71E-04	3.113
SLC9A1	1.538	1.70E-04	3.770
LDHA	1.512	1.20E-04	3.920
GJA1	1.499	7.40E-05	4.131
GAPDH	1.478	1.70E-04	3.768
ITGA6	1.475	1.17E-04	3.931
CHP1	1.467	1.70E-05	4.769
STXBP1	1.422	2.36E-04	3.627
GLOD4	1.376	5.87E-04	3.231
YWHAG	1.361	6.03E-04	3.220
ARPC5	1.334	5.65E-04	3.248
FAM49B	1.324	1.07E-04	3.971
SRI	1.322	7.41E-04	3.130
RALA	1.314	2.91E-04	3.536
GNAS	1.283	9.53E-04	3.021
DCTN2	1.275	3.16E-04	3.501
NOTCH2	1.270	5.34E-04	3.273
CAPZB	1.265	5.76E-04	3.239
YWHAZ	1.243	3.08E-04	3.512
SEPT9	1.241	4.61E-04	3.336
TPT1	1.227	2.28E-04	3.642
PGM1	1.183	2.03E-04	3.693
CAPZA2	0.982	5.23E-04	3.281

Supplementary Table 6. The list of proteins enriched in mesenchymal cells (MES_cells) compared to proneural cells (PN_cells)

The relative abundance of proteins identified in MES_cells and PN_cells was statistically compared, and the ones with adj. pval < 0.001 and $log_2FC > 0$) were listed below. The hits were ranked according to log_2FC.

Gene names	Log_2 (Fold_Change)	adj_pval	-log10 (adj_pval)
ANXA1	11.194	2.29E-09	8.641
TAGLN2	6.238	2.09E-08	7.680
ANXA2	5.495	2.61E-05	4.584
ALDH1A1	4.820	5.18E-06	5.286
ATP2B4	4.741	1.41E-06	5.850
FDXR	4.429	6.82E-04	3.166
LMNA	4.421	5.54E-04	3.256
LAMC1	4.309	9.51E-04	3.022
KIF5C	4.066	4.05E-04	3.393
LMNA	4.036	1.91E-04	3.719
LAMB1	3.685	2.48E-05	4.605
PPP1R18	3.643	3.71E-08	7.430
ROCK1	3.594	1.14E-06	5.944
MAP4K4	3.155	1.61E-06	5.793
CTH	3.078	9.18E-04	3.037
CDH2	3.068	1.28E-07	6.891
LDLR	3.059	3.63E-05	4.440
ACSS2	3.032	5.57E-06	5.254
PLS3	3.023	5.04E-04	3.297
TNKS1BP1	2.969	2.04E-06	5.689
MYO1B	2.833	8.79E-07	6.056
PGM2L1	2.771	2.82E-05	4.549
P4HA2	2.651	8.43E-06	5.074
MYO1C	2.625	8.28E-05	4.082
PSMD5	2.604	1.55E-08	7.809

TRIM16	2.484	2.53E-04	3.596
TUBB3	2.433	8.13E-04	3.090
ITGB1	2.334	1.27E-05	4.895
ANXA11	2.322	5.47E-04	3.262
RAPH1	2.260	4.10E-05	4.387
VCL	2.247	7.54E-04	3.123
CAPN1	2.239	2.57E-04	3.589
EXTL3	2.225	2.20E-08	7.657
CKAP4	2.204	7.73E-04	3.112
RASA1	2.170	6.87E-04	3.163
MPRIP	2.165	8.42E-04	3.075
ALDH3A2	2.154	2.19E-06	5.659
VIM	2.145	7.68E-04	3.115
LGALS1	2.071	8.70E-05	4.061
UTRN	2.021	1.19E-04	3.925
PTK2	1.993	3.59E-05	4.444
CNN3	1.992	9.01E-07	6.045
GBE1	1.983	2.93E-04	3.533
ITGA6	1.905	2.35E-05	4.630
ANXA5	1.901	9.71E-04	3.013
PPP1R12A	1.866	1.96E-04	3.707
CTNNB1	1.857	3.38E-05	4.472
SPTBN1	1.850	2.52E-05	4.598
GNAQ	1.810	2.35E-04	3.629
GNAS	1.809	1.88E-07	6.726
CLIC1	1.758	3.39E-06	5.470
SPTAN1	1.706	2.57E-04	3.589
CD276	1.622	8.99E-06	5.046
RALA	1.616	1.19E-04	3.925

CAMK2D	1.589	2.74E-05	4.562
DBNL	1.571	4.03E-04	3.395
LEPREL2	1.565	3.32E-05	4.478
HSPA1B	1.538	1.70E-05	4.770
CTNND1	1.538	9.54E-07	6.020
PPP1R9B	1.532	2.95E-06	5.531
DPYSL3	1.523	6.37E-07	6.196
TNIK	1.499	2.61E-04	3.584
ARHGAP1	1.464	1.26E-04	3.899
PDPR	1.447	3.36E-04	3.473
SPTAN1	1.432	2.61E-05	4.584
GNAI3	1.406	5.20E-06	5.284
PXK	1.400	2.86E-04	3.544
GSN	1.370	1.51E-04	3.822
CTNNA2	1.366	4.05E-04	3.392
CRYZ	1.362	1.35E-05	4.871
TSG101	1.333	1.26E-05	4.900
PTPN12	1.322	2.81E-04	3.552
WASL	1.296	1.70E-04	3.769
SLC2A1	1.279	7.82E-04	3.107
ACTN4	1.270	5.38E-05	4.269
MSN	1.222	5.54E-06	5.256
ITGAV	1.220	1.28E-04	3.891
CALD1	1.204	3.79E-05	4.421
SLC25A24	1.198	1.42E-04	3.846
USP5	1.172	4.32E-04	3.364
PPM1F	1.154	3.32E-05	4.478
FSCN1	1.152	2.97E-04	3.527
TCEB1	1.129	2.38E-04	3.623

ITCH	1.105	3.49E-04	3.457
SBNO1	1.101	7.38E-04	3.132
CTNNA1	1.079	2.52E-05	4.598
APLP2	1.059	7.33E-04	3.135
GNAI2	1.055	2.84E-05	4.547
PXDN	1.035	3.08E-04	3.511
SF3B4	1.024	1.89E-04	3.724
CCBL2	1.018	3.43E-04	3.465
ARPC3	1.008	1.76E-04	3.754
MKL2	1.003	6.11E-04	3.214
RDX	1.003	7.38E-04	3.132
PURB	0.982	6.90E-04	3.161
ABI2	0.974	7.22E-06	5.142
RAP1B	0.962	5.82E-04	3.235
TPI1	0.946	4.12E-04	3.385
ECE1	0.945	7.63E-04	3.117
AP2B1	0.944	7.53E-04	3.123
HDGF	0.943	4.29E-04	3.368
PRKAA1	0.940	5.76E-04	3.239
AAK1	0.924	8.90E-04	3.051
YKT6	0.921	3.43E-04	3.465
IAH1	0.914	2.84E-05	4.546
AP2M1	0.909	9.36E-04	3.029
DDR2	0.908	3.02E-04	3.520
CAPZB	0.899	2.66E-05	4.575
KIDINS220	0.893	4.79E-04	3.319
RCN1	0.889	1.62E-04	3.791
ACTR3	0.887	2.88E-04	3.541
CAT	0.880	5.08E-04	3.294

CMAS	0.872	4.05E-04	3.393
ACTG1	0.854	3.27E-04	3.485
BCAT2	0.851	2.93E-04	3.533
GARS	0.848	1.61E-04	3.792
NPTN	0.847	4.75E-04	3.323
HNRNPUL1	0.844	3.81E-04	3.419
PTPN11	0.827	6.01E-04	3.221
CROCC	0.819	6.68E-05	4.175
LRSAM1	0.811	2.33E-04	3.633
TSN	0.809	1.42E-04	3.847
GNB1	0.809	1.71E-05	4.767
ARPC4-TTLL3	0.793	5.47E-04	3.262
CPNE3	0.790	2.86E-04	3.544
ACTR2	0.773	6.40E-04	3.194
UBE2H	0.768	6.59E-05	4.181
CNPY4	0.748	5.32E-04	3.274
DNM1L	0.737	6.84E-04	3.165
RECQL	0.736	3.35E-04	3.475
ABR	0.725	5.65E-04	3.248
AP2A1	0.697	5.16E-04	3.287
TCF12	0.678	3.60E-04	3.443
WDR1	0.676	2.66E-04	3.576
DERL1	0.672	8.89E-04	3.051
UBA2	0.592	8.13E-04	3.090

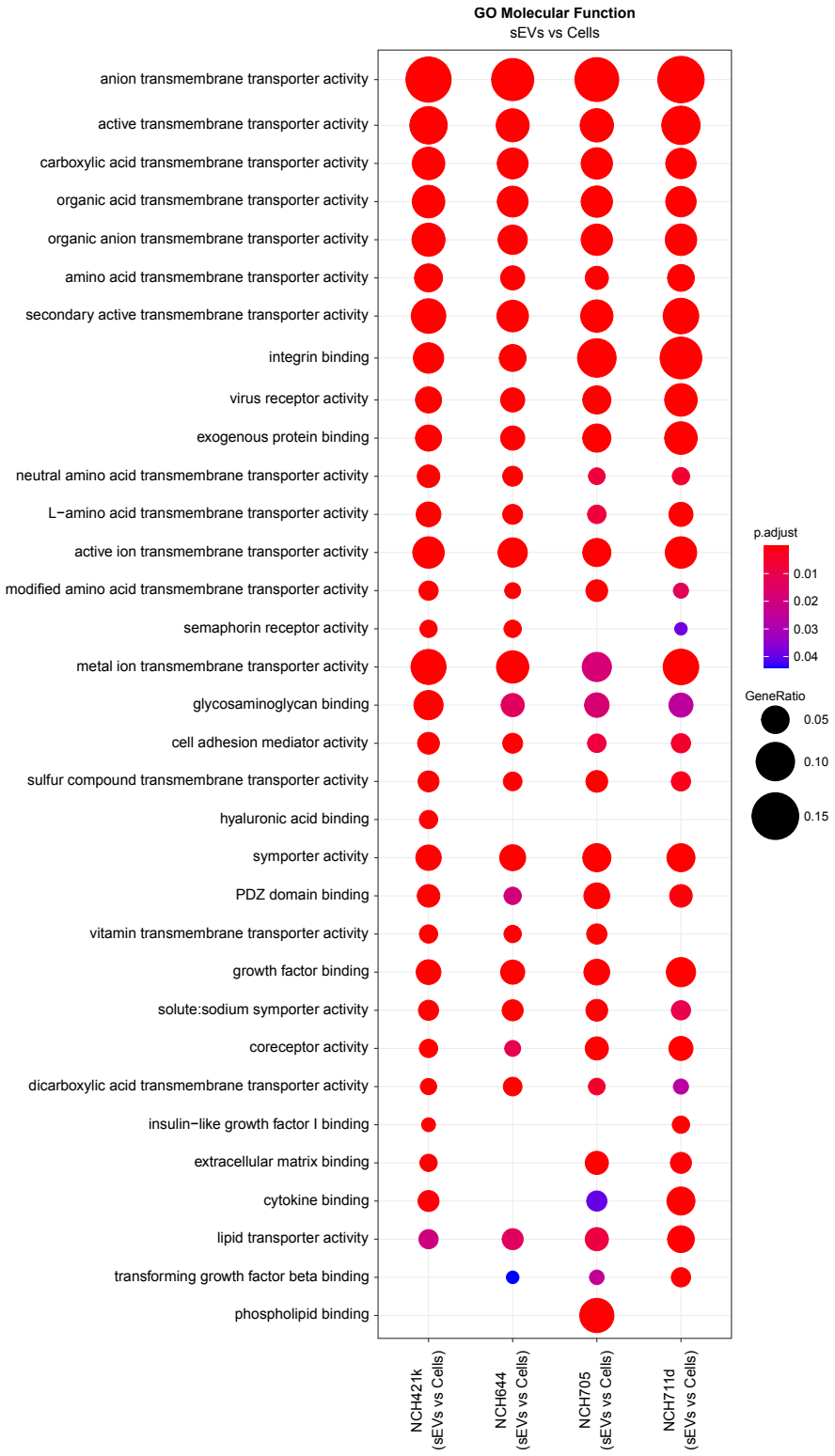

Supplementary Figure 2. Gene ontology (GO) analysis (molecular function) of proteins enriched in sEVs in comparison to their respective cell lines

Dot plot showing the GO molecular function analysis of differentially abundant proteins (sEVs vs Cells, adj. pval < 0.001 and $\log_2$FC > 4) in sEVs. The plot was generated using Top 20 molecular function terms of each comparison.

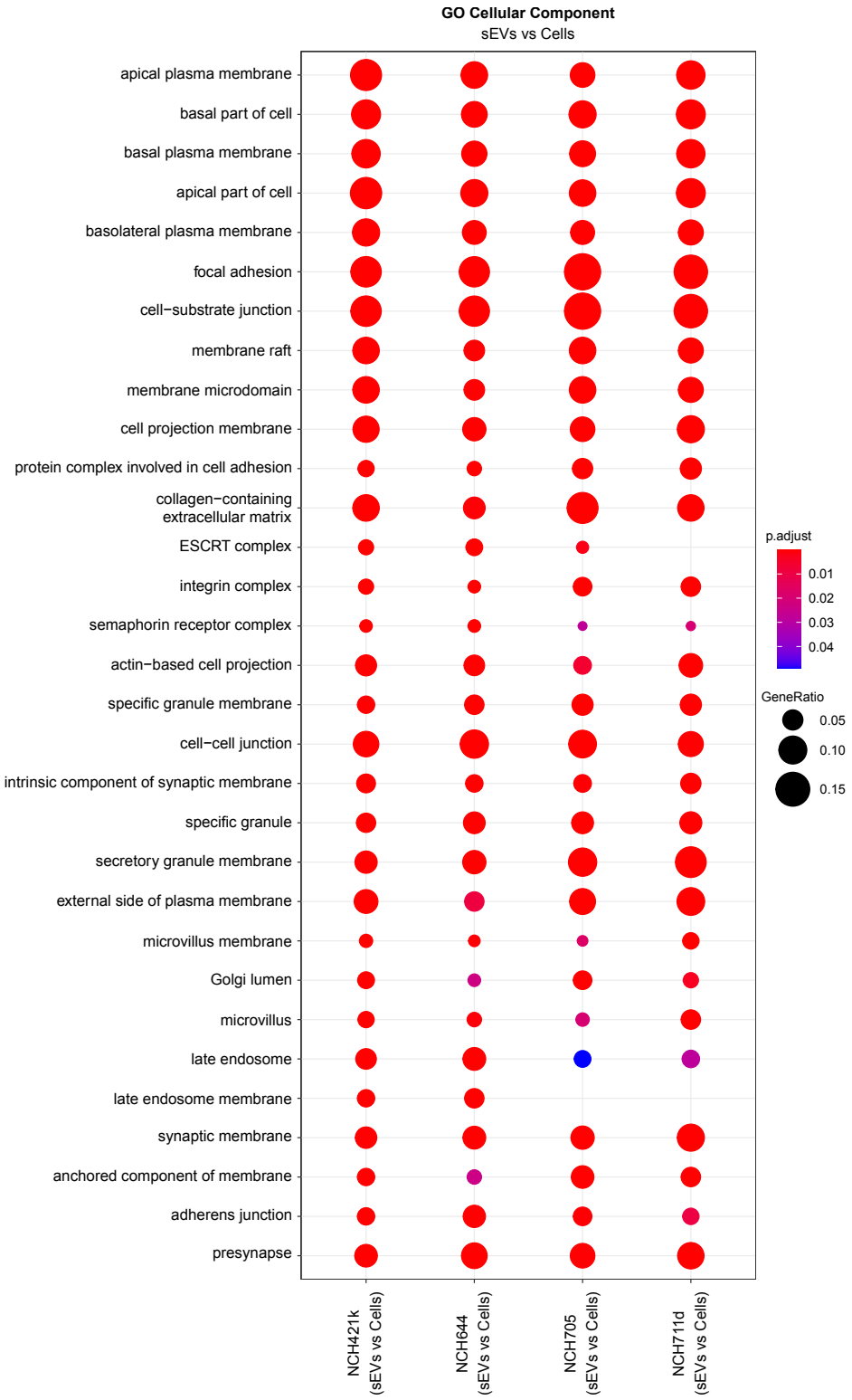

Supplementary Figure 3. Gene ontology (GO) analysis (cellular component) of proteins enriched in sEVs in comparison to their respective cell lines

Dot plot showing the GO cellular component analysis of differentially abundant proteins (sEVs vs Cells, adj. pval < 0.001 and $\log_2$FC > 4) in sEVs. The plot was generated using Top 20 cellular component terms of each comparison.

Plasmid maps

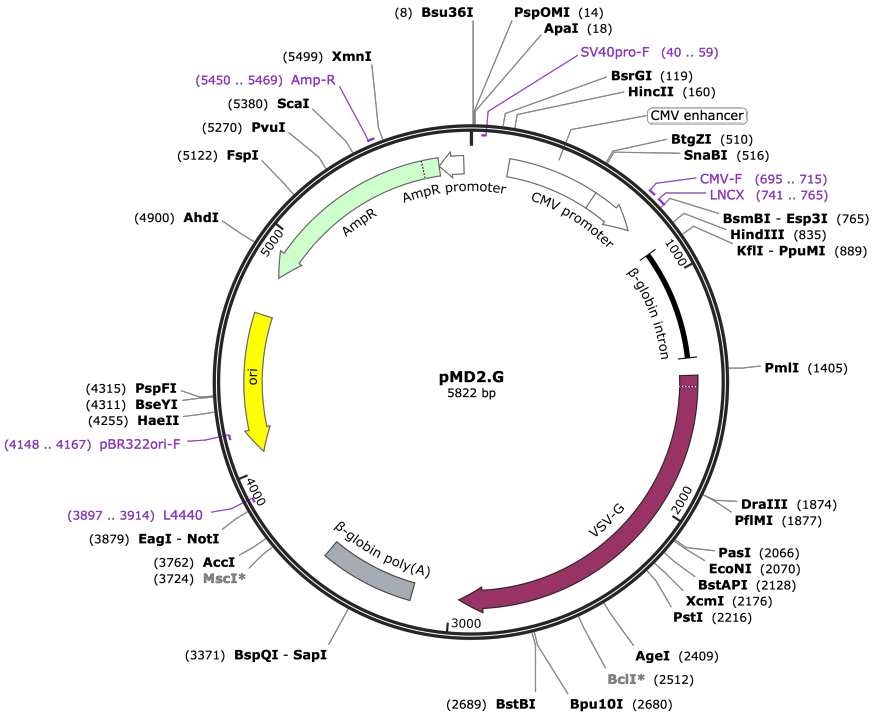

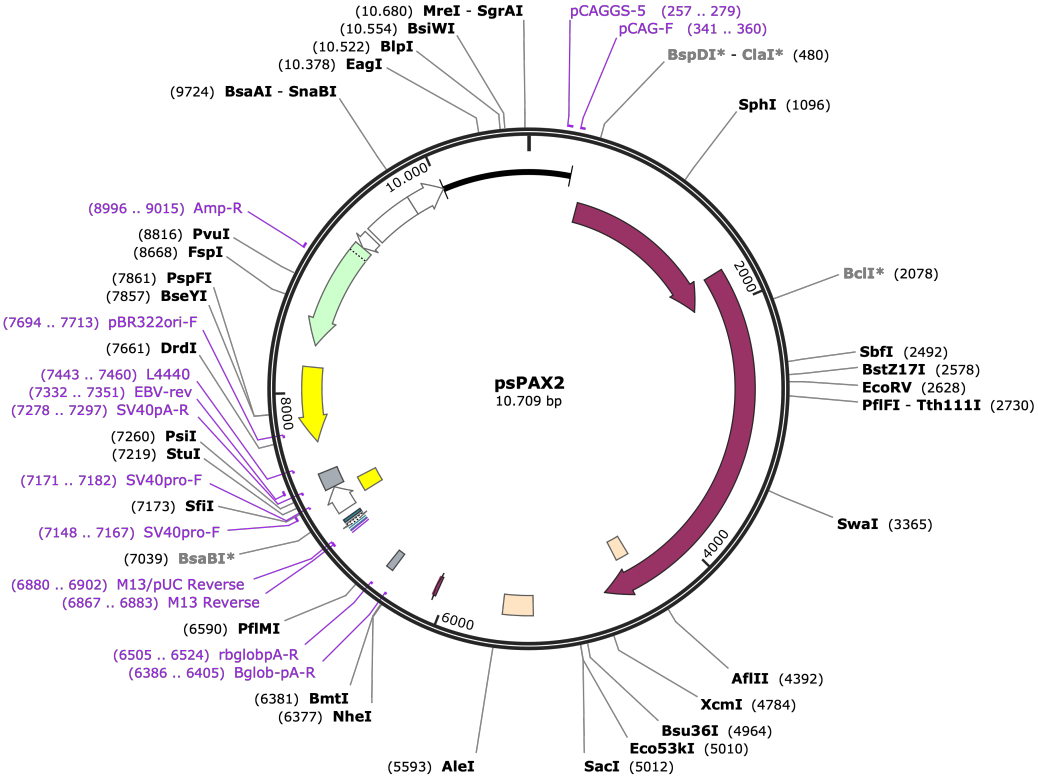

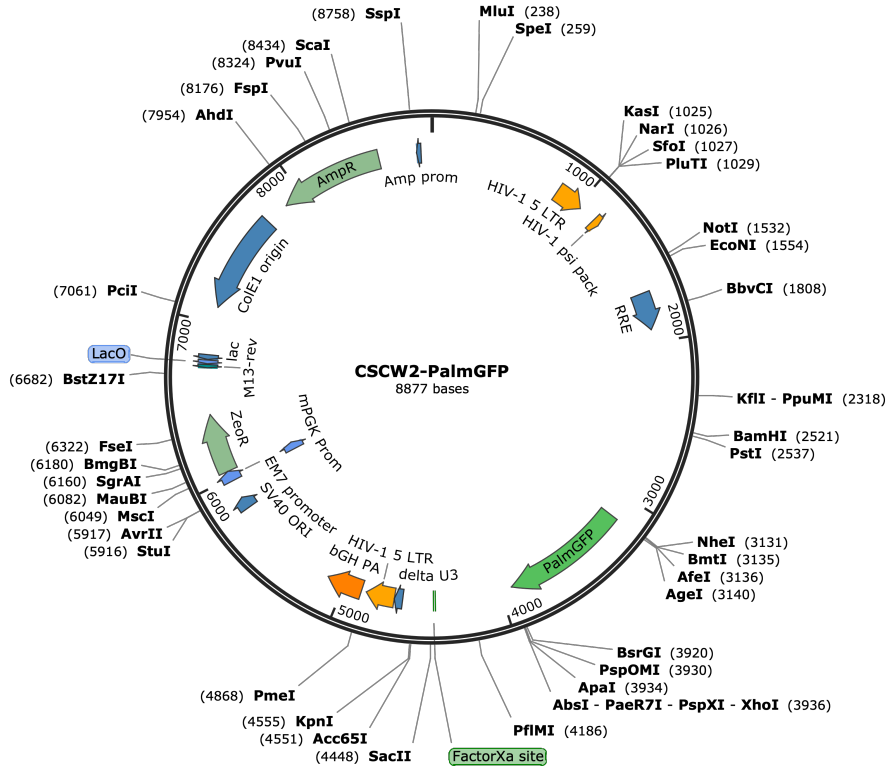
CSCW2-PalmGFP
8877 bases
(8758) SspI
MluI (238)
SpeI (259)
(8434) ScaI
(8324) PvuI
(8176) FspI
(7954) AhdI
KasI (1025)
NarI (1026)
SfoI (1027)
PluTI (1029)
NotI (1532)
EcoNI (1554)
BbvCI (1808)
KflI - PpuMI (2318)
BamHI (2521)
PstI (2537)
NheI (3131)
BmtI (3135)
AfeI (3136)
AgeI (3140)
BsrGI (3920)
PspOMI (3930)
ApaI (3934)
AbsI - PaeR7I - PspXI - XhoI (3936)
PflMI (4186)
FactorXa site
(4868) PmeI
(4555) KpnI
(4551) Acc65I
(4448) SacII
(7061) PciI
LacO
(6682) BstZ17I
(6322) FseI
(6180) BmgBI
(6160) SgrAI
(6082) MauBI
(6049) MscI
(5917) AvrII
(5916) StuI
AmpR
Amp prom
ColE1 origin
HIV-1 5 LTR
HIV-1 psi pack
RRE
lac
M13-rev
ZeoR
mPGK Prom
EM7 promoter
SV40 ORI
HIV-1 5 LTR
bGH PA
delta U3
PalmGFP
1000
2000
3000
4000
5000
6000
7000
8000

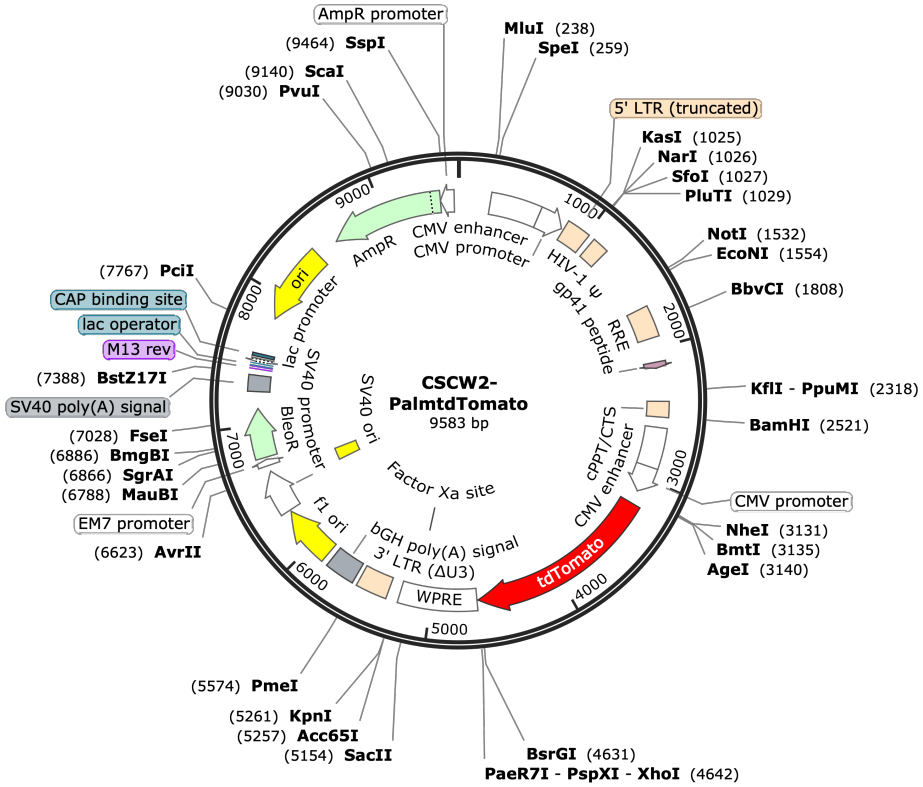
CSCW2-
PalmtdTomato
9583 bp
AmpR promoter
(9464) SspI
MluI (238)
SpeI (259)
(9140) ScaI
(9030) PvuI
5' LTR (truncated)
KasI (1025)
NarI (1026)
SfoI (1027)
PluTI (1029)
NotI (1532)
EcoNI (1554)
BbvCI (1808)
KflI - PpuMI (2318)
BamHI (2521)
CMV promoter
NheI (3131)
BmtI (3135)
AgeI (3140)
(5574) PmeI
(5261) KpnI
(5257) Acc65I
(5154) SacII
BsrGI (4631)
PaeR7I - PspXI - XhoI (4642)
(7767) PciI
CAP binding site
lac operator
M13 rev
(7388) BstZ17I
SV40 poly(A) signal
(7028) FseI
(6886) BmgBI
(6866) SgrAI
(6788) MauBI
EM7 promoter
(6623) AvrII
AmpR
CMV enhancer
CMV promoter
HIV-1 ψ
gp41 peptide
RRE
cPPT/CTS
CMV enhancer
tdTomato
WPRE
3' LTR (ΔU3)
bGH poly(A) signal
f1 ori
Factor Xa site
SV40 ori
SV40 promoter
BleoR
lac promoter
ori
1000
2000
3000
4000
5000
6000
7000
8000
9000

8. Acknowledgements

I would like to express my gratitude and appreciation to the following people:

Violine Goidts for her supervision during my PhD and for helpful discussions about the project.

Ursula Klingmüller, Stefan Pfister, and Christel Herold-Mende for being member of my thesis advisory committee and for fruitful discussions about my PhD project.

Rüdiger Hell, Peter Angel, Ursula Klingmüller, and Stefan Pfister for being on my defense committee.

Martin Schneider and Dominik Helm for their never-ending support and an excellent collaboration on the proteomic profiling.

Glynis Klinke and Michael Büttner for a great collaboration in metabolite screening and fatty acid profiling.

Almut Schulze and Lisa Schlicker for a great collaboration and their help on analyzing/interpreting metabolomics/fatty acid data.

Karsten Richter for the TEM imaging of sEVs.

Mark Zapatka and Murat Iskar for a great collaboration and bioinformatics support.

Frederic Bethke for his technical support on sEVs separations.

Peter Lichter, Martina Seiffert, Bernhard Radlwimmer, Daniel Mertens, Aurelie Ernst, and Stefan Pfister for all their helpful comments and fruitful discussions in B060 seminars.

Umar Khalid, Ka-Hou Man, Mona Göttman, Michael Persicke, Jasmin Mangei, Himanshu Soni, Magdalena Schlotter, Yuan Peng, Obada Alhalabi, Emma Phillips, Gabriele Müller, Silja Schlue, Laura Puccio, Theresa Schmid, Liliana Francois Martin del Campo, Lavinia Arseni, Marie Bordas, Mariana Coelho, Milena Simovic, and Rithu Kumar for all the great times.

All the other members of B06x for providing such a great working atmosphere.

And finally, my family and my partner Burcu Kuyumcu for the emotional support throughout this journey.